

PRELIMINARY INVESTIGATION OF THE EFFECT  
OF SURFACE FLUCTUATIONS ON SOUND AMPLITUDE  
IN GUIDED MODE PROPAGATION

By

Wesley Earl Jordan



# United States Naval Postgraduate School



## THESIS

PRELIMINARY INVESTIGATION OF THE EFFECT  
OF SURFACE FLUCTUATIONS ON SOUND AMPLITUDE  
IN GUIDED MODE PROPAGATION

by

Wesley Earl Jordan, Jr.

December 1970

*This document has been approved for public release and sale; its distribution is unlimited.*

T137070



Preliminary Investigation of the Effect  
of Surface Fluctuations on Sound Amplitude  
in Guided Mode Propagation

by

Wesley Earl Jordan, Jr.  
Lieutenant Commander, United States Navy  
B.S., United States Naval Academy, 1963

Submitted in partial fulfillment of the  
requirements for the degree of

MASTER OF SCIENCE IN ENGINEERING ACOUSTICS

from the

NAVAL POSTGRADUATE SCHOOL  
December 1970



# ABSTRACT

A simple theoretical relation between a one-dimensional surface wave and the amplitude fluctuations of an acoustic standing wave in a cavity with idealized boundaries is presented. An experiment was designed to investigate the applicability of the theory to a more complicated configuration. A 237 cm x 117 cm x 9 cm water-filled cavity with pressure-release walls was excited in a normal mode by a source placed in one corner. The resulting acoustic signal was monitored at various locations throughout the cavity with a small probe receiver. Wind-driven surface waves were generated by a multi-fan blower placed at one end of the cavity. The relationship between the resulting fluctuation of the acoustic signal and the surface fluctuation above the receiver was investigated. The results are consistent with the simple theory at low surface-wave frequencies. Anomalous behavior was observed for the higher frequencies of the surface wave spectrum. Possible mechanisms for this inconsistency are postulated and discussed.



## TABLE OF CONTENTS

I.	INTRODUCTION-----	9
II.	THEORY-----	11
III.	PROCEDURE AND ANALYSIS-----	20
	A. THE EXPERIMENT-----	20
	B. DESCRIPTION-----	24
	C. PROCEDURE-----	33
	D. ANALYSIS-----	43
	E. ERROR ANALYSIS-----	49
IV.	RESULTS AND CONCLUSIONS-----	51
	APPENDIX A: Computer Program for $a/\epsilon$ Calculation-----	66
	APPENDIX B: Observed Data-----	67
	APPENDIX C: Measured Values of $a/\epsilon$ -----	86
	BIBLIOGRAPHY-----	105
	INITIAL DISTRIBUTION LIST-----	106
	FORM DD 1473-----	107



## LIST OF FIGURES

### FIGURE

1.	Theoretical Cavity for Guided Mode Propagation-----	11
2.	Predicted Values of $a/\epsilon$ vs Surface Wave Frequency ( $\Omega/2\pi$ )(at an Antinode of the Standing Wave)-----	15
3.	Predicted Values of $a/\epsilon$ vs Surface Wave Frequency ( $\Omega/2\pi$ )(at a Node of the Standing Wave)-----	16
4.	Surface Propagation Constant ( $\gamma$ ) vs Surface Wave Frequency ( $\Omega/2\pi$ )-----	19
5.	Schematic Cross Section of Experimental Setup-----	22
6.	Tank Construction-----	25
7.	Tank with Fan Manifold in Place-----	27
8.	Wind Generator Operation-----	28
9.	The Wave Probe-----	29
10.	The Wave Height Measuring System-----	31
11.	The Wave Data Processing System-----	34
12.	The Acoustic System-----	35
13.	The Analog Frequency Analysis System-----	36
14.	Acoustic Amplitude vs Depth (at an Antinode of the Standing Wave in x and y)-----	38
15.	The Selected Receiver Positions-----	39
16.	Tank Modification for Isolation of Acoustic Amplitude Fluctuation Due to Fans-----	41
17.	Example of Graphical Determination of the Estimated Value of Mean Squared Amplitude-----	44



18.	The Graphical Determination of the Fan Contribution to the Acoustic Amplitude Fluctuation (Wind 4)-----	48
19.	Measured Value of $a/\epsilon$ vs Surface Wave Frequency ( $\Omega/2\pi$ ) for Each Wind Condition-----	54
20.	The Tank Surface Disturbed by a Typical Wind-----	61
21.	The Distribution of RMS Wave Heights in the Vicinity of the Receiver Positions-----	63
22.	Surface Fluctuation ( $\epsilon$ ) vs Surface Wave Frequency ( $\Omega/2\pi$ ) for Wind 6-----	64



## LIST OF SYMBOLS

$x, y, z$	Rectangular Coordinates
$l_x, l_y, l_z$	Cavity Dimensions
$n_i$	Wave Numbers
$k_i$	Acoustic Propagation Constant for $i^{\text{th}}$ Direction
$\gamma$	Surface Wave Propagation Constant
$\Phi$	Total Velocity Potential
$\Phi_1$	Steady State Velocity Potential
$\epsilon$	Perturbation Constant
$\epsilon\Phi_2$	Velocity Potential Contributed by Boundary Fluctuation
$\epsilon F(x, y, t)$	Surface Fluctuation (Eq. 2.2)
$\Omega$	Circular Frequency of Surface Wave
$\omega$	Circular Frequency of Acoustic Signal
$\psi$	Relative Phase of the Amplitude Fluctuation
$a$	Acoustic Amplitude Fluctuation
$a_a$	Observed Acoustic Amplitude Fluctuation
$a_f$	Contribution to Acoustic Amplitude Fluctuation from the Fans
$a_s$	Contribution to Acoustic Amplitude Fluctuation from Source Modulation
$c$	Free Field Acoustic Phase Speed
$V$	Surface Wave Phase Speed
$T_s$	Surface Tension



$\rho$	Density of Water
$g$	Acceleration of Gravity
$c(\tau)$	Autocorrelation Function
$T$	Integration Time of Correlator
$t$	Time
$\mu_i$	Term Involving Acoustic and Surface Wave Propagation Constants (Eq. 2.7)



## ACKNOWLEDGEMENTS

The author wishes to express his gratitude to Associate Professor A.B. Coppens for his many hours of consultation and patient guidance. A special note of thanks is due my wife, Sue Jordan, for the many hours of tireless work she contributed.



## I. INTRODUCTION

In A.B. Wood's model study of shallow water propagation [1], a sound amplitude fluctuation, synchronized with the passage of surface waves, is reported. Wood suggested the cause was an appreciable change in water depth in the vicinity of the source and/or specular scatter from the surface. The reflection and scattering of sound from uneven surfaces has been given considerable attention in the past twenty years [2]. Most treatments in the open literature have involved ray theoretic approaches, treating the reflection and scattering of plane waves from irregular surfaces, and have assumed no interaction with a second boundary. When a second boundary is present, the possibility of ducted propagation arises. A practical mathematical tool for investigation of surface irregularities affecting this type of propagation would be normal mode theory. Normal mode approaches [3,4] have been rare.

Several experimental investigations involving normal mode propagation have been conducted. J.A. Scrimger [5] reported correlation between surface-wave heights and sound-amplitude fluctuations both in magnitude and in frequency content. O.S. Tonakanov [6] found a linear relationship between surface-wave heights and percentage fluctuation in sound amplitude and phase.

The present work describes an experimental method for the investigation of the effect of surface variation on sound-fluctuation in guided mode propagation. Sound-amplitude fluctuations,



caused by a wind-driven surface, were measured and compared to the surface irregularity in the vicinity of the receiver. The surface was treated as a Fourier superposition of various sinusoidal waves, and the experimental results at each frequency were compared to a theoretical prediction for sound-amplitude fluctuations based on a monofrequency sinusoidal wave surface.



## II. THEORY

A normal mode solution to the wave equation for a rectangular enclosure with smooth boundaries (Figure 1) can be expressed as

$$\Phi = \cos k_1 x \cos k_2 y \sin k_3 z \cos \omega t \quad (2.1)$$

where  $\omega$  = circular frequency of excitation

$k_i$  = propagation constant for the  $i^{\text{th}}$  direction.

If the boundaries perpendicular to the  $z$  axis are pressure-release and are located at  $z = 0$  and  $z = l_z$ , then  $k_3 l_z = n_3$  is required. In all that follows, it is assumed that the system is excited at frequencies allowing only  $n_3 = 1$  so that the eigenvalue  $k_3$  is as small as possible.

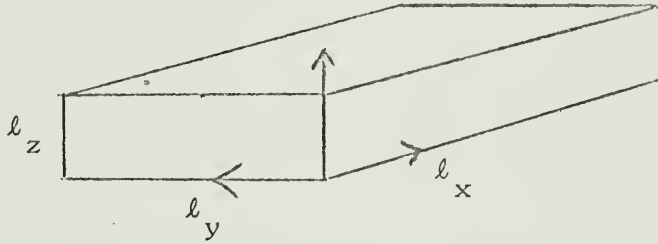


Figure 1. Theoretical Cavity for Guided Mode Propagation

If the upper boundary is disturbed, the boundaries in the  $z$  direction then occur at

$$z = 0$$

$$z = l_z + \epsilon F(x, y, t) \quad (2.2)$$



where  $\epsilon F(x,y,t)$  describes the change in depth of the cavity resulting from the surface fluctuation.

If  $\epsilon F(x,y,t)$  is small, then a solution of the form

$$\Phi = \Phi_1 + \epsilon \Phi_2 \quad (2.3)$$

is sought where  $\Phi_1$  is the solution for smooth boundaries shown above and  $\epsilon \Phi_2$  expresses a perturbation due to the altered boundary at  $z = l_z$ .

When  $\epsilon$  is sufficiently small, the following boundary conditions on  $\Phi_2$  result [7]:

$$\Phi_2 \Big|_{z=l_z} = \frac{-\partial \Phi_1}{\partial z} \Big|_{z=l_z} F(x,y,t) \quad (2.4)$$

$$\Phi_2 \Big|_{z=0} = 0$$

and  $\Phi_2$  must satisfy the wave equation

$$\square^2 \Phi_2 = 0.$$

If the surface fluctuation is a monofrequency wave propagating across the surface  $z = l_z$  in the x direction,  $F(x,y,t)$  may be written

$$F(x,y,t) = l_z \cos(\gamma x - \Omega t) \quad (2.5)$$

where  $\gamma$  = surface wave propagation constant

$\Omega$  = circular frequency of the surface wave.



The solution for  $\phi_2$  under these conditions is

$$\phi_2 = \frac{1}{4} k_3^{\ell} z \cos k_2 y \left[ \begin{aligned} & \frac{\sin \mu_1 z}{\sin \mu_1^{\ell} z} \cos[(k_1 + \gamma)x - (\omega + \Omega)t] + \\ & \frac{\sin \mu_2 z}{\sin \mu_2^{\ell} z} \cos[(k_1 - \gamma)x + (\omega + \Omega)t] + \\ & \frac{\sin \mu_3 z}{\sin \mu_3^{\ell} z} \cos[(k_1 + \gamma)x + (\omega - \Omega)t] + \\ & \frac{\sin \mu_4 z}{\sin \mu_4^{\ell} z} \cos[(k_1 - \gamma)x - (\omega - \Omega)t] \end{aligned} \right] \quad (2.6)$$

where  $\mu_1^2 = \left(\frac{\omega + \Omega}{c}\right)^2 - (k_1 + \gamma)^2 - k_2^2 \quad (2.7)$

$$\mu_2^2 = \left(\frac{\omega + \Omega}{c}\right)^2 - (k_1 - \gamma)^2 - k_2^2$$

$$\mu_3^2 = \left(\frac{\omega - \Omega}{c}\right)^2 - (k_1 + \gamma)^2 - k_2^2$$

$$\mu_4^2 = \left(\frac{\omega - \Omega}{c}\right)^2 - (k_1 - \gamma)^2 - k_2^2 .$$

If  $\Omega \ll \omega$ , then the approximation

$$\mu_1^2 \doteq \mu_3^2 \doteq k^2 - (k_1 + \gamma)^2 - k_2^2 \quad (2.8)$$

$$\mu_2^2 \doteq \mu_4^2 \doteq k^2 - (k_1 - \gamma)^2 - k_2^2$$

can be made and the complete solution simplifies to

$$\phi = \cos \omega t \cos k_2 y [\cos k_1 x \sin k_3 z + \frac{1}{2} \epsilon k_3^{\ell} z A \cos(\Omega t + \psi)] \quad (2.9)$$

where

$$A = \sqrt{\left(\frac{\sin \mu_1 z}{\sin \mu_2^{\ell} z}\right)^2 + \left(\frac{\sin \mu_2 z}{\sin \mu_2^{\ell} z}\right)^2 + 2 \left(\frac{\sin \mu_1 z}{\sin \mu_1^{\ell} z}\right) \left(\frac{\sin \mu_2 z}{\sin \mu_2^{\ell} z}\right) \cos 2k_1 x}$$



and

$$\tan \psi = - \frac{\left( \frac{\sin \mu_1 z}{\sin \mu_1 \frac{\ell}{2}} \right) \sin(k_1 + \gamma)x + \left( \frac{\sin \mu_2 z}{\sin \mu_2 \frac{\ell}{2}} \right) \sin(k_1 - \gamma)x}{\left( \frac{\sin \mu_1 z}{\sin \mu_1 \frac{\ell}{2}} \right) \cos(k_1 + \gamma)x + \left( \frac{\sin \mu_2 z}{\sin \mu_2 \frac{\ell}{2}} \right) \cos(k_1 - \gamma)x}.$$

Notice that it is the second term in the brackets of Eq. 2.9 that describes the fluctuation in the acoustic amplitude and that this term depends only on  $x$  and  $z$ . For the subsequent analysis Eq. 2.9 will be written in the form

$$\Phi = \cos \omega t \cos k_2 y [\cos k_1 x \sin k_3 z + a \cos(\Omega t + \psi)] \quad (2.10)$$

where  $k_3 \frac{\ell}{2} = \pi$

$$a/\epsilon = (\pi/2) A.$$

When  $k_1 x = \pi$  (an antinode of the standing wave in  $x$ ),  $a/\epsilon$  becomes

$$a/\epsilon = \sqrt{\left( \frac{\sin \mu_1 z}{\sin \mu_1 \frac{\ell}{2}} \right)^2 + 2 \left( \frac{\sin \mu_1 z}{\sin \mu_1 \frac{\ell}{2}} \right) \left( \frac{\sin \mu_2 z}{\sin \mu_2 \frac{\ell}{2}} \right) + \left( \frac{\sin \mu_2 z}{\sin \mu_2 \frac{\ell}{2}} \right)^2} \quad (2.11)$$

At  $z = \ell/2$ , this expression further reduces to

$$a/\epsilon = \pi/4 \left| \frac{1}{\cos \frac{\mu_1 \ell}{2}} + \frac{1}{\cos \frac{\mu_2 \ell}{2}} \right| \quad (2.12)$$

and

$$\Phi = \cos \omega t \cos k_2 y [1 + a \cos(\Omega t + \psi)]. \quad (2.13)$$



Predicted Values of  $a/c$   
vs  
Surface Wave Frequency ( $\Omega/2\pi$ )  
(at an Antinode of the Standing Wave)

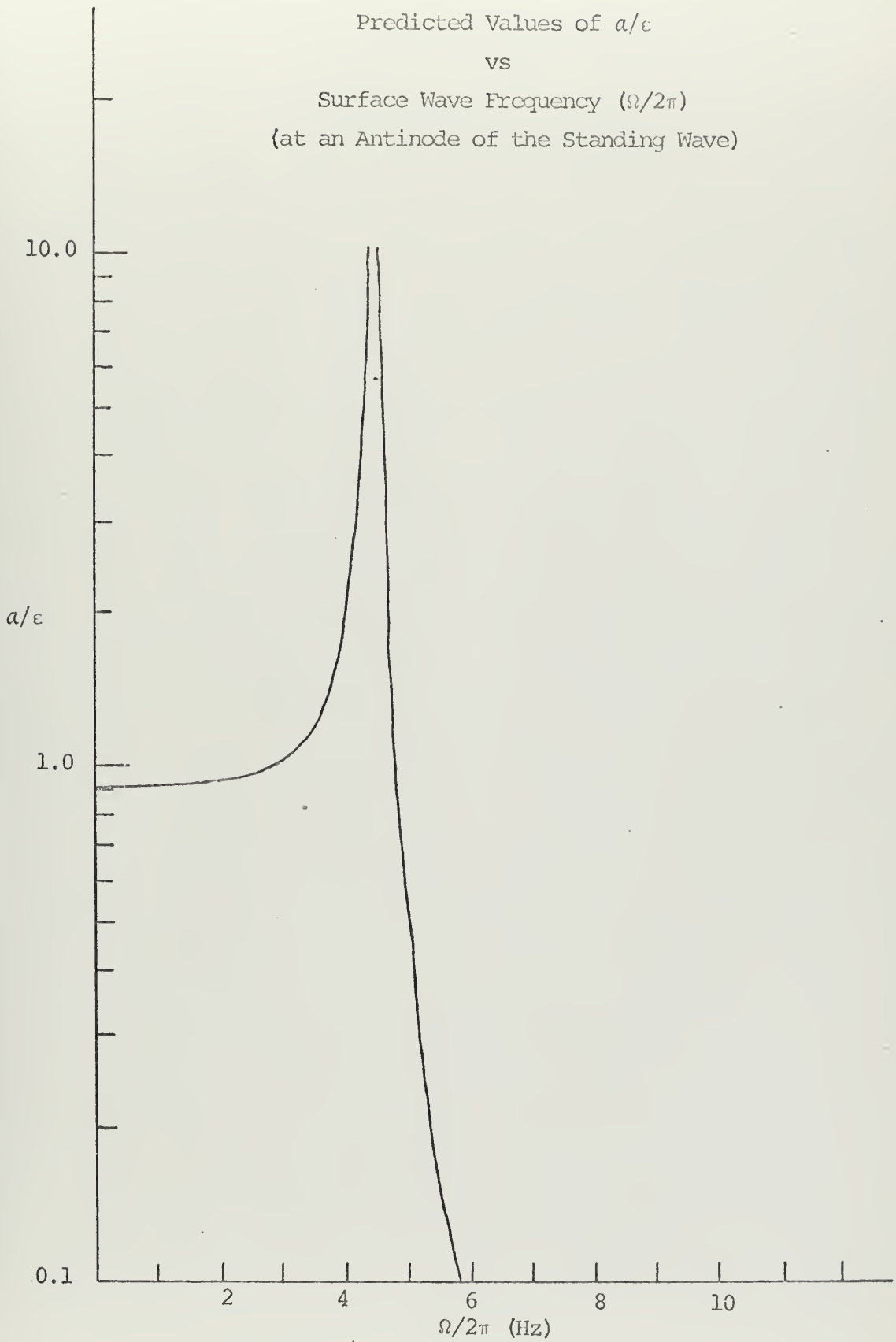


Figure 2



Predicted Values of  $a/\epsilon$   
vs  
Surface Wave Frequency ( $\Omega/2\pi$ )  
(at a Node of the Standing Wave)

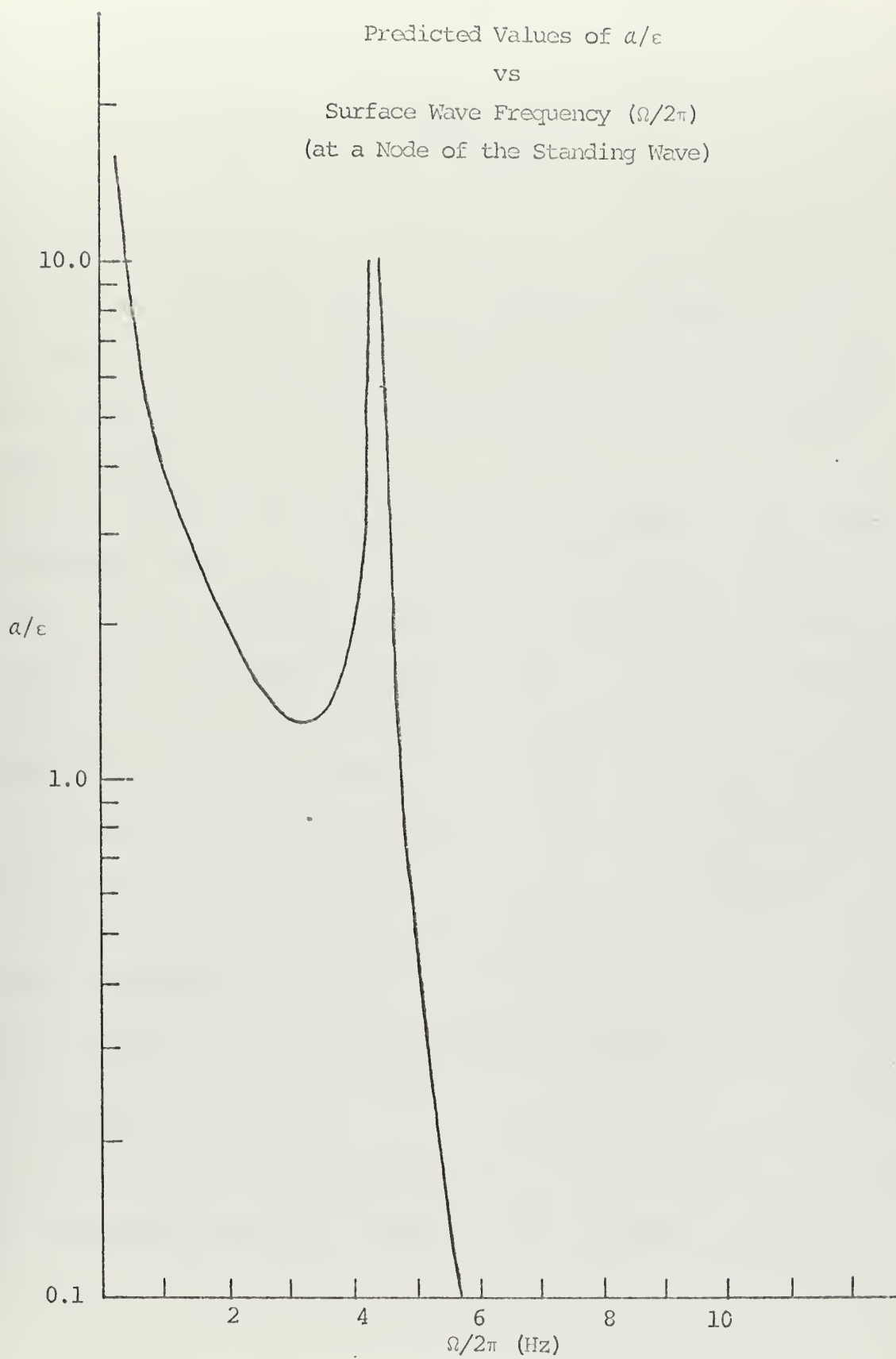


Figure 3



On the other hand, at a node where  $k_1 x = \pi/2$  and for  $x = \ell_z/2$ , Eq. 2.12 becomes

$$a/\epsilon = \pi/4 \left| \frac{1}{\cos \mu \frac{\ell_z}{2}} - \frac{1}{\cos \mu \frac{2\ell_z}{2}} \right| \quad (2.14)$$

$$\text{and } \Phi = a \cos \omega t \cos k_2 y \cos(\Omega t + \psi). \quad (2.15)$$

Plots of  $a/\epsilon$  as functions of surface wave frequency for the two cases are presented in Figures 2 and 3. These functions display strong dependence on both acoustic and surface-wave propagation constants.

Notice that when  $\gamma = k_1$ , there is a "resonance" effect. The perturbation analysis may fail in this region, because  $\epsilon\phi_2$  may no longer be small compared to  $\phi_1$ . If bulk absorption of the medium is included,  $a/\epsilon$  no longer becomes infinite, but is still extremely large. For  $\gamma < k_1$ , the surface fluctuation tends to behave as a rather uniform change in depth of the cavity, and the amplitude fluctuation behaves as if the standing wave in the  $z$  direction were squeezed and then released. When  $\gamma > k_1$ , the amplitude fluctuation appears to react to the average fluctuation over many surface wavelengths, and approaches the steady-state solution  $\phi_1$ .

The relation between frequency and propagation constant is

$$\omega/k = c \quad (2.16)$$

for the acoustic wave and

$$\Omega/\gamma = v \quad (2.17)$$

for the surface wave where  $c$  and  $v$  are the respective phase speeds.



The surface-wave speed  $V$  is dispersive and the governing equation [8] is

$$V^2 = (g/\gamma + \frac{T_s \gamma}{\rho}) \tanh(\gamma l_z) \quad (2.18)$$

where  $g$  = acceleration resulting from gravity  $980 \text{ cm/sec}^2$

$\rho$  = density

$T_s$  = surface tension  $75 \text{ dynes/cm}^2$ .

Because of this,  $\gamma$  varies with  $\Omega/2\pi$  as shown in Figure 4.

In this experiment,  $\Omega$  is of magnitude  $10 \text{ rad/sec}$  and

$\omega \approx 90 \times 10^5 \text{ rad/sec}$ . Therefore,  $\gamma \sim k_1$  and  $\omega/\Omega \sim 90 \times 10^4$ . For this reason, the perturbation term in Eq. 2.13 appears as a low-frequency modulation of the acoustic signal, and  $a$  becomes a measure of the modulation amplitude. The great inequality in acoustic and surface wave speeds means that the surface can be treated as effectively "frozen" with respect to the acoustic processes.

The solution for  $\epsilon\phi_2^*$  in terms of  $\epsilon F(x,y,t)$  obeys superposition. Thus, if the surface were a spectrum of  $\Omega$ , the solution for  $\epsilon\phi_2$  would be superposition of the solutions for each component of  $\Omega$  according to Eq. 2.13.

In particular, for a narrow band of surface wavelengths, a localized disturbance on the surface leads to a local disturbance in the acoustic standing wave. Scrimger [5] observed that the fluctuations in the acoustic signal were strongest when generated surface waves were in the vicinity of the source or receiver. This localization of effect is assumed to apply in this experiment.



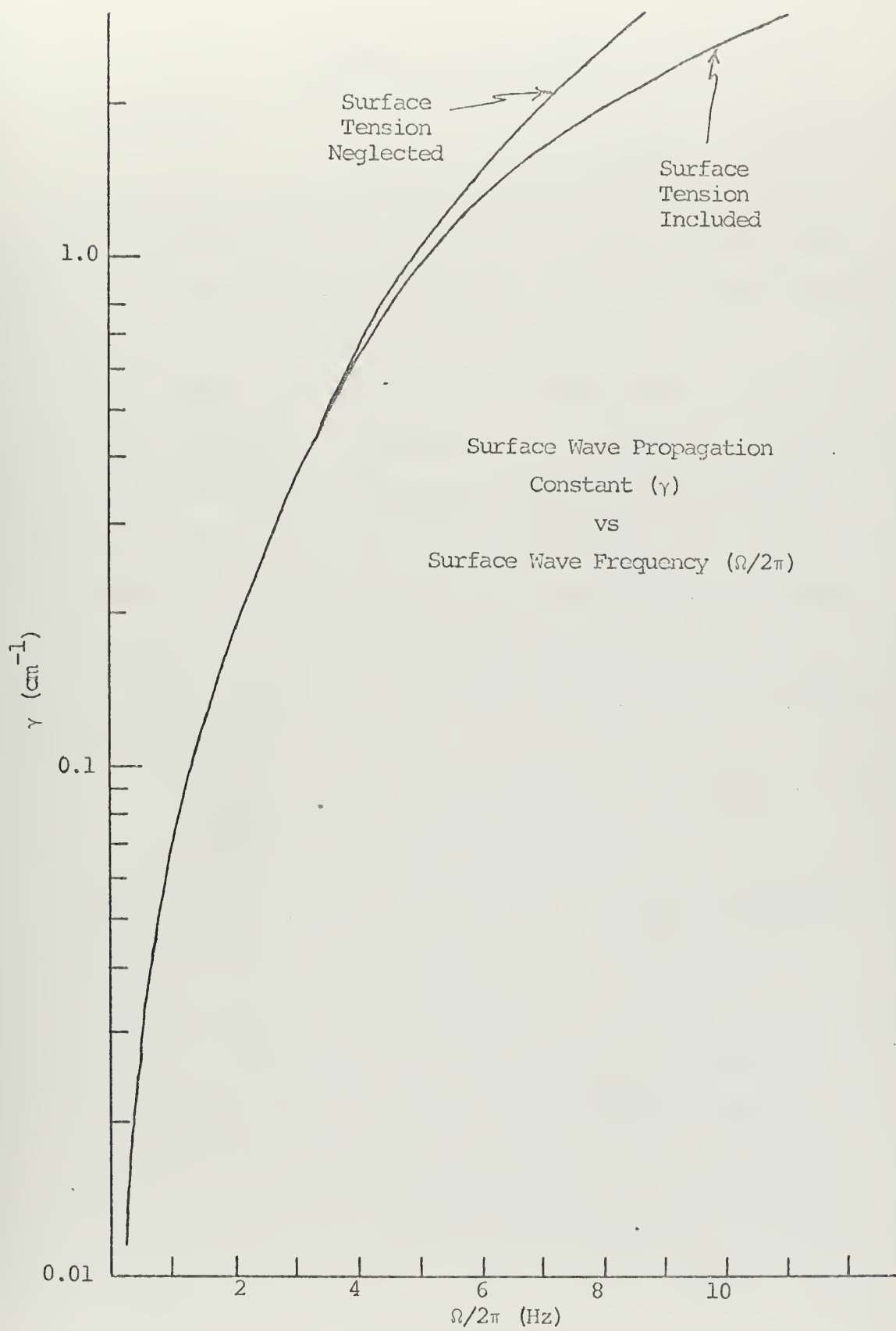


Figure 4



### III. PROCEDURE AND ANALYSIS

#### A. THE EXPERIMENT

The goal of the experimental investigation was to achieve guided-mode propagation in a shallow water layer, disturb one surface with a measurable perturbation, and observe the resultant fluctuations in the acoustic pressure amplitude.

In the original concept of the experiment design, one end of a shallow tank with pressure-release boundaries was to be lined with sound absorbing material and a fan manifold for generating wind-driven "seas" was to be suspended over the other end. By using a highly directive source aimed into the anechoic area, a cylindrically spreading acoustic traveling wave, which excited the  $n_3 = 1$  family of modes, could be transmitted. This approach would have yielded the following advantages:

1. Elimination of effects resulting from reflections at the vertical sides of the tank.
2. A simple traveling wave configuration corresponding to propagation in the lowest mode of a cylindrically diverging wave.
3. Limitation of the ensonified surface to a region excluding that in the vicinity of the fans used to generate the surface fluctuations.

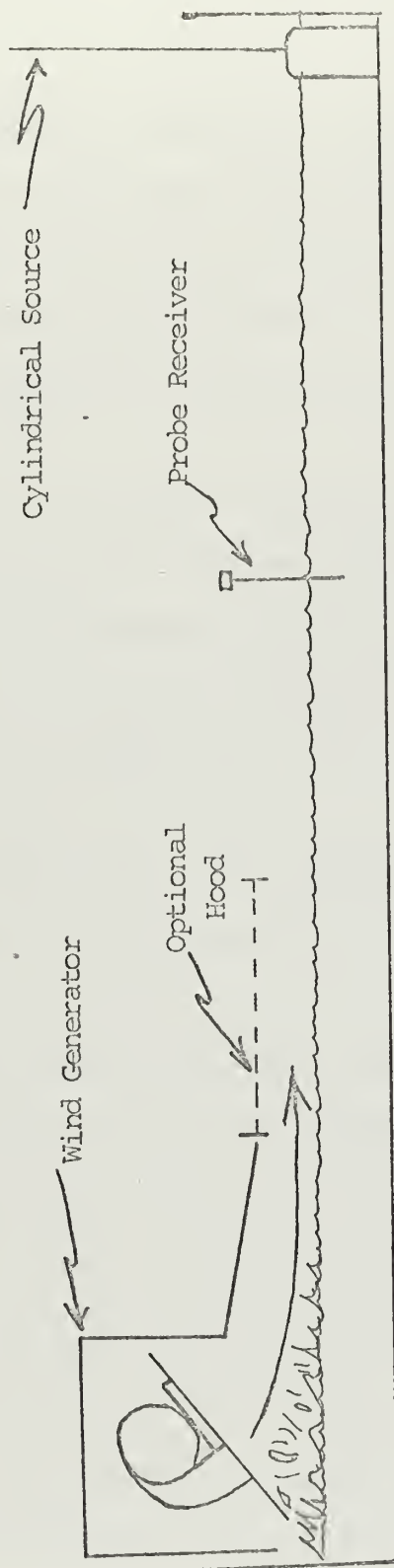


It was impossible within the available time to construct a sufficiently anechoic tank in the frequency range of interest, so the method had to be abandoned. The alternative was to place a cylindrically symmetrical source in a corner of the tank and excite a normal mode of the bounded cavity. This method raised the immediate problem of the effects of the highly agitated surface directly under the fans. (See Figure 5.) (The surface under the fans was beaten about by the air stream generated by the fans directed at the water surface.)

The theory suggests (as discussed earlier) that it may be possible to assume that for small  $\epsilon F(x,y,t)$ , the cause of the acoustic amplitude fluctuation observed at the receiver is the surface in the immediate vicinity. Therefore, acoustic noise from the turbulence under the fans could be treated as a "distant source" combining incoherently with the effects generated by the local surface.

Excitation of the  $n_3 = 1$  family of modes was a primary consideration; the complications coming from modal interference were to be avoided. To ensure efficient excitation of these modes, a source active over a height greater than the depth of the cavity was chosen. This insured that, as the depth at the source changed with passing waves, source strength exciting the desired normal mode would be smoothly changing and closely related to the local surface. Since sea state at the source was essentially uncorrelated with that at the receiver in the cavity, and since the propagation speed of the acoustic energy far exceeded the





Schematic Cross Section of Experiment Set Up

Figure 5



speed of the surface waves, the effect was the equivalent of simply changing the amplitude of  $\phi_1$ . Equation 2.13 must then be modified to

$$\Phi = [1 + a_s \cos(\Omega t + \psi_s)] \cos \omega t \cos k_2 y [1 + a \cos(\Omega t + \psi)] \quad (3.1)$$

where  $a$  is the amplitude fluctuation at the receiver resulting from the changing conditions at the source, and  $\psi_s$  and  $\psi$  are assumed incoherent. For small  $a_s$  and  $a$  this becomes

$$\Phi \doteq \cos \omega t \cos k_2 y [1 + \sqrt{a_s^2 + a^2} \cos(\Omega t + \psi')]. \quad (3.2)$$

In a similar manner, the "distant acoustic sources" contributed by the strong surface-fluctuations in the neighborhood of the fans combine incoherently at the receiver with the acoustic amplitude fluctuations resulting from the local surface state. Inclusion of these "distant sources" modifies Eq. 3.2 to

$$\Phi \doteq \cos \omega t \cos k_2 y [1 + \sqrt{a^2 + a_s^2 + a_f^2} \cos(\Omega t + \psi'')] \quad (3.3)$$

where  $a_f$  = the amplitude fluctuation at the receiver resulting from the distant sources.

Thus, the sound-amplitude fluctuations resulting from the local surface state must be obtained from the measured fluctuations and

$$a_a = \sqrt{a^2 + a_f^2 + a_s^2} \quad (3.4)$$

and results in

$$a = \sqrt{a_a^2 - a_f^2 - a_s^2}. \quad (3.5)$$

Extraction of the desired values of  $a$  and then  $\epsilon$  from the experimental data is accomplished by the following steps:



1. Measure the statistics of the sea surface to obtain  $\epsilon$  as a function of surface wave frequency ( $\Omega$ );
2. Measure the acoustic amplitude fluctuations ( $a_a$ ) at the various positions in the tank;
3. Determine the values of  $a_s$ , and  $a_f$  as functions of surface wave frequency;
4. Compute  $a$  by Eq. 3.5 and divide it by  $\epsilon$  at each frequency of interest.

## B. DESCRIPTION

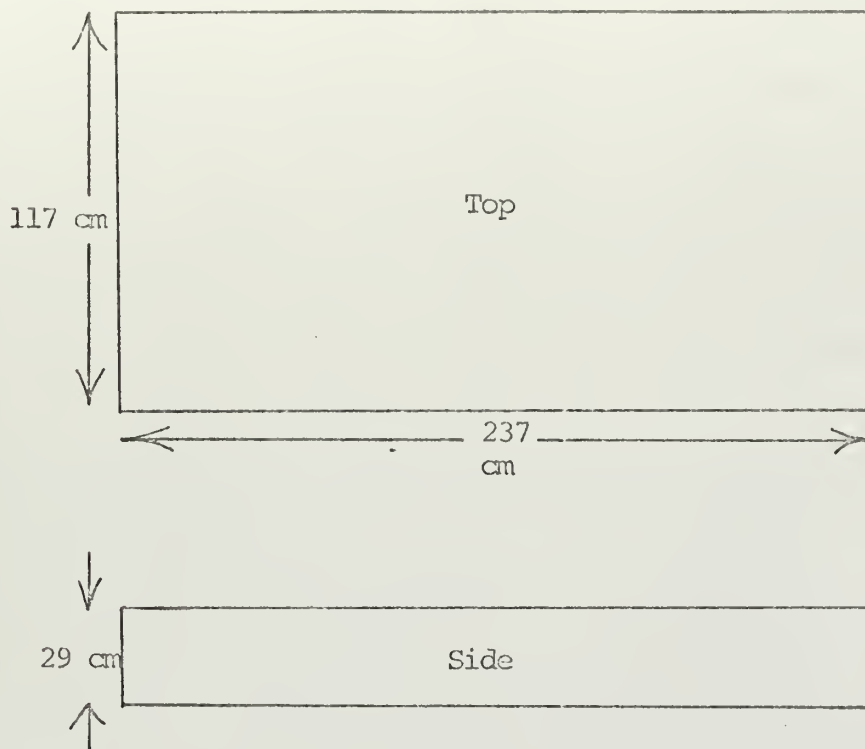
The experiment was conducted in a shallow water tank whose dimensions are shown in Figure 6. The tank was constructed of 3/4 inch marine plywood set on 2 inch x 6 inch supports to prevent sagging. Water depth could be maintained uniform to within  $\pm 1$  mm throughout the tank.

A 3/8 inch neoprene<sup>1</sup> envelope, set in the tank and held in place by hydrostatic pressure, served as a pressure release boundary. The reflection coefficient of the neoprene was measured by terminating an acoustic waveguide with a sample of the material and conducting reflectivity tests. Values of around 0.95 for the reflection coefficient were obtained. The boundary condition in the tank was confirmed by probing the sound field and verifying that the pressure extrapolated to zero, within experimental accuracy, as the probe was brought near a boundary.

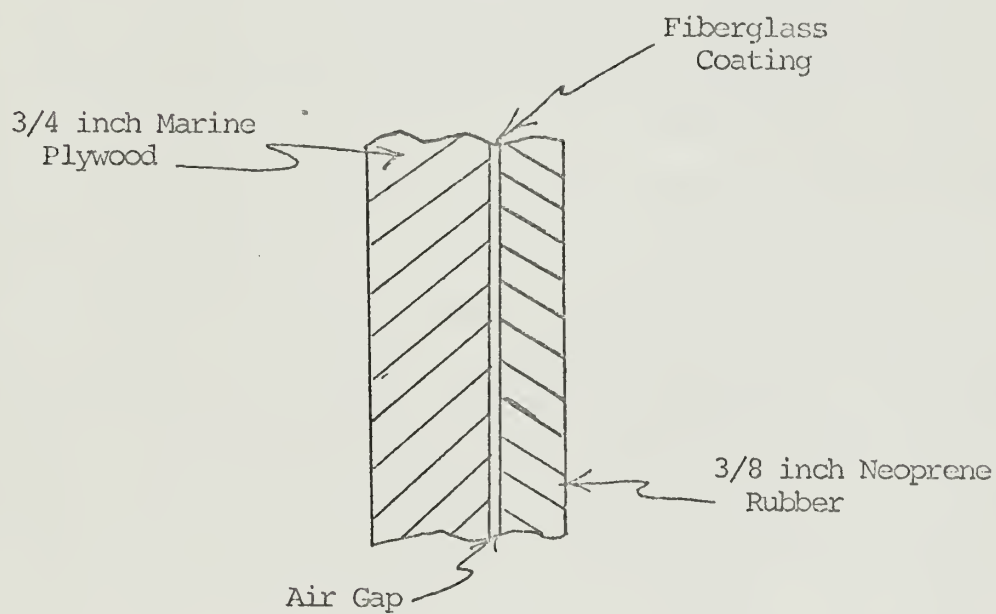
---

<sup>1</sup>The neoprene rubber used is foam containing nitrogen and is the type used in suits for SCUBA divers. It is commonly known as "wetsuit" material.





Inside Dimensions



Tank Construction

Figure 6

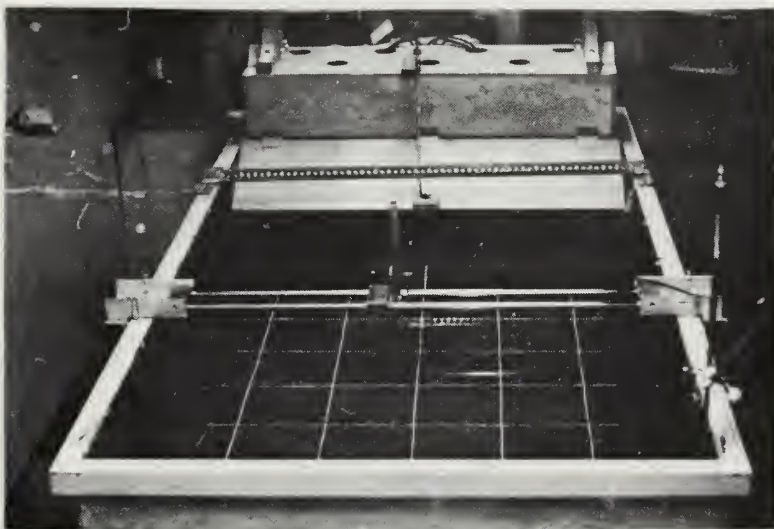


A "wind-driven sea" was created by five equally-spaced squirrel-cage blowers in a manifold at one end of the tank. The manifold was suspended over the tank to prevent coupling of mechanical vibration to the tank (Figure 7). Each fan had a rated capacity of  $100 \text{ ft}^3/\text{min}$ . Various seas could be generated by varying the angle of attack of the fan output, the height of the manifold, orifice size, and the number of fans (Figure 8). Greater sea heights were obtained by placing a 16 inch wide cover over the water adjacent to the fan manifold in order to hold the wind down on the surface (Figure 5).

The wave heights were measured by an immersion probe whose impedance varied inversely with its submerged length. This wave probe consisted of two submerged electrodes with a 10 kHz current flowing between them. The passing surface waves modulated the current amplitude by changing the amount of submerged electrode. This produced a current whose envelope amplitude was a measure of the passing wave height. After amplification, the information was retrieved by filtering and detecting the amplitude envelope of the current.

Wave probe construction is shown in Figure 9. The positive electrode was made from 20-mil nikomel wire soldered to 1/16 inch brazing rod. The ground return was 1/16 inch brazing rod coated with neoprene paint over its vertical length. The last 4 cm were kept bare and bent at a right angle to the vertical. The electrodes were soldered to standard banana plugs and held in place by a connector (Pomona Electronics Connector model #1681).

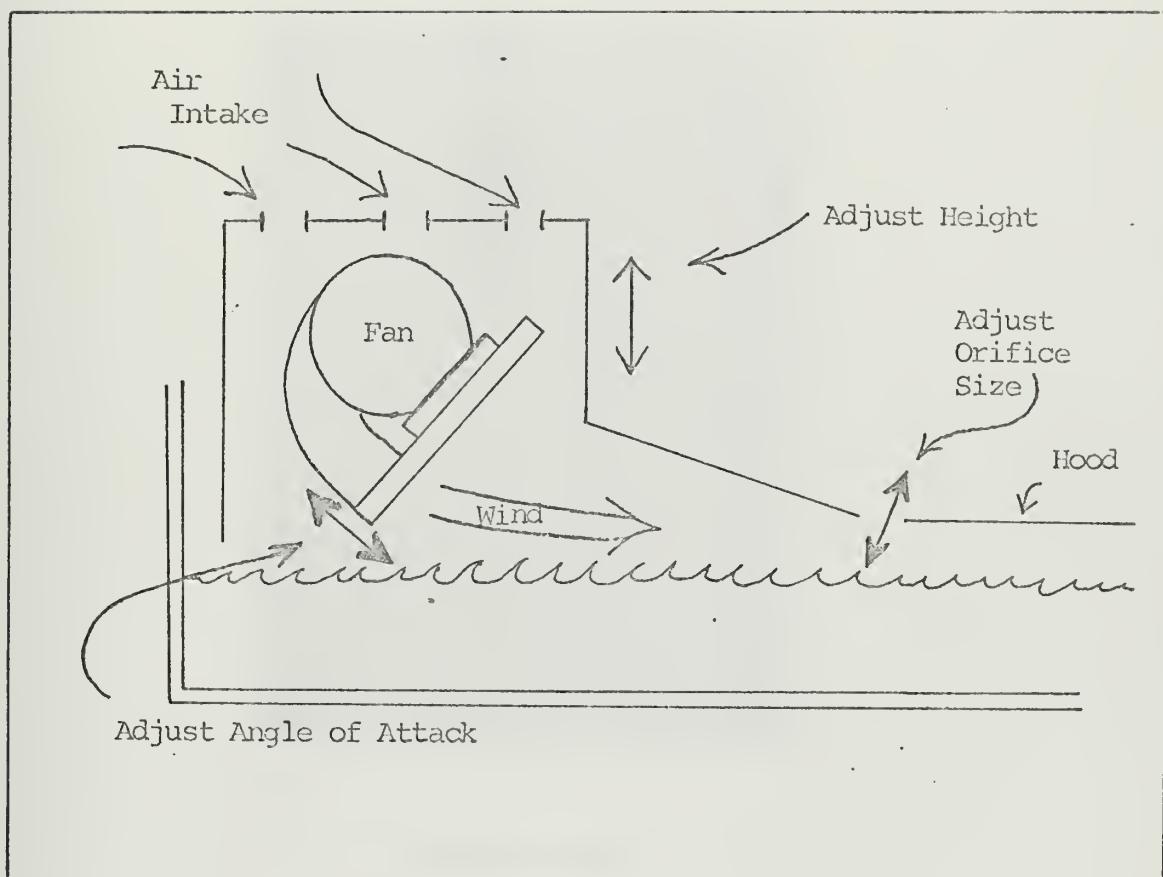




Tank with Fan Manifold in Place

Figure 7

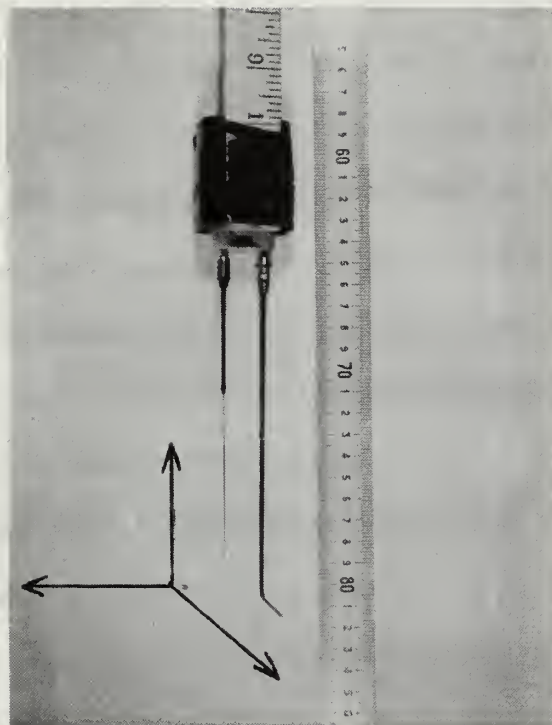




Wind Generator (Fan Manifold) Operation

Figure 8





The Wave Probe  
Figure 9

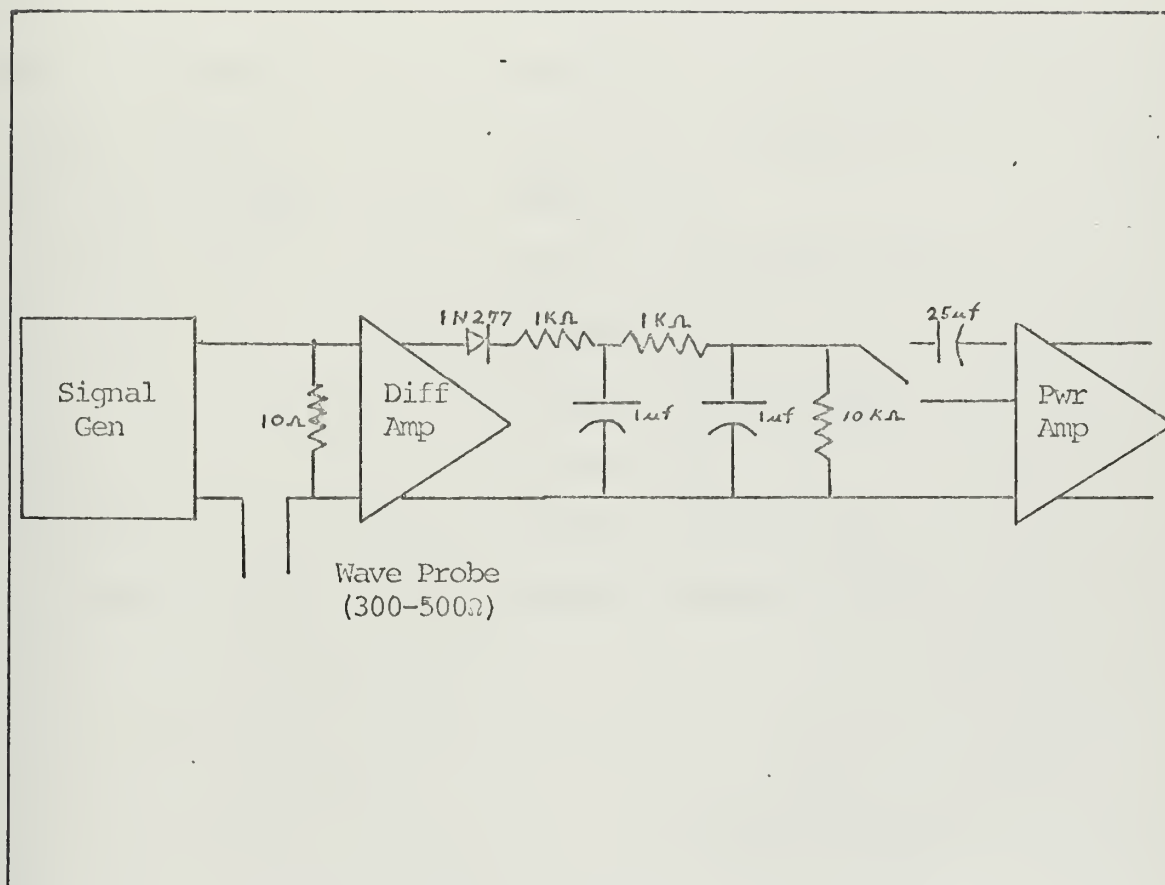


The detection and filtering network (see Figure 10) consisted of a switching diode for half-wave rectification, two successive low-pass filters with cutoff frequencies of 159.5 Hz, and a blocking capacitor. The 25  $\mu$ F capacitor with the 50 k $\Omega$  input impedance of the following amplifier formed a high-pass filter with 0.126 Hz cutoff. The network was tested with an unmodulated 10 kHz tone which ideally would generate zero DC and AC outputs. The AC signal which leaked through the filter amounted to no more than 0.05 percent of the input amplitude, and the DC appearing at the output was equally insignificant.

The relation between submerged length of the wave probe and current flow was non-linear, the effect being more or less severe depending on the positioning of the probe with respect to the cavity boundaries. (If the electrodes were placed too near the bottom, the non-linearity was aggravated.) By bending the ground return and adjusting the probe current level, an adequately linear operating range was established for the wave heights expected.

Due to the bottom effects mentioned, a static probe calibration method was used: With the probe in place, the water level in the tank was varied and the output voltage measured on the probe side of the blocking capacitor. (It was verified by use of an AN/URM-26 AM modulation test set that there was no measurable loss in amplitude across the blocking capacitor in the frequency range of interest.)





The Wave Height Measuring System

Figure 10



## LIST OF EQUIPMENT

Signal Generator	WAVETEK Multipurpose VCG Model 116
Diff. Amp.	HEWLETT PACKARD 2470A
Power Amp.	HEWLETT PACKARD 467A
Amp. 1	TEKTRONICS Model 1121
Amp. 2	HEWLETT PACKARD 460A
Signal Correlator	PRINCETON APPLIED RESEARCH Model 100A
FM Tape Recorder	PRECISION INSTRUMENT 6200
Audio Tape Recorder	AMPEX PR-10
0.1 Octave Filter	GENERAL RADIO Model 1564A
XY Plotter	MOSELEY 7035B
CRO	HEWLETT PACKARD 120B
Filter	ALLISON Model 2C
Voltmeter	HEWLETT PACKARD 427A
True RMS Voltmeter	HEWLETT PACKARD 3400A



The system for processing wave information is shown in Figure 11. The wave information, contained in the envelope of the wave probe signal, was first amplified; this information was then recorded on an FM tape recorder and simultaneously sent to a signal correlator. The output of the correlator was graphically recorded on the XY plotter.

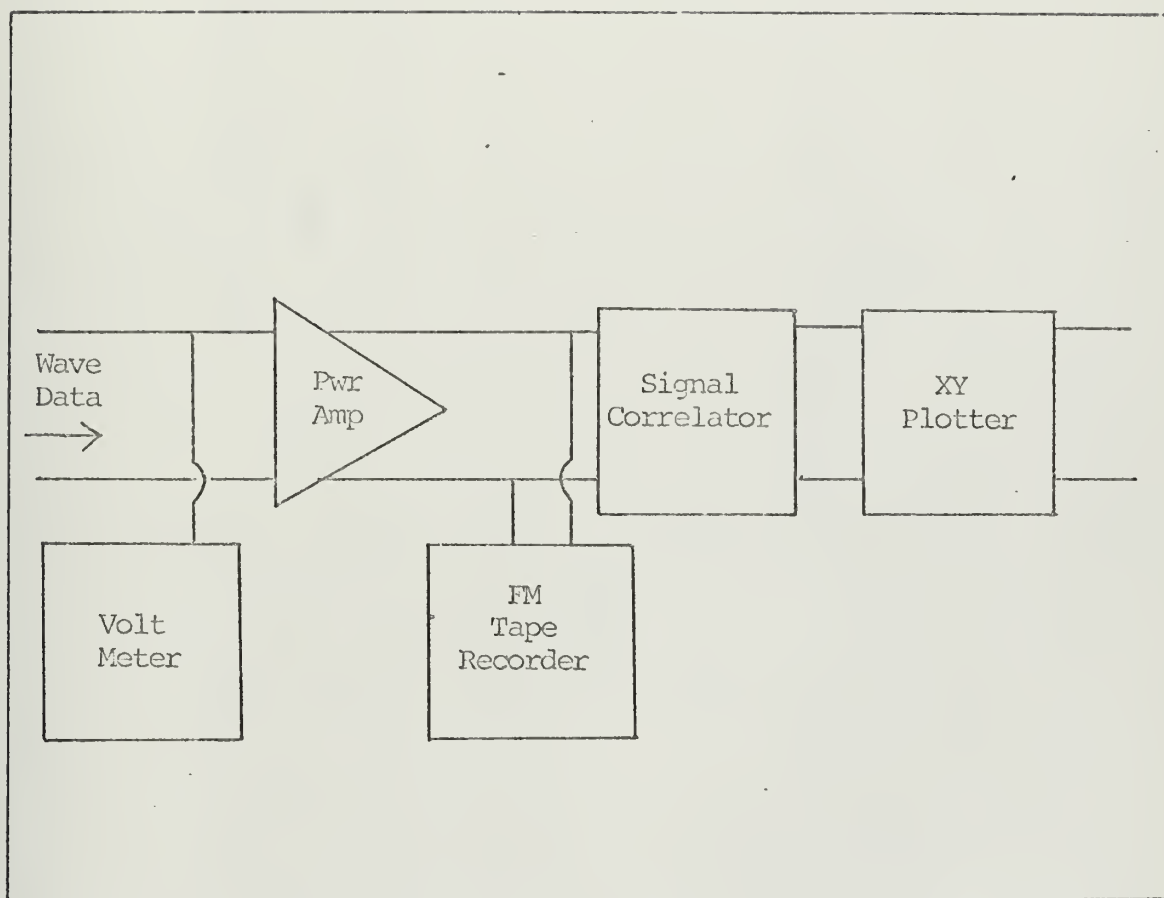
The sound source used was a  $\text{BaTiO}_3$  cylinder, 4.5 cm in diameter and 10.5 cm tall. The receiver was a 1/8 inch  $\text{BaTiO}_3$  probe. The sound processing system is shown in Figure 12. The received signal was pre-amplified in a low-noise 40 db amplifier, bandpass filtered at carrier  $\pm 2.5$  kHz and then amplifier further. The amplitude modulation of the acoustic signal was analyzed in like manner with the same detector network used in the wave probe system. This information was then recorded in the same manner as the wave height data.

The wave and acoustic amplitude fluctuation data were analyzed for frequency content. The system used is shown in Figure 13. The original tapes, recorded in the systems previously described, were replayed 100 times faster and recorded on tape loops with a standard audio recorder. The tape loops were then replayed through a 0.1 octave filter as shown.

### C. PROCEDURE

The experiment was conducted in water of 8.8 cm depth. A strong normal mode was found at 14.1 kHz, a frequency well below cutoff of the  $n_3 = 2$  family of modes. The sound field was probed

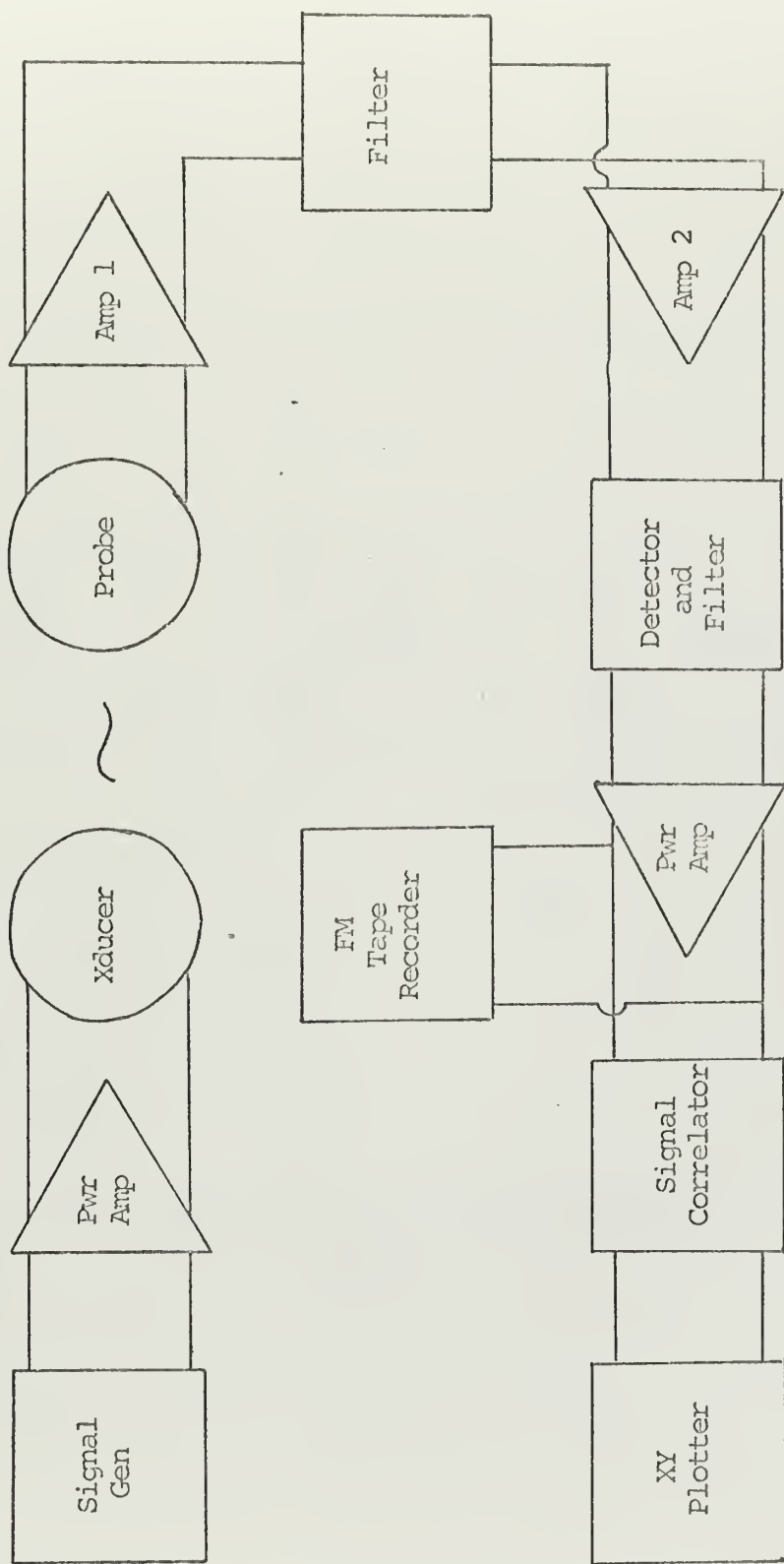




Wave Data Processing System

Figure 11

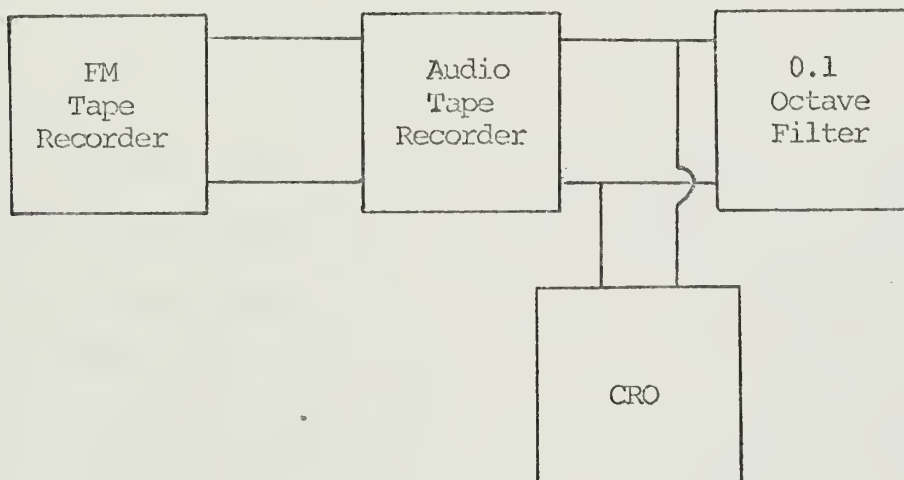




The Acoustic System

Figure 12





The Analog Frequency Analysis System

Figure 13



in order to identify the modes model pressures other than zero were found in the tank, indicating excitation of more than one mode or more likely imperfections in the boundaries. The criterion for a strong mode was taken to be the average standing wave ratio, which in this case was approximately 60.

The mode was identified by measuring the lengths of the standing waves and estimating the wave numbers. The mode with  $n_1 = 28$ ,  $n_2 = 9$ ,  $n_3 = 1$  appeared to be excited. This mode has a calculated frequency of 13.6 kHz (4.25 percent less than the observed frequency). The vertical sound profile verified that the  $n_3 = 1$  family of modes was being excited (Figure 14) as assumed in Section II.

Once the desired mode was excited and identified, three receiver stations were selected at strong antinodes of the horizontal wave pattern (Figure 15). The procedure now described was followed at each receiver position.

The acoustic probe was set at a depth of 4.4 cm in still water, and the sound carrier amplitude measured. The surface was then disturbed with a preselected wind condition. The following observations were then made of the envelope of the modulated sound carrier:

1. A 500 second record was made of the mean square amplitude of the modulation from the output of the correlator on the XY plotter.



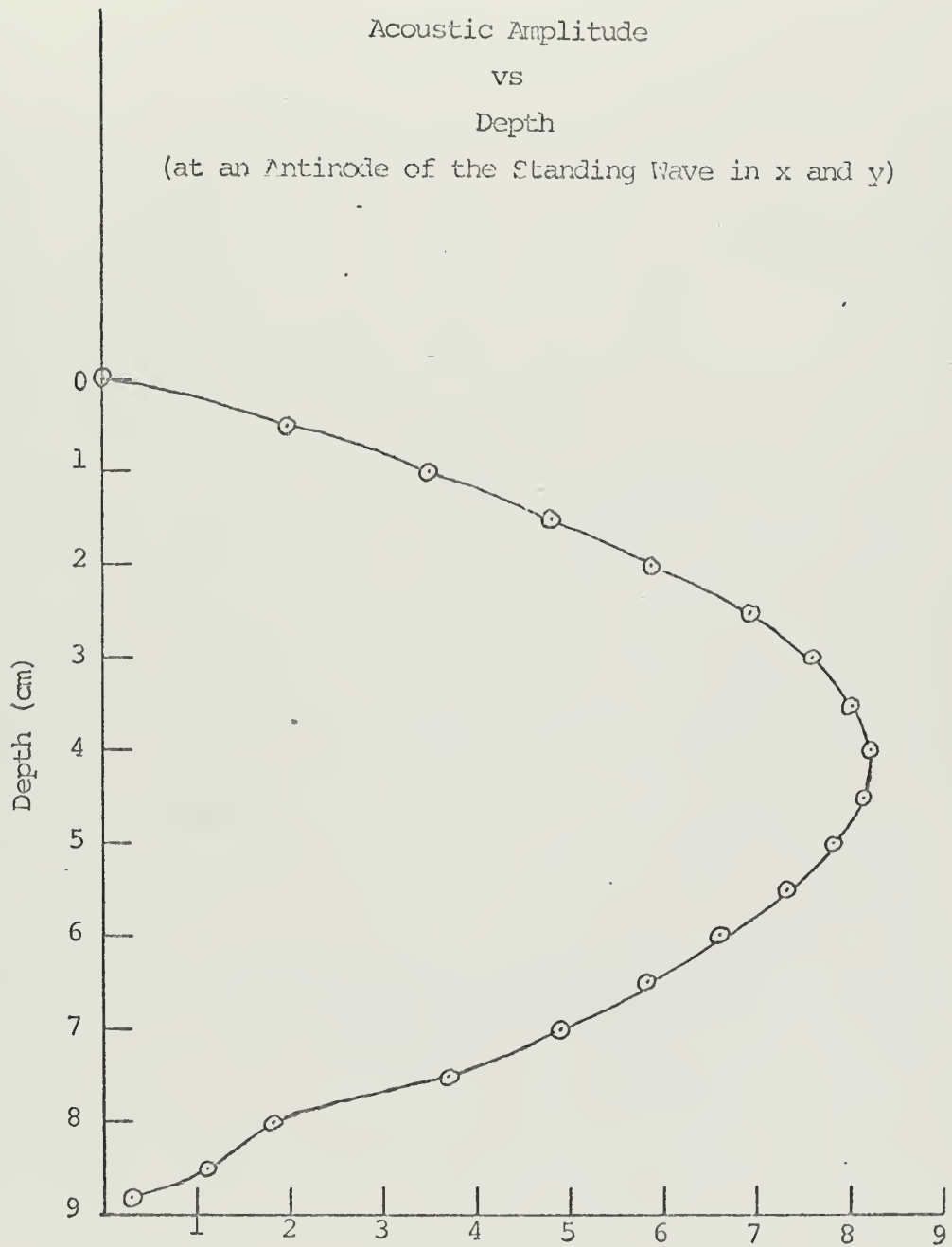
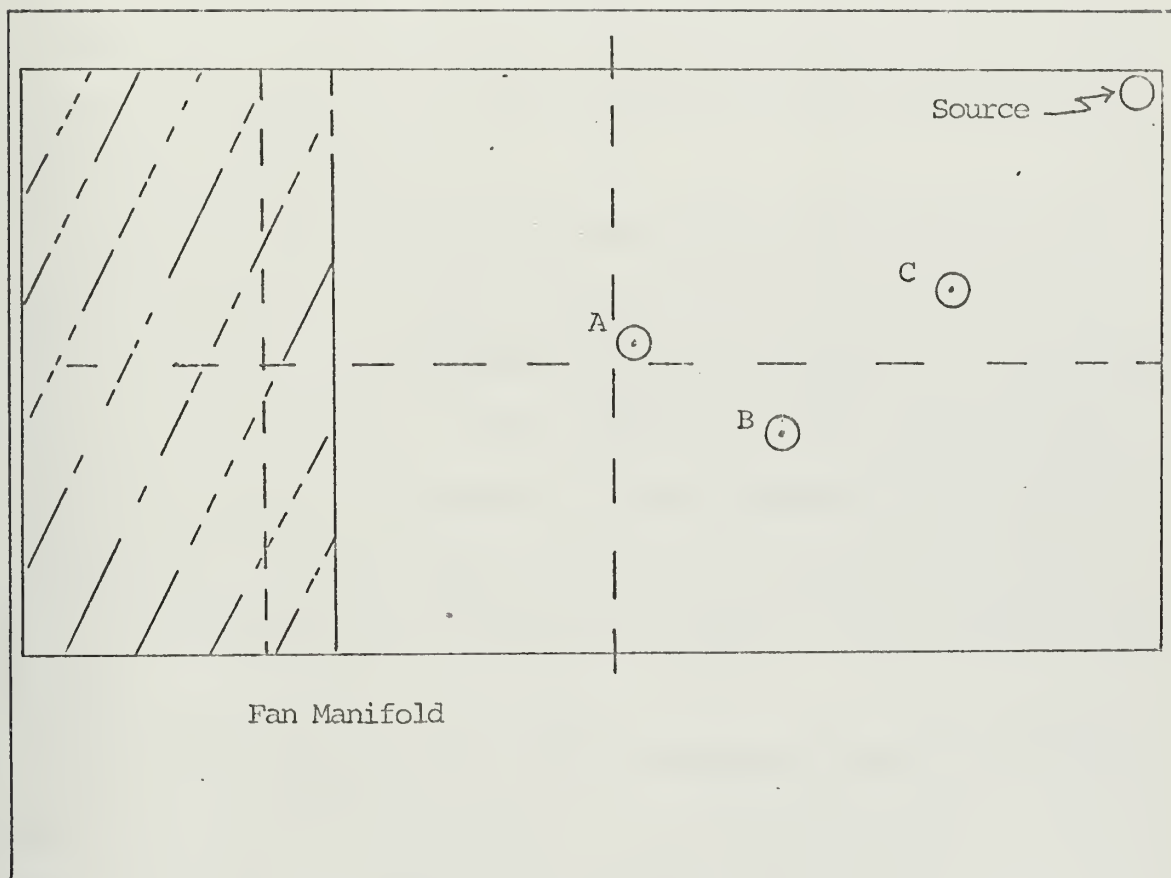


Figure 14





Selected Receiver Positions  
Figure 15



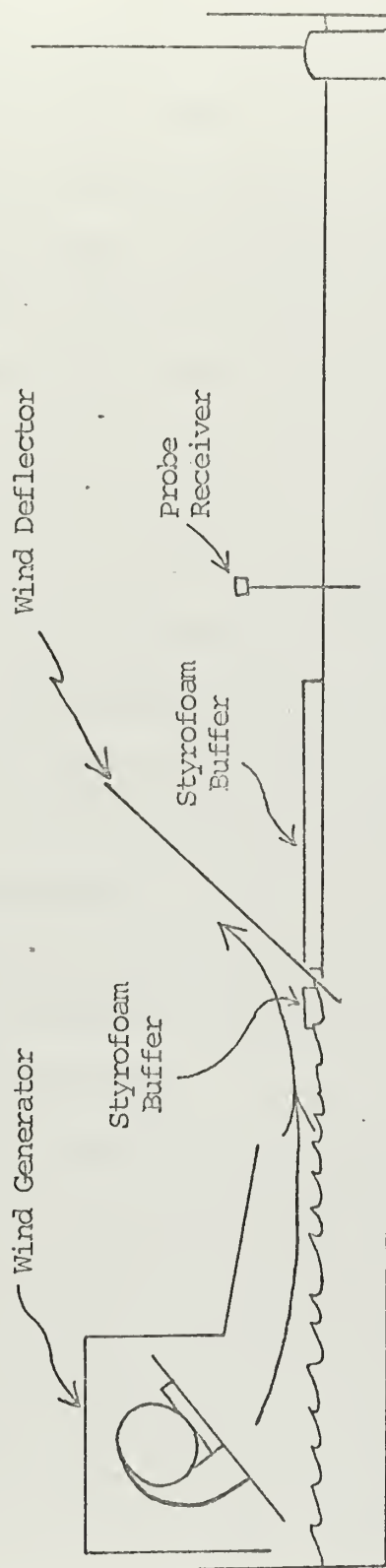
2. A 20 minute FM tape recording was made of the acoustic modulation.
3. The autocorrelation function was computed at two different times by the correlator and recorded by the XY plotter.

The wind generator was then stopped and the surface allowed to calm. The carrier amplitude was again measured to verify that the amplitude of the standing wave had not changed. The acoustic data for six different sea states at each receiver position were obtained in this fashion.

The area directly under the fans of the wind generator was intensely agitated relative to the rest of the sea surface. In order to isolate this contribution to the modulation of the signal, the tank was modified as shown in Figure 16. The reverse flap lifted the wind off the surface, and the styrofoam prevented the propagation of surface waves. Since the styrofoam was pressure-release, its presence had a negligible effect on the standing wave pattern.

With the probe in position at a designated receiver station and the wind machine operating at a specified setting, the amplitude of the acoustic modulation was measured through a 0.1 octave filter and average modulation amplitude as a function of frequency was recorded. These data were recorded at positions "B" and "C" only; position "A" was obstructed by the styrofoam buffer.





Tank Modification for Isolation  
of Acoustic Amplitude Fluctuations due to Fans

Figure 16



Once all sound data had been collected, the statistics of the sea surface were measured. A calibration of the wave probe was always conducted before a data run. With the probe in place, the tank was filled with water to a depth of 10 cm. The water was then slowly siphoned out and the DC output of the wave probe was recorded as a function of depth. A calibration factor was determined from this curve. Probe performance did not vary with position in the tank except very near the walls.

A static calibration of the wave probe is considered valid; however, a dynamic check was performed by simultaneously measuring the height of a passing wave visually and comparing it with the output of the probe. The passing waves were measured on a metric scale, printed on heavy photographic paper and taped to the side of the probe holder. (The thin paper ruler caused negligible disturbance in the passing surface waves.) The output of the probe was observed on an oscilloscope.

Once the probe was calibrated, it was placed at each receiver position and measurements were made of the amplitudes of the waves generated on the surface.

The statistics of the surface at the position of the sound source were also required. These data could not be taken with the wave probe, so the behavior of the various frequency components of the sea were measured as they propagated down the tank and a projection of the behavior of each water surface at the position of the acoustic source was made. This estimate was checked visually and appeared to be valid within experimental error.



Analog frequency analysis of the FM tape recording was made by a tape loop method. The 20 minute tape records were played back 100 times faster and recorded on 7 second tape loops with an audio-magnetic tape recorder.

These loops were then played through a 0.1 octave filter with slow integration time. Average amplitude as a function of frequency was recorded. The tape loop output was also played through a true RMS voltmeter to measure overall RMS amplitude for comparison with the mean square amplitude prediction of the correlator.

#### D. ANALYSIS

The RMS wave height was computed by having the correlator set to compute the autocorrelation function. In this mode the correlator output is

$$c(\tau) = \frac{1}{T} \int_0^T v_{in}^2(t) dt \quad (3.6)$$

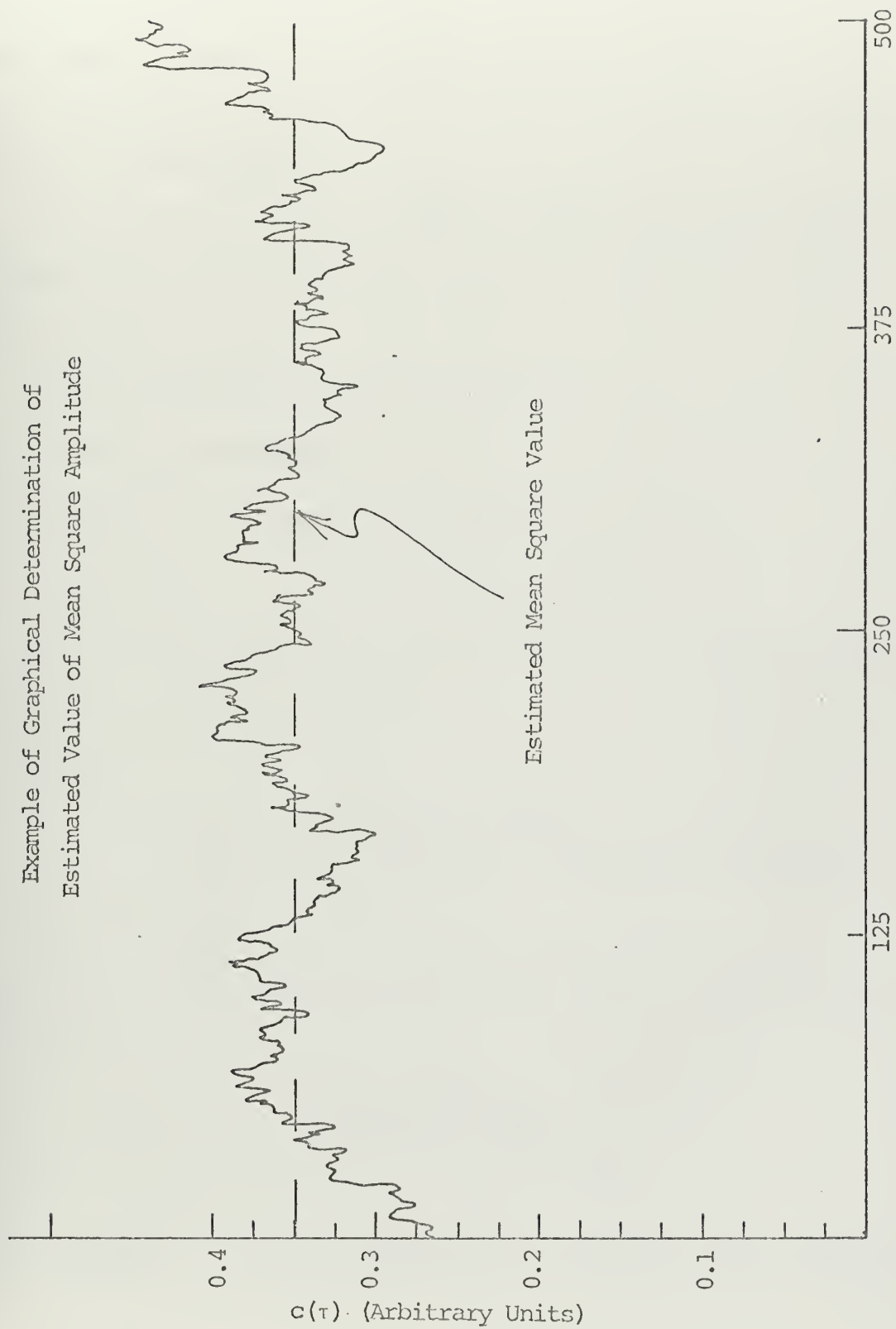
which equals the mean square value of the input when T approaches infinity. The correlator integration time is only 20 seconds, so a good estimate of the mean square value was obtained by taking the average of a 500 second graphical record of the correlator output (Figure 17). The various equipment amplification factors were divided out and the square root taken.

The RMS value of the envelope amplitude of the wave probe signal was computed in the same manner.

The average surface wave and acoustic amplitudes as functions of frequency were obtained as previously discussed. As the data



Example of Graphical Determination of  
Estimated Value of Mean Square Amplitude



Time (sec)  
Figure 17



were recorded, a 100 Hz tone was recorded on another channel of the tape. The system amplification was checked by monitoring this test signal at various stages in the frequency analysis. This check also gave assurance that the data were not being distorted during the processing.

In order that  $\alpha$  and  $\epsilon$  be computed, the gains of the equipment through which the data was sent had to be divided out of the observations.

Refer to Figures 11 and 12 and let

$GAIN_{AMP}$  = the amplifier gain

$GAIN_{TAPE\ 1}$  = the FM tape recorder

$GAIN_{TAPE\ 2}$  = the audio tape recorder.

The average amplitude measured through the 0.1 octave filter is converted to the average value of  $\epsilon$  for each frequency interval as follows:

$$WAVE\ PROBE\ OUTPUT = \frac{FILTER\ OUTPUT}{GAIN_{AMP} \cdot GAIN_{TAPE\ 1} \cdot GAIN_{TAPE\ 2}}$$

The wave probe output can be expressed in centimeters of wave height by dividing by the DC calibration factor determined before each run:

$$WAVE\ HEIGHT = \frac{PROBE\ OUTPUT}{CALIBRATION\ FACTOR}$$

The normalized fluctuation  $\epsilon$  then becomes

$$\epsilon = \frac{WAVE\ HEIGHT}{DEPTH} = \left( \frac{FILTER\ OUTPUT}{GAIN_{AMP} \cdot GAIN_{TAPE\ 1} \cdot GAIN_{TAPE\ 2}} \right) \left( \frac{1}{CAL\ FACTOR} \right) \left( \frac{1}{DEPTH} \right) \quad (3.7)$$



$$= \frac{\text{FILTER OUTPUT}}{\text{GAIN}_{\text{AMP}} \cdot \text{CAL FACTOR} \cdot \text{DEPTH}} \left( \frac{1}{\text{GAIN}_{\text{TAPE 1}} \text{GAIN}_{\text{TAPE 2}}} \right).$$

The sound amplitude fluctuation  $a$  at each frequency of interest is

$$a = \frac{\text{ENVELOPE AMPLITUDE AT THAT FREQUENCY}}{\text{CARRIER AMPLITUDE}}.$$

Since the sound information was processed with the same system as the surface data,  $a$  was computed as follows:

$$a = \frac{\text{AVERAGE AMPLITUDE}}{(\text{GAIN}_{\text{AMP}})(\text{CARR}_{\text{AMP}})} \frac{1}{(\text{GAIN}_{\text{TAPE 1}})(\text{GAIN}_{\text{TAPE 2}})} \quad (3.8)$$

Notice that no calibration factor is required in the calculation of  $a$ .

In the ratio  $a/\epsilon$ , the factor  $\frac{1}{\text{GAIN}_{\text{TAPE 1}} \text{GAIN}_{\text{TAPE 2}}}$  vanishes;

therefore, all data were treated in arbitrary units with this factor included.

The carrier amplitude by which the envelope amplitude was divided was an average of the amplitude measured before and after each run. If, however, the difference in these amplitudes was greater than 2 percent, the run was re-executed.

The presence of high frequency sound fluctuations, unpredicted by the theory, and the persistence of these fluctuations throughout the tank strongly suggested the fans as a source. The acoustic amplitude fluctuation due to the agitation under the fans was obtained for positions "B" and "C" and described above. For any given sea state, these data were very similar at the two



positions. Therefore, an average (fan noise) level for each sea state was assumed (Figure 18) for all the receiver stations.

The other factor to be accounted for was source modulation. The sea state at the source was predicted as previously described. The effect of the waves on the acoustic output of the source was determined by raising the source a given distance out of the water and measuring the reduction in sound amplitude at position "B". With a 10 percent reduction in the radiating surface, the sound amplitude at position "B" was reduced by 6 percent. This relation was found to be linear within the range of interest. Therefore, the amplitude modulation of the source was assumed to be

$$a_s = 0.6 \epsilon. \quad (3.9)$$

(This result was checked by shading the upper part of the transducer the same amount with 3/8 inch neoprene foam rubber and comparing the results, which agreed within experimental error.) The amplitude fluctuation due to the local surface effect was then computed with Eq. 3.5:

$$a = \sqrt{a_a^2 - a_s^2 - a_f^2}. \quad (3.5)$$

As a check on the validity of the data, several quantities were measured by two methods and the results compared. The tape loops, for instance, were played through the true RMS voltmeter in order to measure the RMS amplitude fluctuation and wave height. The results, adjusted for system gain, agreed to within 10 percent with the RMS values computed through the correlator.



Graphical Determination of the  
Fan Contribution to the Observed  
Acoustic Amplitude Fluctuation  
(Wind 4)

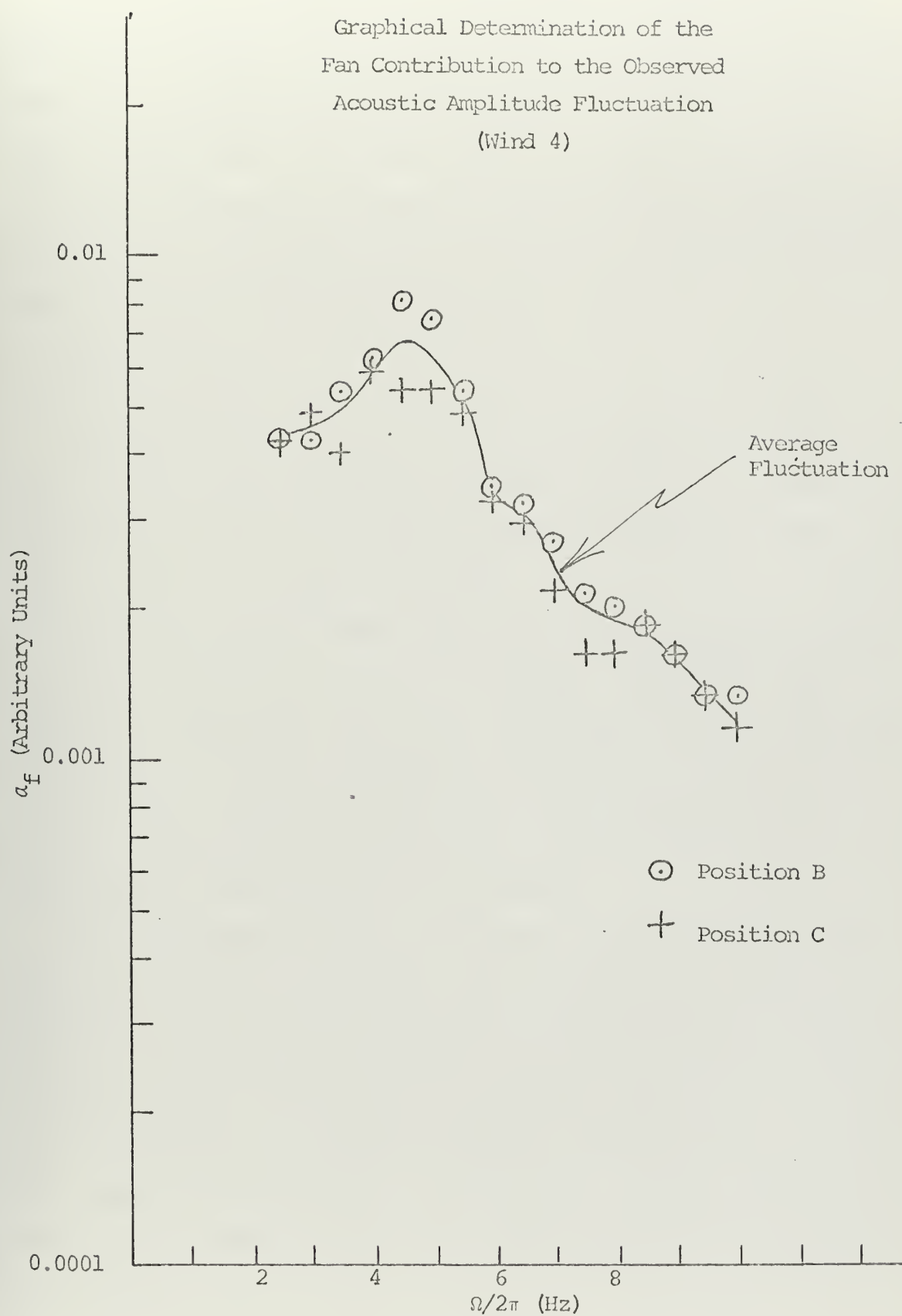


Figure 18



The frequency distribution of the modulation data was also determined from the autocorrelation function plotted during each data run. The cosine Fourier transform of the autocorrelation function  $c(\tau)$  equals the power spectral density. The transform of  $c(\tau)$  was computed by numerical integration of 100 points taken from the plots described above. The resulting spectra confirmed the distributions obtained from the tape loops.

#### E. ERROR ANALYSIS

The major cause of error in this experiment was the non-stationarity of the processes. The variation in mean square amplitude (see Figure 17) gives a qualitative measure of the degree of non-stationarity involved.

Measuring equipment with sufficiently long integration times to overcome this problem was not available. Therefore, long "effective" integration times were achieved by visual integration of the meter readings or graphical averaging as previously discussed. Study of Figure 17 suggests that an integration time of 500 seconds is sufficient for our purposes.

In the frequency analysis, 15 minutes of FM tape record was compressed onto a 7 second tape loop (see page 33). Visually averaging the meter reading on the 0.1 octave filter, provided an integration time in excess of 500 seconds. The estimated error in the value assigned to acoustic amplitude fluctuation ( $a_a$ ) or surface height fluctuation ( $\epsilon$ ) is  $\pm 10$  percent. (This estimate was determined by comparing the values estimated by two independent observers.)



The tape loop method was not used in obtaining the acoustic amplitude fluctuation due to the fans; in this case the filter was placed directly on the output of the filtering and detecting network (page 40). Averaging two sets of observations together at each wind setting, minimized the error in the fan contribution ( $a_f$ ) to an estimated 15 percent, so that the more elaborate tape loop analysis was not deemed necessary.

Recall that the acoustic amplitude fluctuation term  $a_s$  resulted from the source modulation, which was extracted from the  $\epsilon$  curves. The estimated error in  $\epsilon$  is  $\pm 10$  percent. Adding a  $\pm 5$  percent error for the graphical extrapolation yielding the surface at the source position, results in a total error in the source modulation term,  $a_s$ , of  $\pm 15$  percent.

The RMS amplitude values computed from the graphical output of the correlator are considered reliable. In order to test the validity of the average amplitudes obtained from the tape loops, RMS amplitudes computed in this manner were compared to those from the correlator. The values were consistently within 10 percent.

The error in  $a_a$ ,  $a_s$ ,  $a_f$  and  $\epsilon$  were assumed statistically independent at each receiver position. Therefore the error in the value of  $a/\epsilon$  at each frequency was computed using standard RMS error analysis.



#### IV. RESULTS AND CONCLUSIONS

The experimental results consist of eighteen sets of data: measurements were taken at three different receiver positions for six different winds. The six winds generated can be grouped in pairs: (1,2), (3,4) and (5,6). Each pair of winds was generated with the same settings of manifold height, angle of attack, and orifice size of the wind machine. The even-numbered winds were generated with five fans; the odd-numbered ones, with three. The receiver positions were previously shown in Figure 15.

The frequency distribution of the measured acoustic-amplitude fluctuation ( $a_a$ ), the fluctuation induced by the fans ( $a_f$ ), and the amplitude fluctuation due to source modulation ( $a_s$ ) are plotted for each wind setting at a given receiver position (see Appendix B).

These graphs reveal certain general features:

1. The frequency spectrum of the measured acoustic fluctuation ( $a_a$ ) closely resembles that of the local surface fluctuation ( $\epsilon$ ). In all cases each curve computed for  $a$  closely resembles the curve for the equivalent  $a_a$ .
2. At each receiver position, the frequency spectra for both "B" and "C" are similar for each wind pair. The stronger winds produce greater amplitudes as would be expected.
3. The curves of  $a_a$  are similar at all receiver positions for any given wind setting. The difference in values of  $a_a$  for positions "B" and "C" is very small.



4. The higher frequency components of  $\epsilon$  appear to die out as the surface waves progress down the tank. (See Figure 22.) The corresponding values of  $a_a$  fall off much more slowly.

5. In computing the values of the acoustic amplitude fluctuation resulting from the local surface

$$a = \sqrt{(a_a)^2 - (a_f)^2 - (a_s)^2}, \quad (3.5)$$

we see that  $a_f$  becomes significant at the higher frequencies while  $a_s$  is significant at the lower frequencies.

6. There appears to be evidence of generation in  $a_a$  of second harmonics of frequencies in the region corresponding to resonance.

The computed values of  $a/\epsilon$  (using Eq. 2.13) are plotted as functions of surface-wave frequency for each wind condition at each receiver position. (Appendix C.) The results are summarized in Figure 19 where the curves are collected on single graphs according to wind condition.

In the region below the predicted "resonance" the measured values of  $a/\epsilon$  compared favorably with the theoretical prediction. Very little evidence for a resonance effect exists in the results of any run. Above the predicted resonance the observed values of  $a/\epsilon$  are consistently greater than the theoretical values. The absence of any peaking of  $a/\epsilon$  in the vicinity of resonance cannot be explained.



Several important factors could be contributing to the high-frequency behavior mentioned. Recall that the term  $a_f$  is extremely important in determining the acoustic amplitude fluctuation  $a$  in this region. It is suspected that perhaps the entire observed acoustic amplitude fluctuation  $a_a$  above 6 Hz can be attributed to the surface agitation under the fans.

In the design of the fan isolation experiment, it was assumed that the surface agitation directly under the fans was responsible for the additional amplitude fluctuation at the receiver. The styrofoam buffer was therefore placed under the orifice flap. This, however, suppressed large surface waves generated in this region. It is conceivable that these waves contribute to the "distant sources", but this possibility was not investigated at the time. Recall also that analyses of the fan-generated noise were not conducted with the more accurate tape-loop method because of time and equipment limitations. Therefore, the  $a_f$  term may be larger than recorded. This hypothesis would have been investigated further if time had been available.

Since accuracy in  $a_f$  becomes critical when computing the ratio  $a/\epsilon$  for the higher frequencies, increasingly anomalous behavior in  $a_a$  in this frequency range at distances further removed from the fans cannot be considered as unequivocally contradicting the theory.

The discrepancy between experiment and theory for values of  $a/\epsilon$  at the higher frequencies could also be attributed to violations of the assumptions in the theory. For instance,



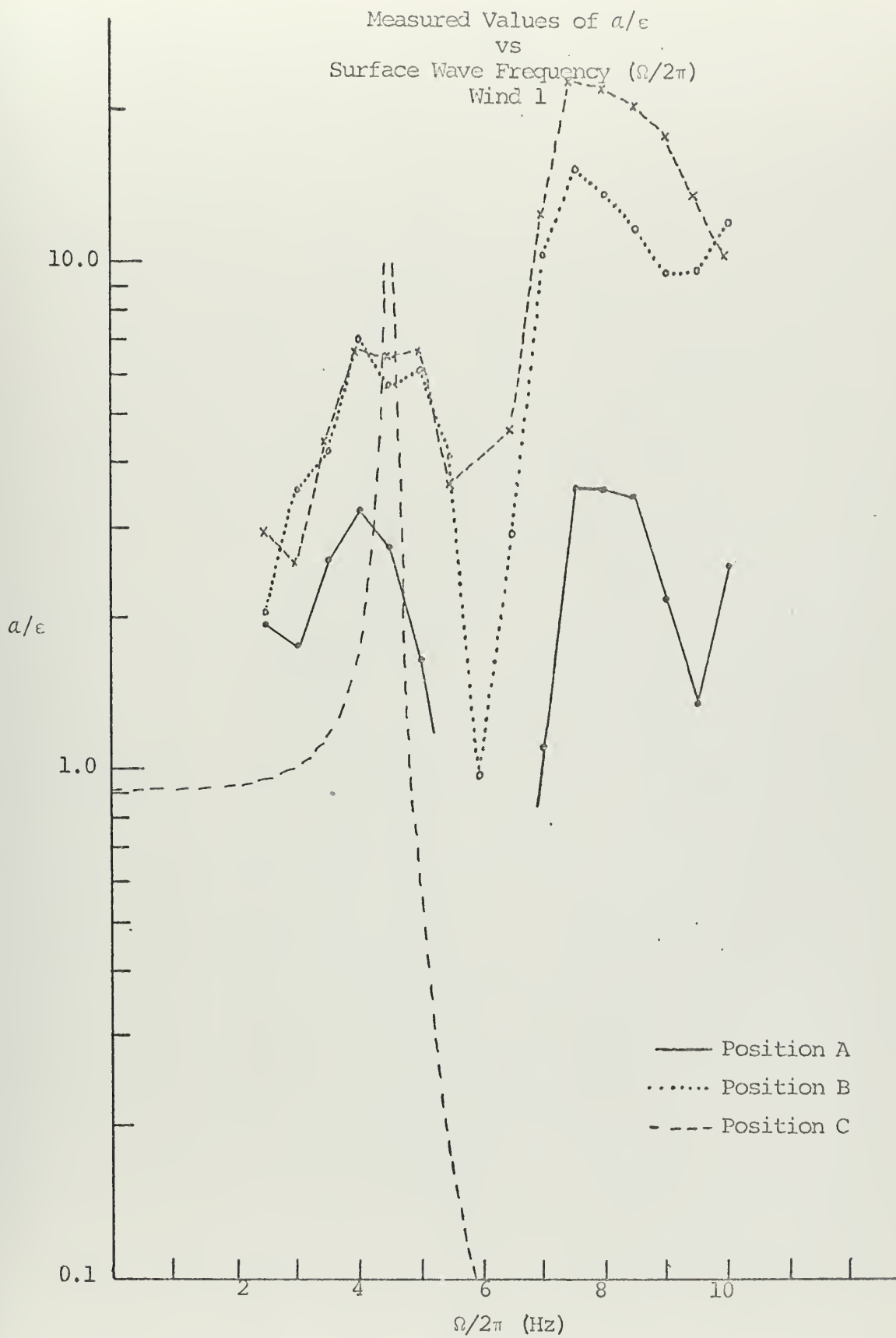


Figure 19a



Wind 2

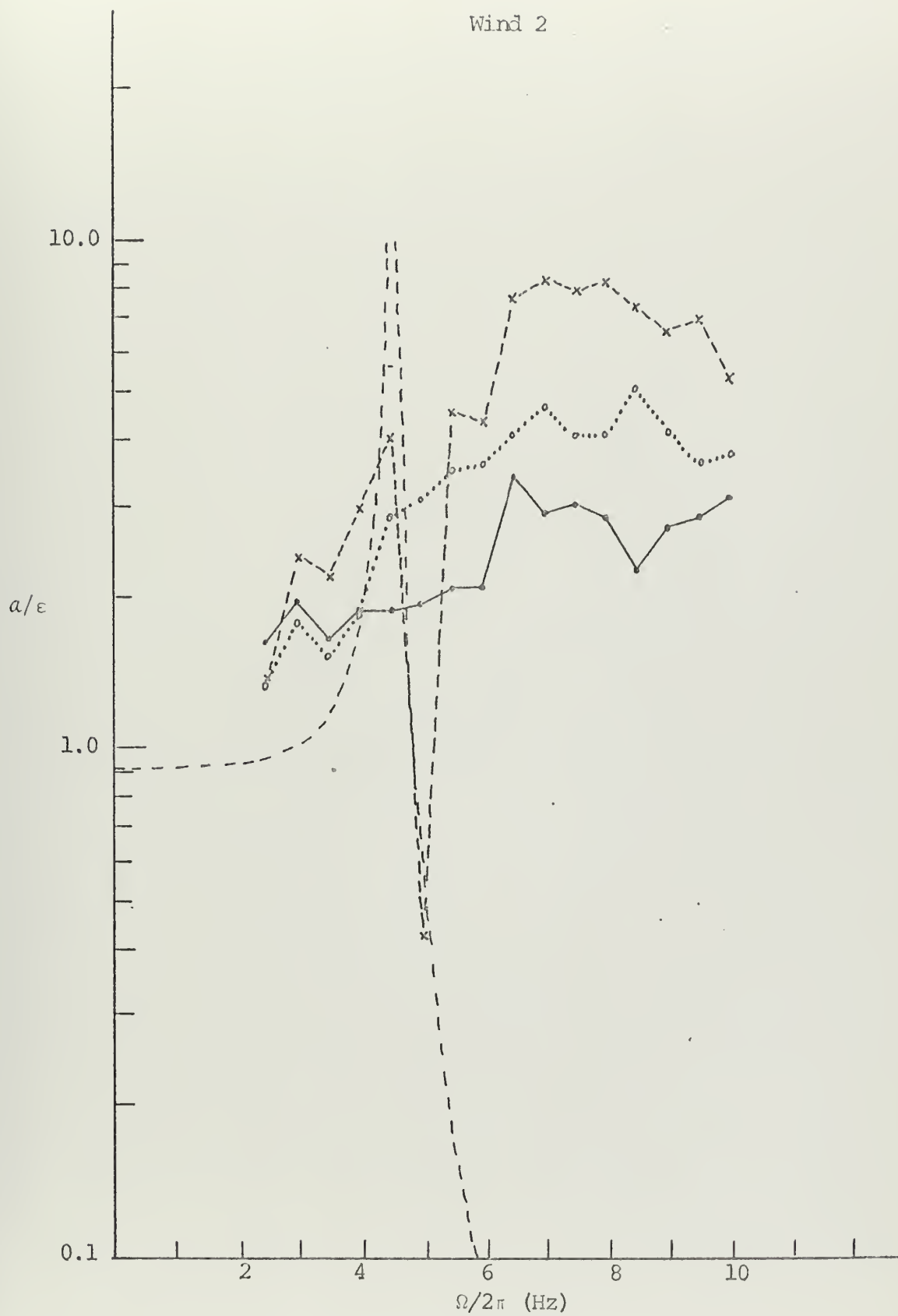


Figure 19b



Wind 3

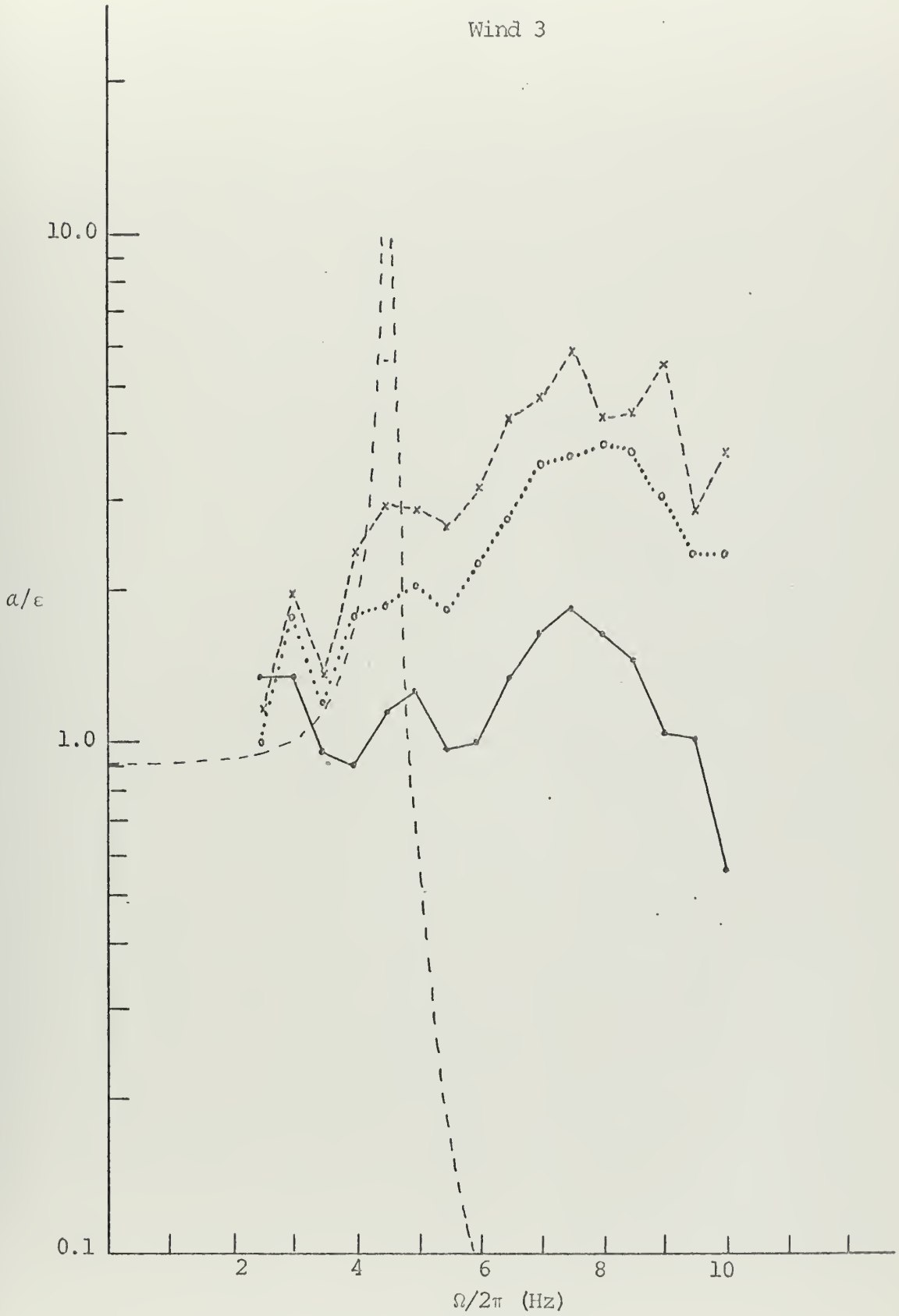


Figure 19c



Wind 4

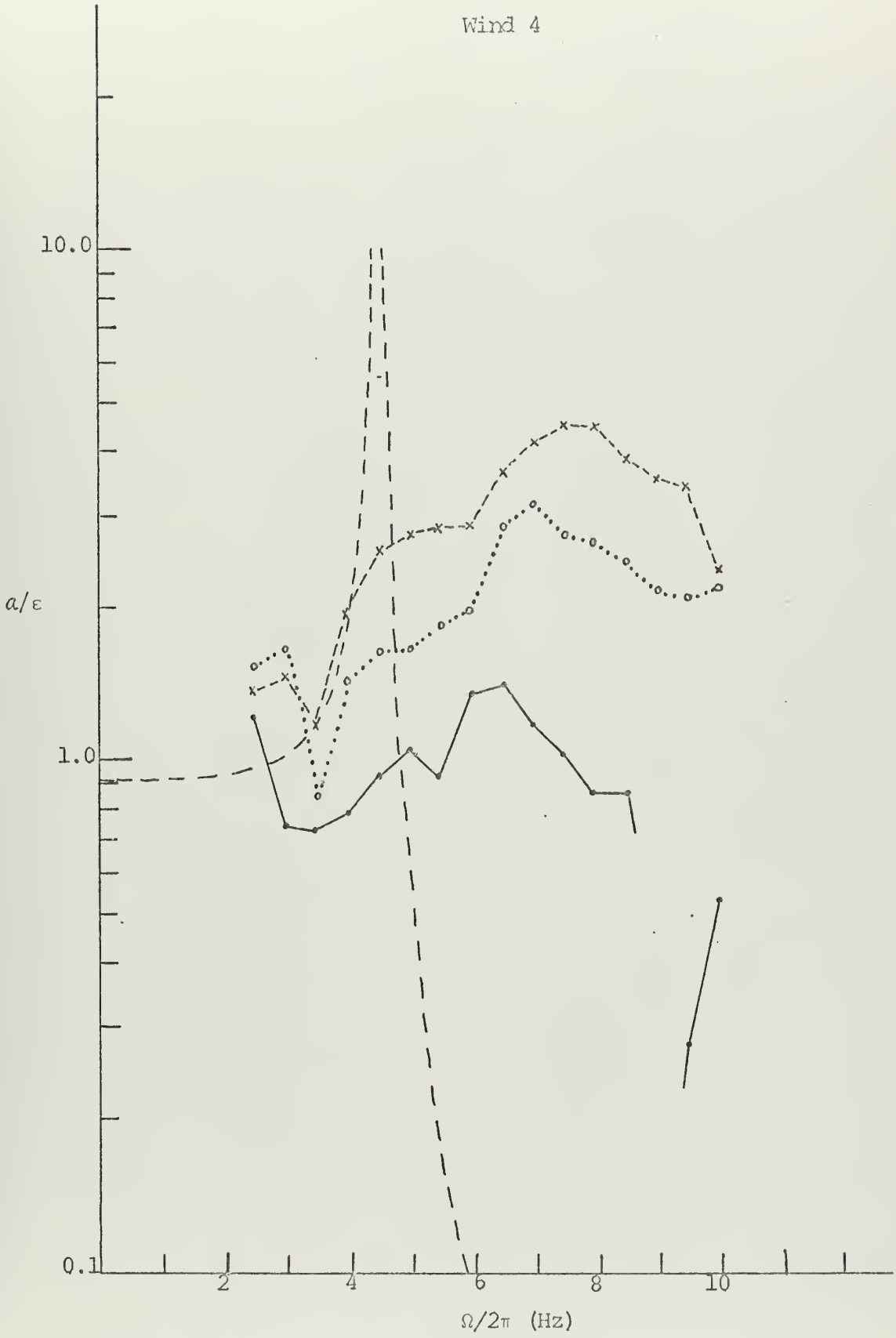


Figure 19d



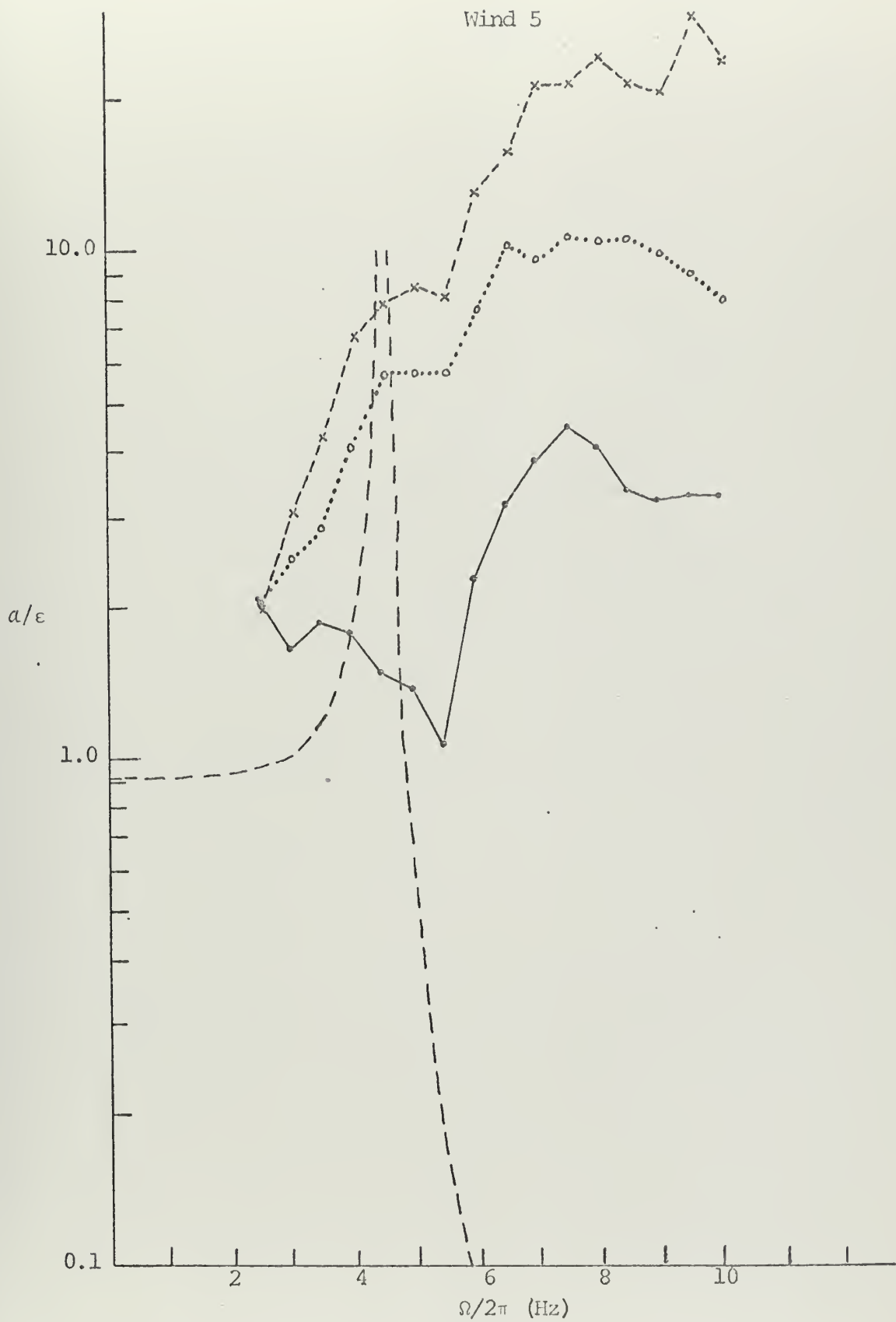


Figure 19e



Wind 6

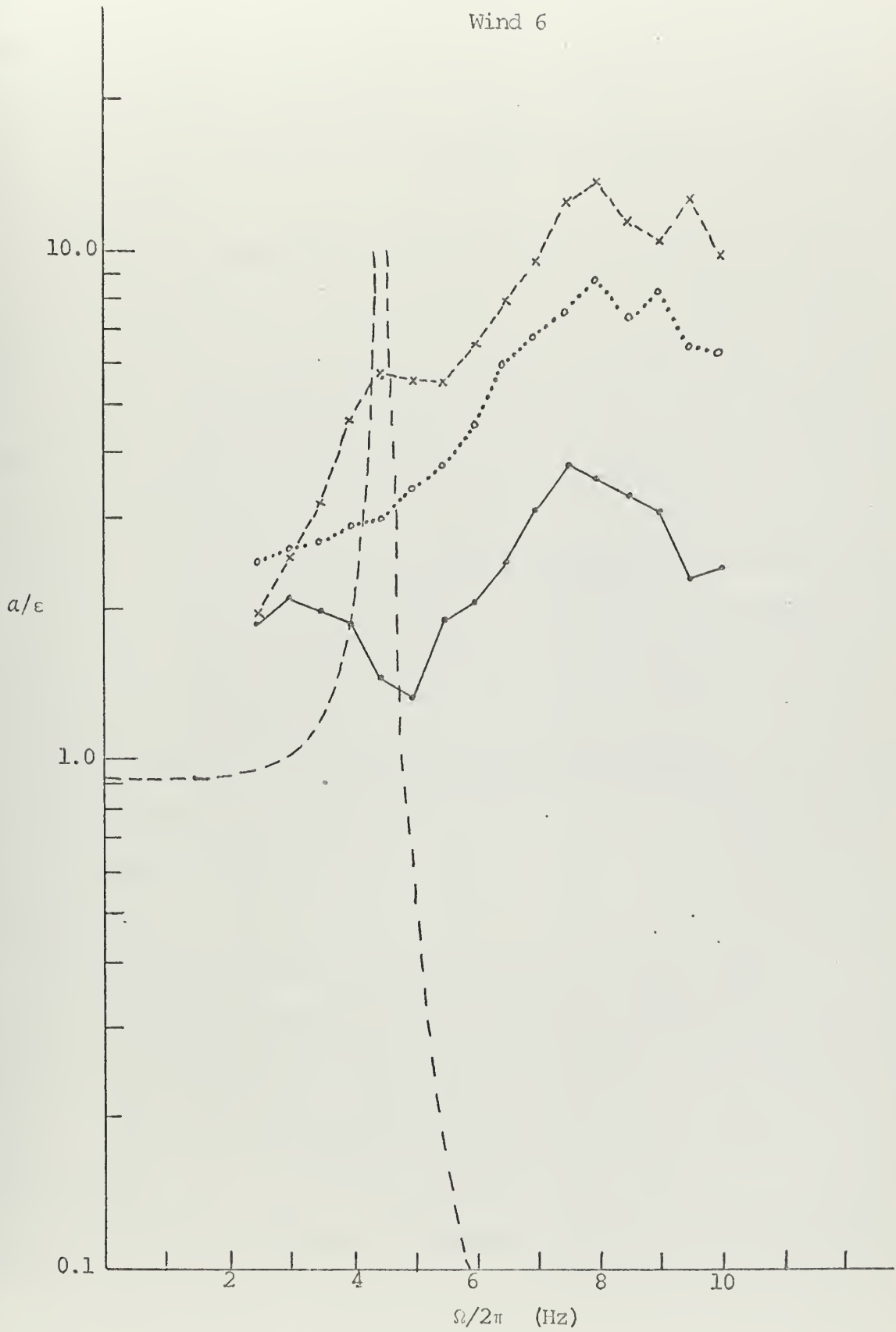


Figure 19f



Figure 20 shows that the surface fluctuations were functions of both  $x$  and  $y$ , rather than just of  $x$  as was assumed. Investigation of a more realistic expression for  $F(x,y,t)$  would require extensive auto- and cross-correlation on measurements of the generated surface fluctuation.

It is also assumed in the theory that the properties of the surface fluctuations are uniform in the vicinity of the receiver. Figure 21 shows the distribution of RMS wave heights for a typical wind over the area of the surface in the vicinity of the receiver stations. This figure shows that the waves are dying out as they propagate down the tank. Figure 22 shows that the frequency spectrum for the surface waves above the frequency corresponding to the "resonance" is also changing. The effect of the inhomogeneity of the surface could not be determined but is probably most severe at position "A".

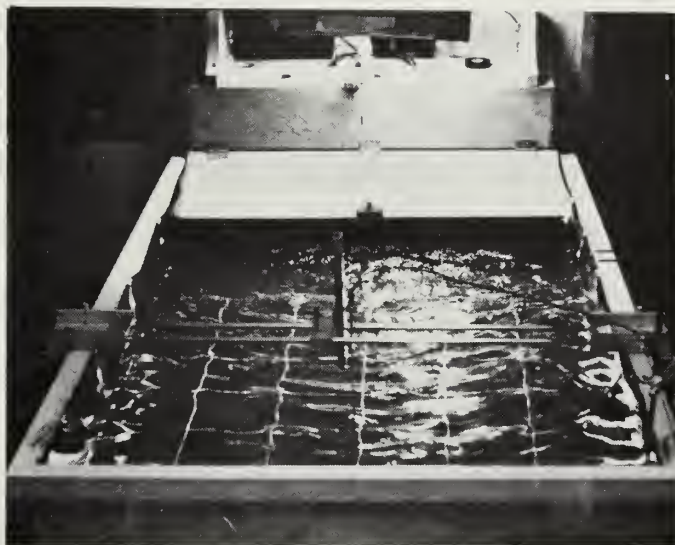
A basic assumption in the theory is that the mechanism for the acoustic fluctuation is the local surface state. In the investigation of the validity of this assumption, the following points merit study:

1. With the normal mode excited and the water surface calm, the surface in the vicinity of the source was disturbed by quadrigital agitation<sup>2</sup>. An immediate amplitude fluctuation was observed at the distant

---

<sup>2</sup>Trickling four fingers in the water, making small capillary waves.





The Tank Surface Disturbed  
by a Typical Wind

Figure 20



receiver (station "B"). The surface above the receiver was disturbed in the same manner and the acoustic signal was again immediately perturbed. However, when the water surface was disturbed at a point removed from both source and receiver, an effect on the received acoustic signal was observed only after the surface disturbance had propagated into the vicinity of the source, receiver, and region in between.

2. The treatment of the extreme agitation under the fans as a distant source (page 14) contributing to observed acoustic-amplitude fluctuation appears valid from the results of the fan isolation experiment, but this would appear to be inconsistent with the result just discussed. Recall, however, that the violent agitation of the surface under the fans is a clear violation of the assumption that  $\epsilon F(x,y,t)$  be small.

The first point above appears to validate the assumption that the driving mechanism for the acoustic fluctuation at the receiver is the local surface. The fan isolation experiment (point two) showed that severe surface disturbances at a remote location could cause amplitude fluctuations under a smooth surface. It is plausible that the distinction between these two cases results from the difference in magnitude of  $\epsilon F(x,y,t)$  in the two regions.

The stringent assumptions of the simple theory were all clearly violated to some degree during the conduct of the experiment. It



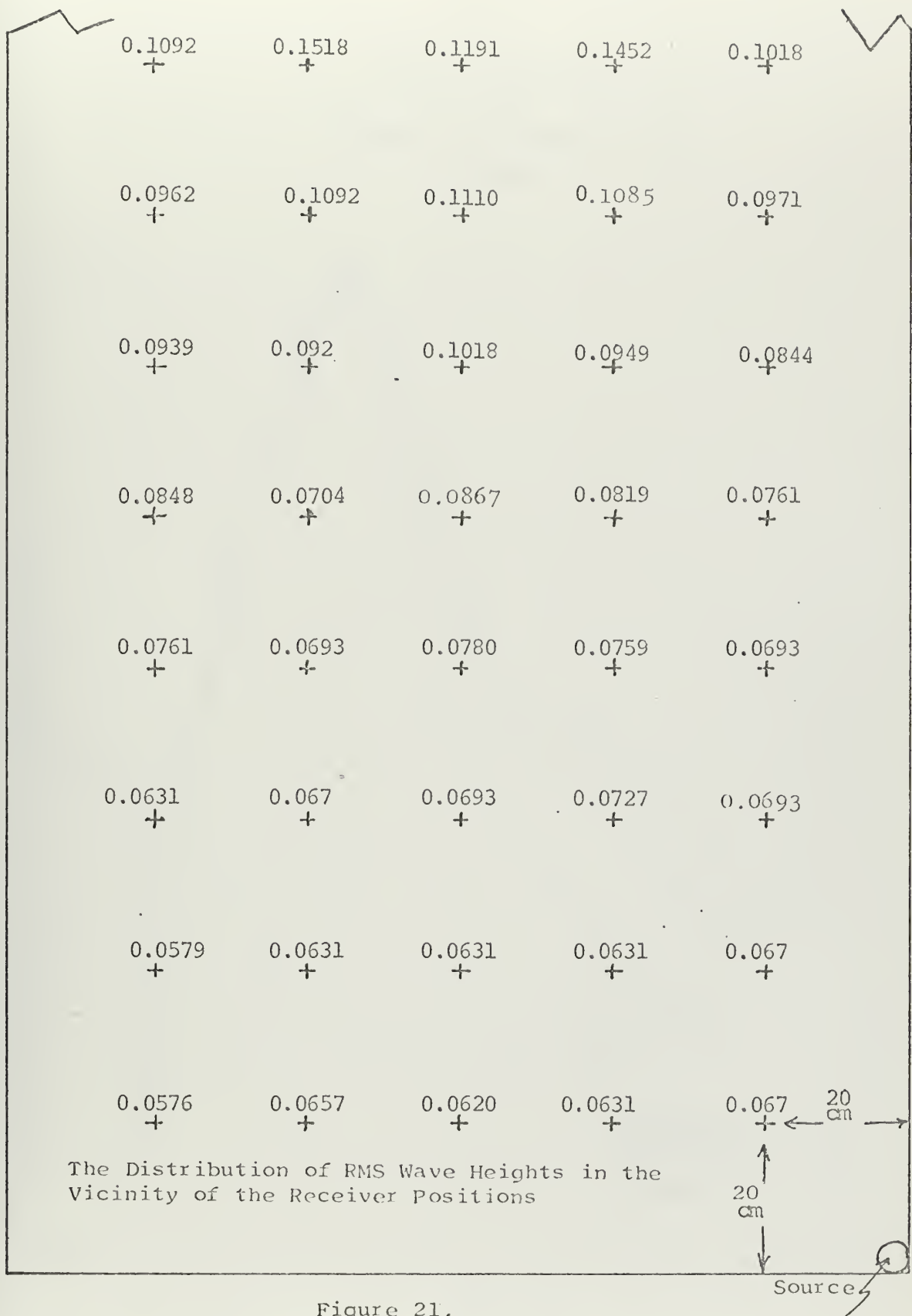


Figure 21.



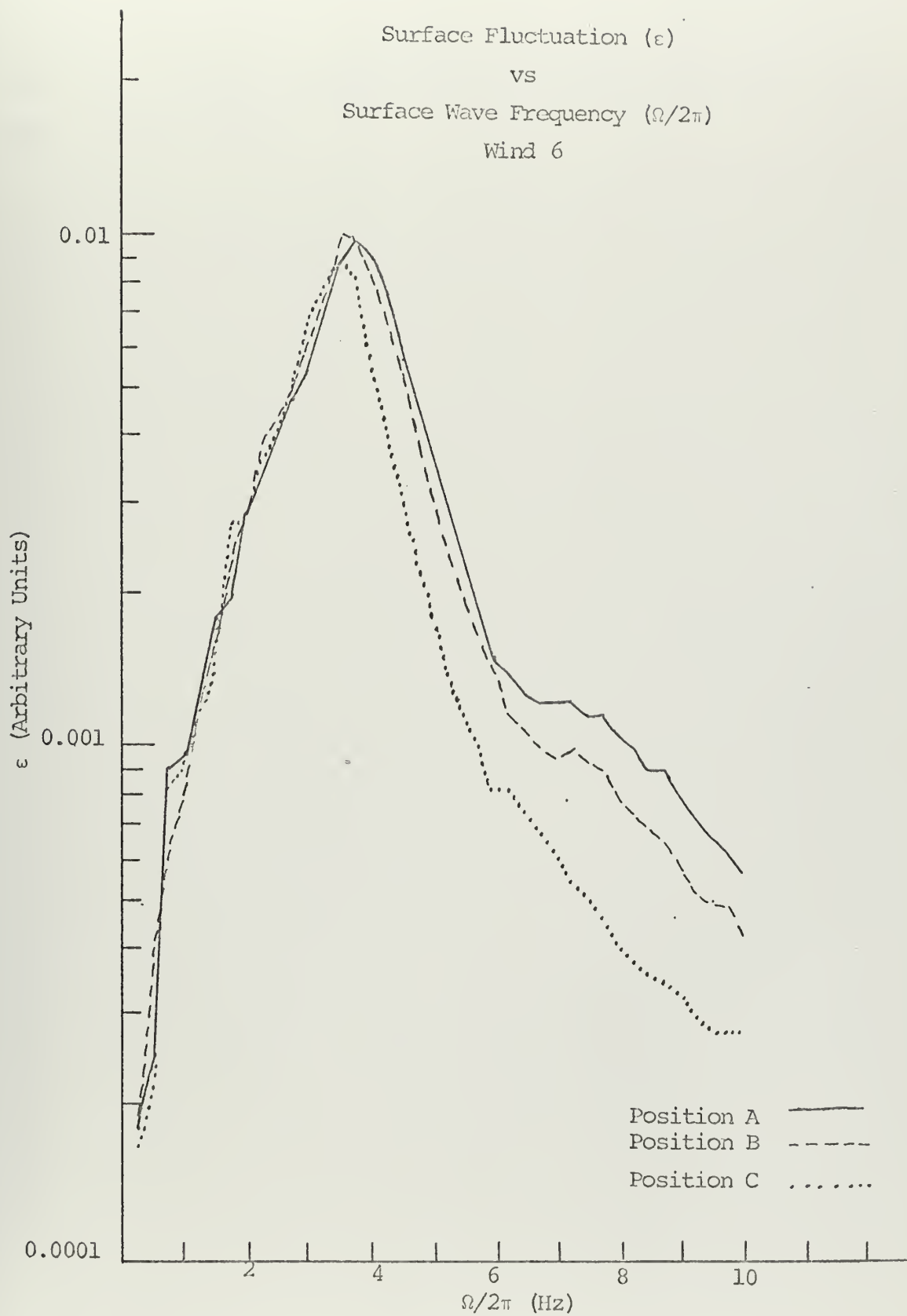


Figure 22



is concluded, however, that the measured values of  $a/\epsilon$  below the frequency of predicted "resonance" are sufficiently close to the theoretical values to claim consistency between experiment and theory in this range.



## APPENDIX A

### Computer Program for $a/\epsilon$ Calculation

```
1.      IMPLICIT REAL*8(A, K, P,)
2.      REAL*8(DCOS, DCOSH, DABS, DSQRT)
3.      DO 100 I=1, 500
4.      GAM = (I-1)*.01
5.      K1=2.*3.1415926535/16.4
6.      K3=3.1415926535/8.8
7.      PI=3.1415926535
8.      AR1=2.*GAM*K1
9.      AR2=K3**2
10.     AR3=GAM**2
11.     AR4=PI/2.
12.     AR5=(1.-((AR3+AR1)/AR2))
13.     AR6=(1.-((AR3-AR1)/AR2))
14.     IF(AR5.LT.0.)GO TO 50
15.     AR7=DCOS(AR4*DSQRT(AR5))
16.     GO TO 60
17. 50   AR7=DCOSH(AR4*DSQRT(DABS(AR5)))
18. 60   IF(AR6.LT.0.) GO TO 70
19.     AR8=DCOS(AR4*DSQRT(AR6))
20. 70   AR8=DCOSH(AR4*DSQRT(DABS(AR6)))
21. 80   AR9=DABS(1./AR7-1./AR8)
22.     ABE=PI*AR9/4.
23.     PRINT, GAM, ABE
24. 100  CONTINUE
25.     STOP
26.     END
```



## APPENDIX B

### Observed Data

The eighteen sets of data described on page 51 are plotted as functions of surface wave frequency ( $\Omega/2\pi$ ).

$a_a$  = the measured acoustic amplitude fluctuation

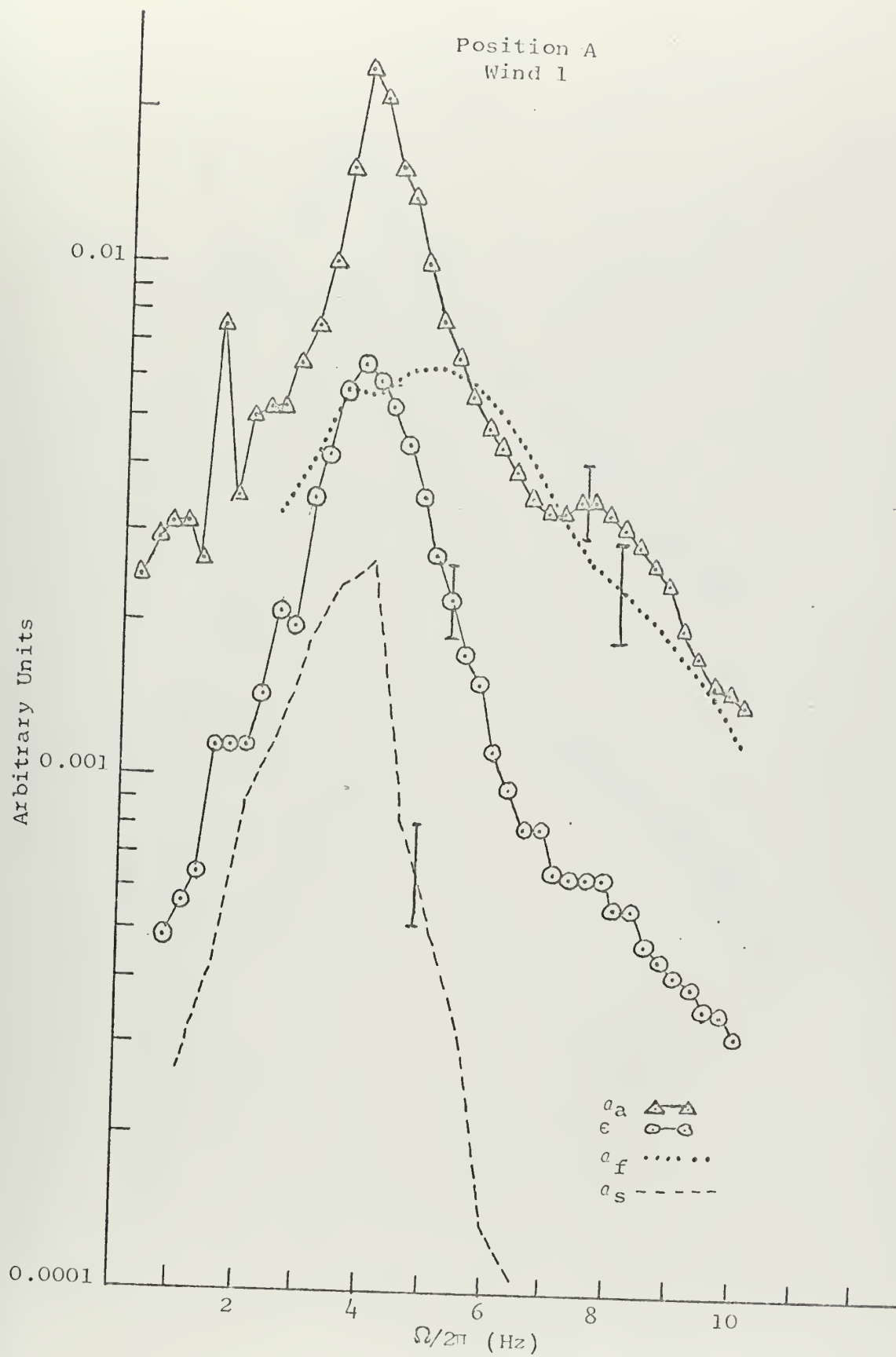
$\epsilon$  = the normalized surface wave fluctuation in the  
vicinity of the receiver

$a_f$  = the acoustic amplitude fluctuation generated by the  
severe agitation under the fans

$a_s$  = the acoustic amplitude fluctuation due to source  
modulation

Representative error flags for these data are presented in  
Figure B1.







Position A

Wind 2

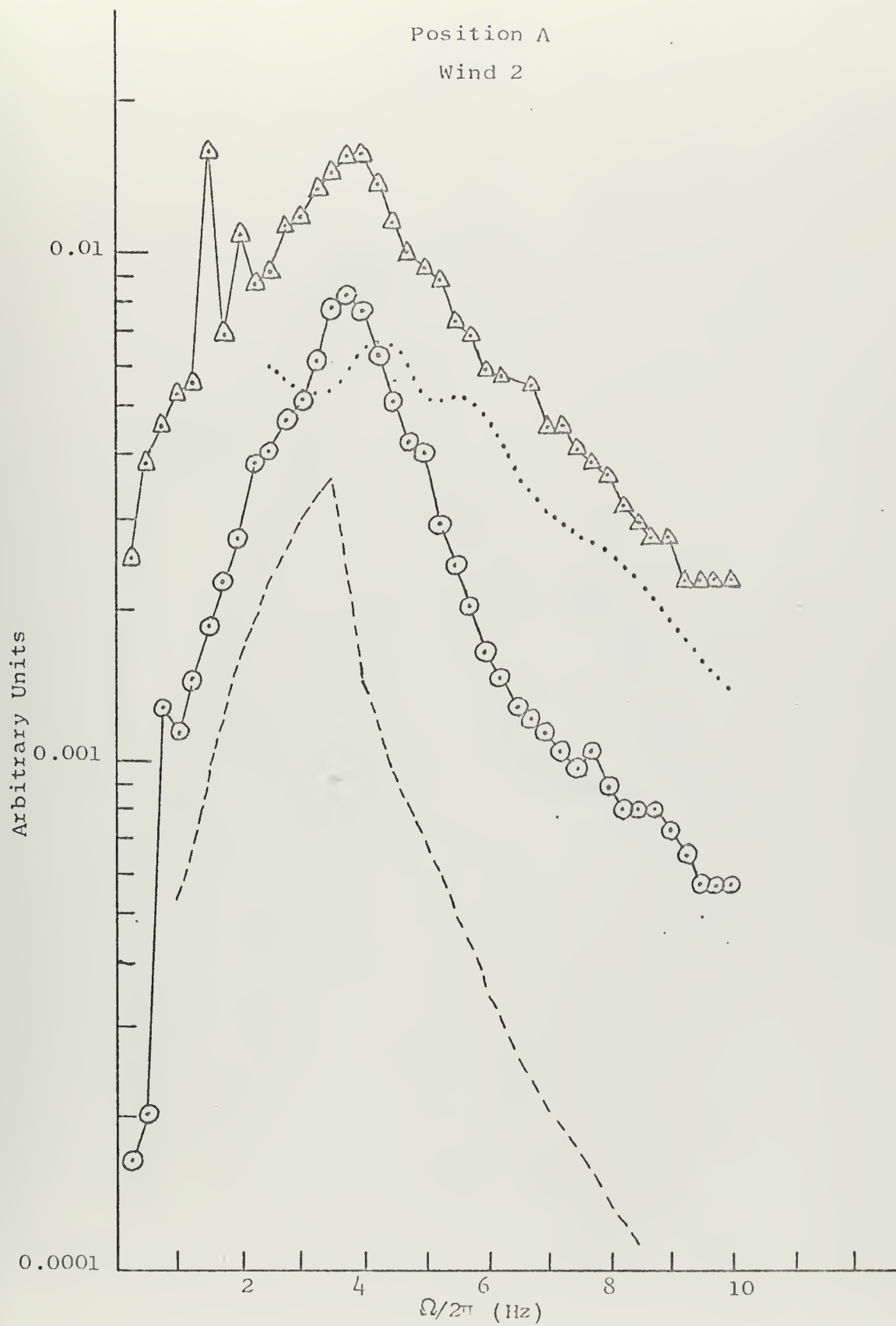


Figure B2



Position A  
Wind 3

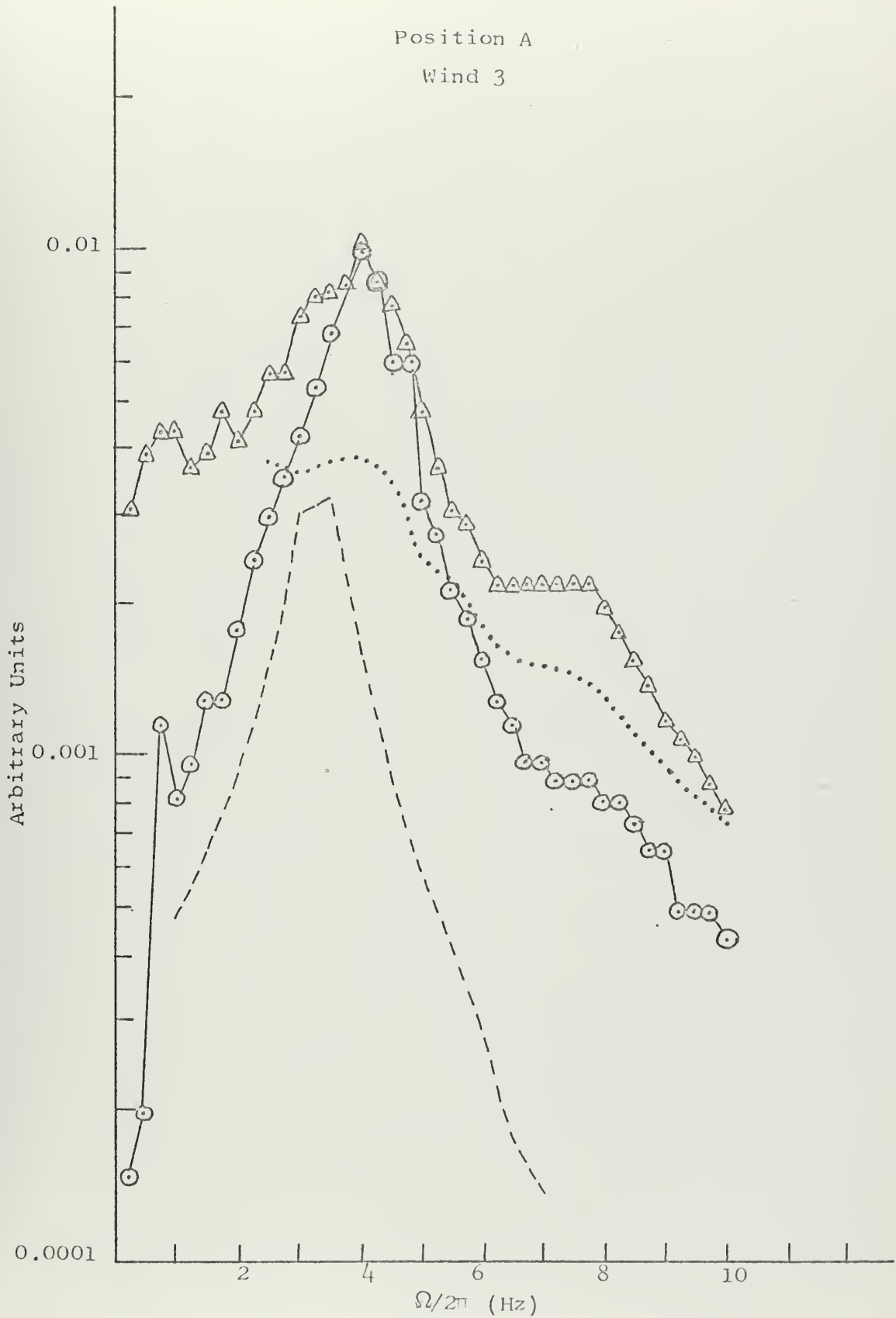
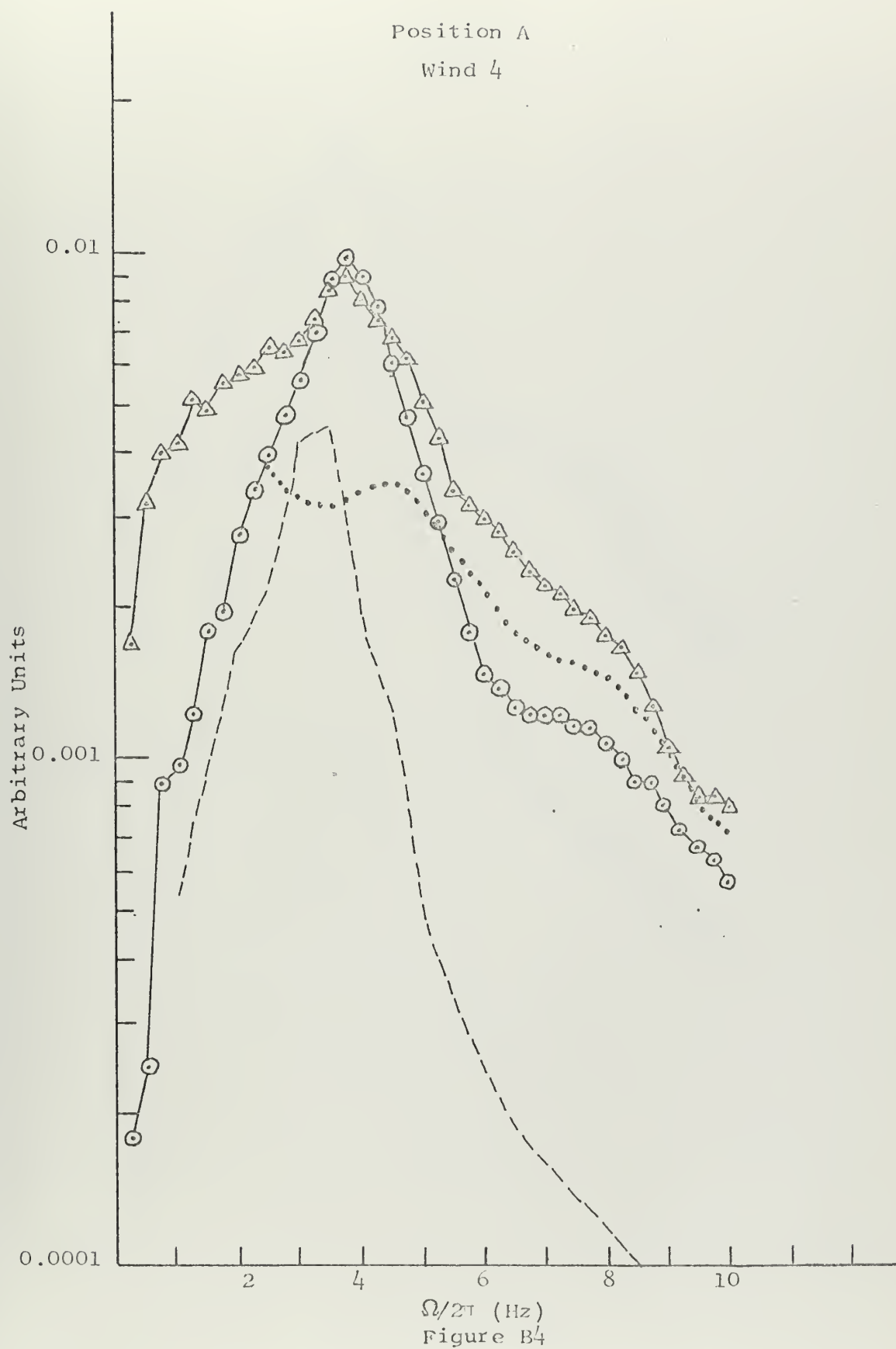


Figure B3



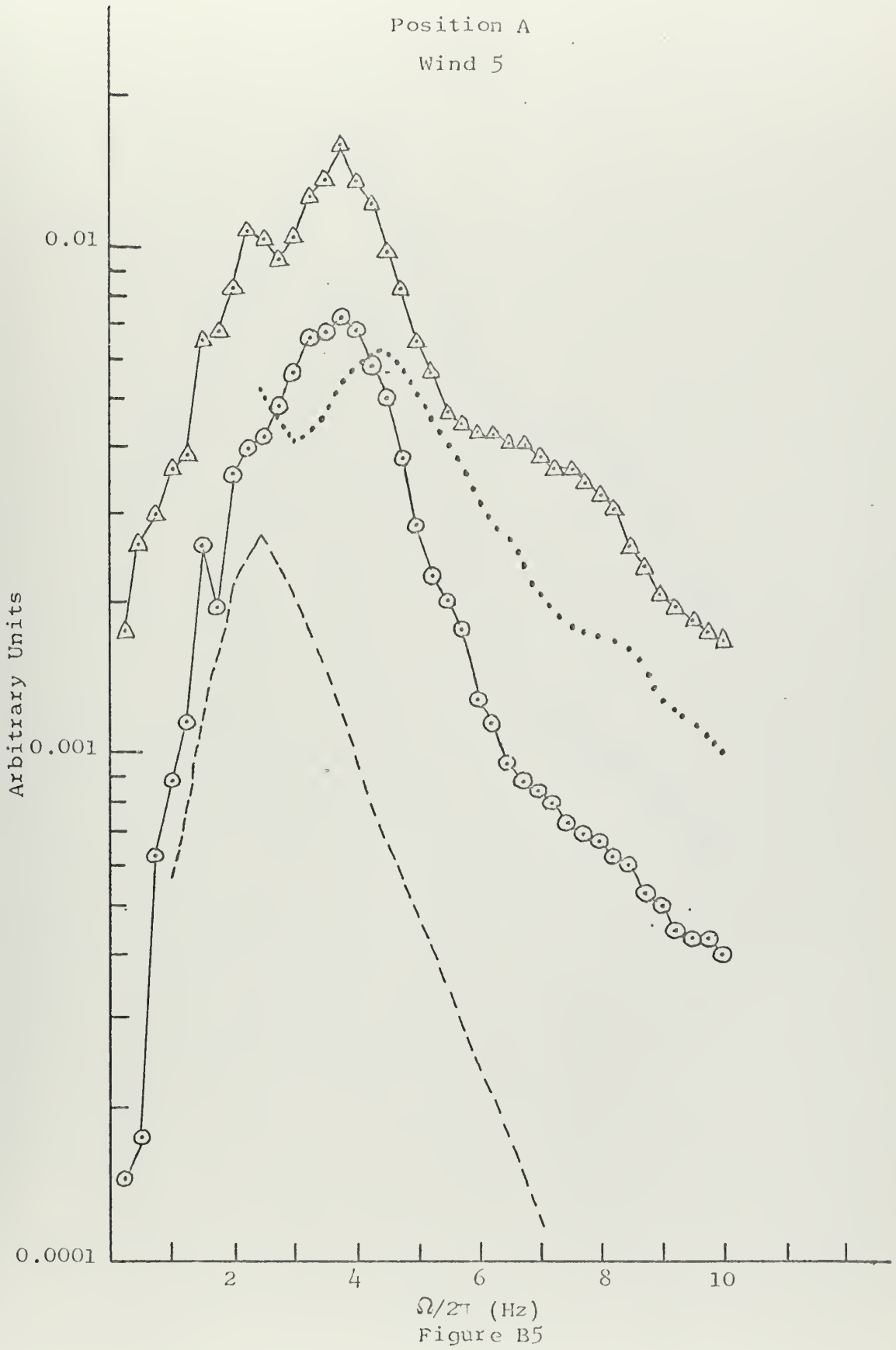
Position A

Wind 4





Position A  
Wind 5





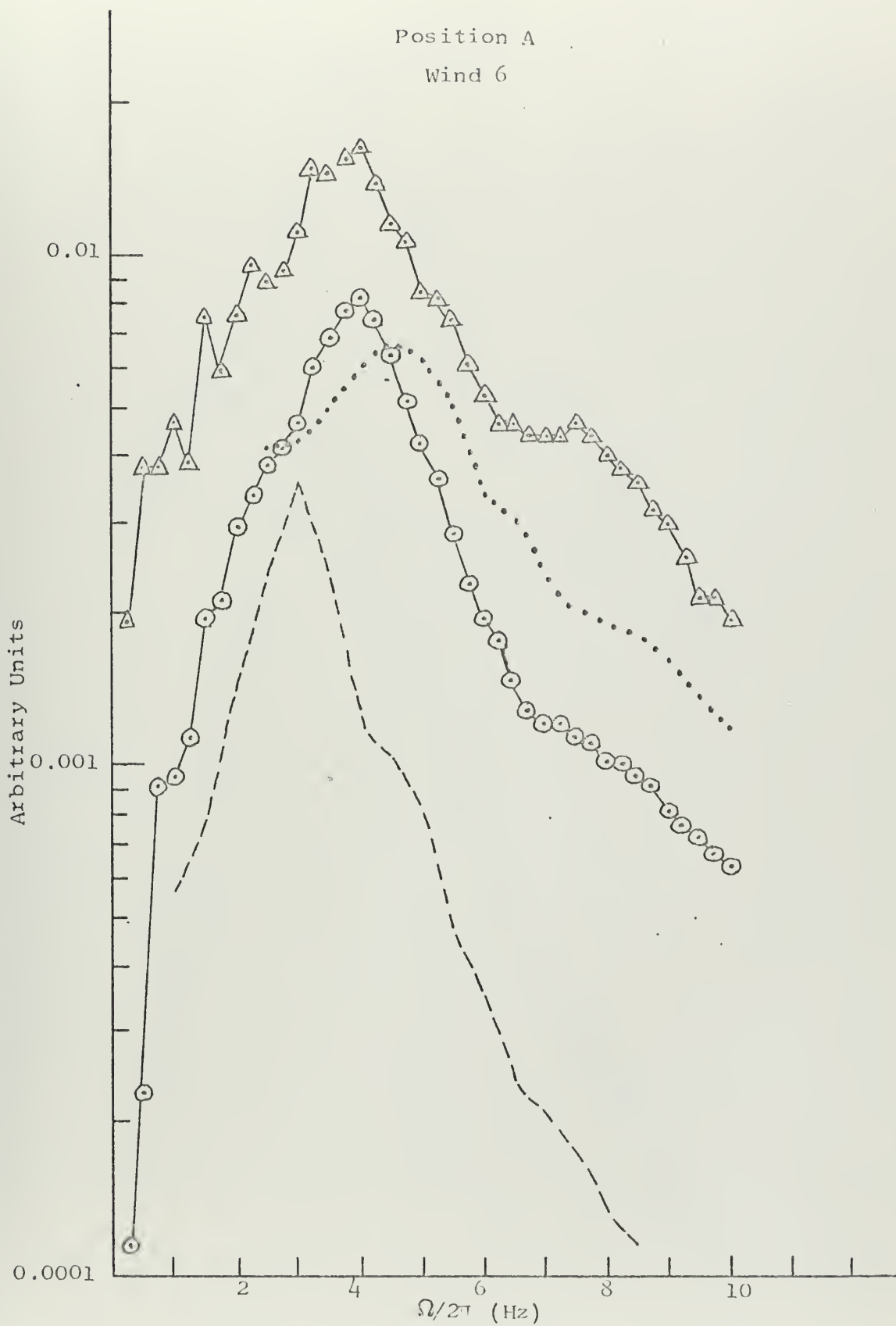
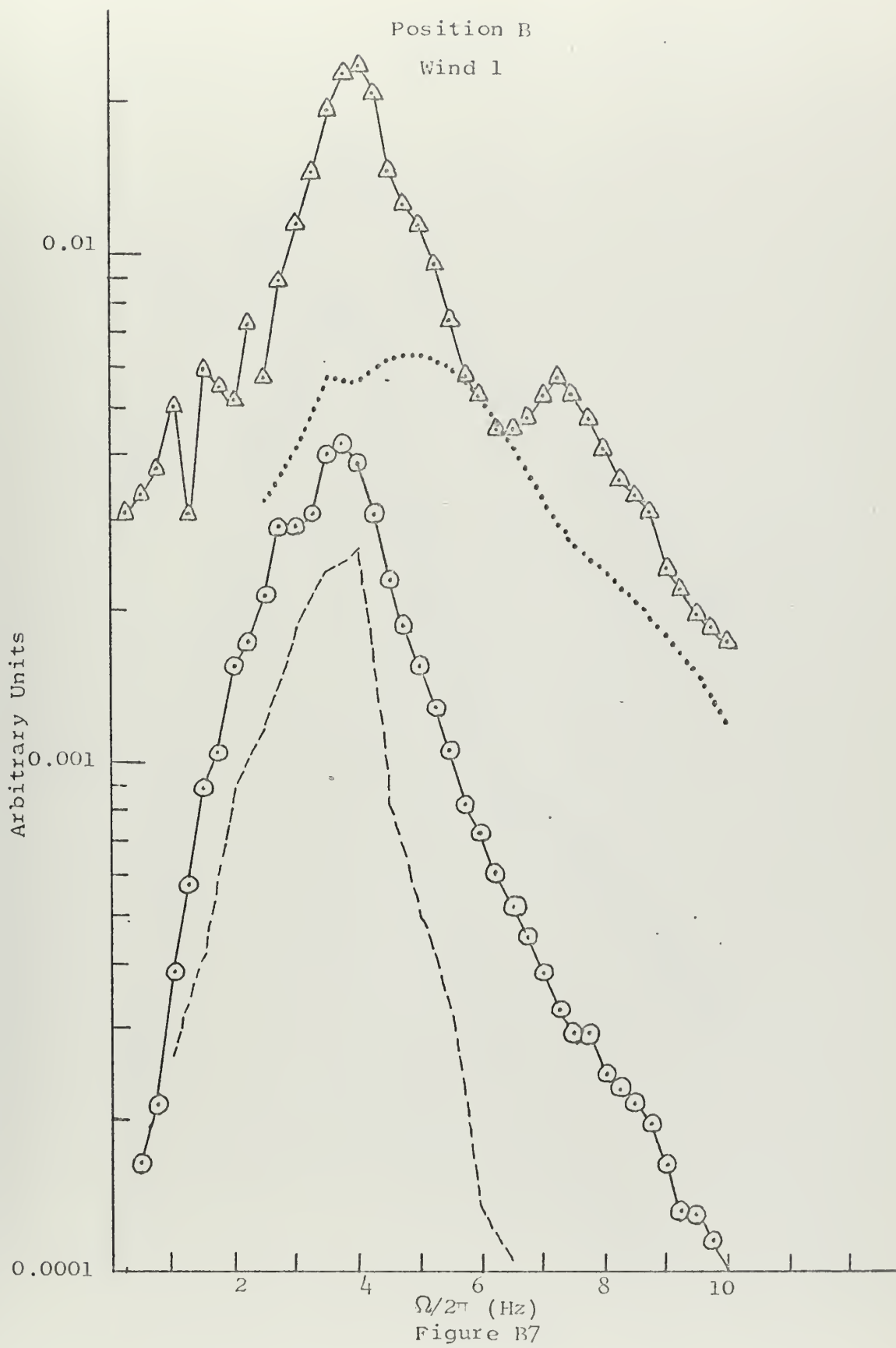
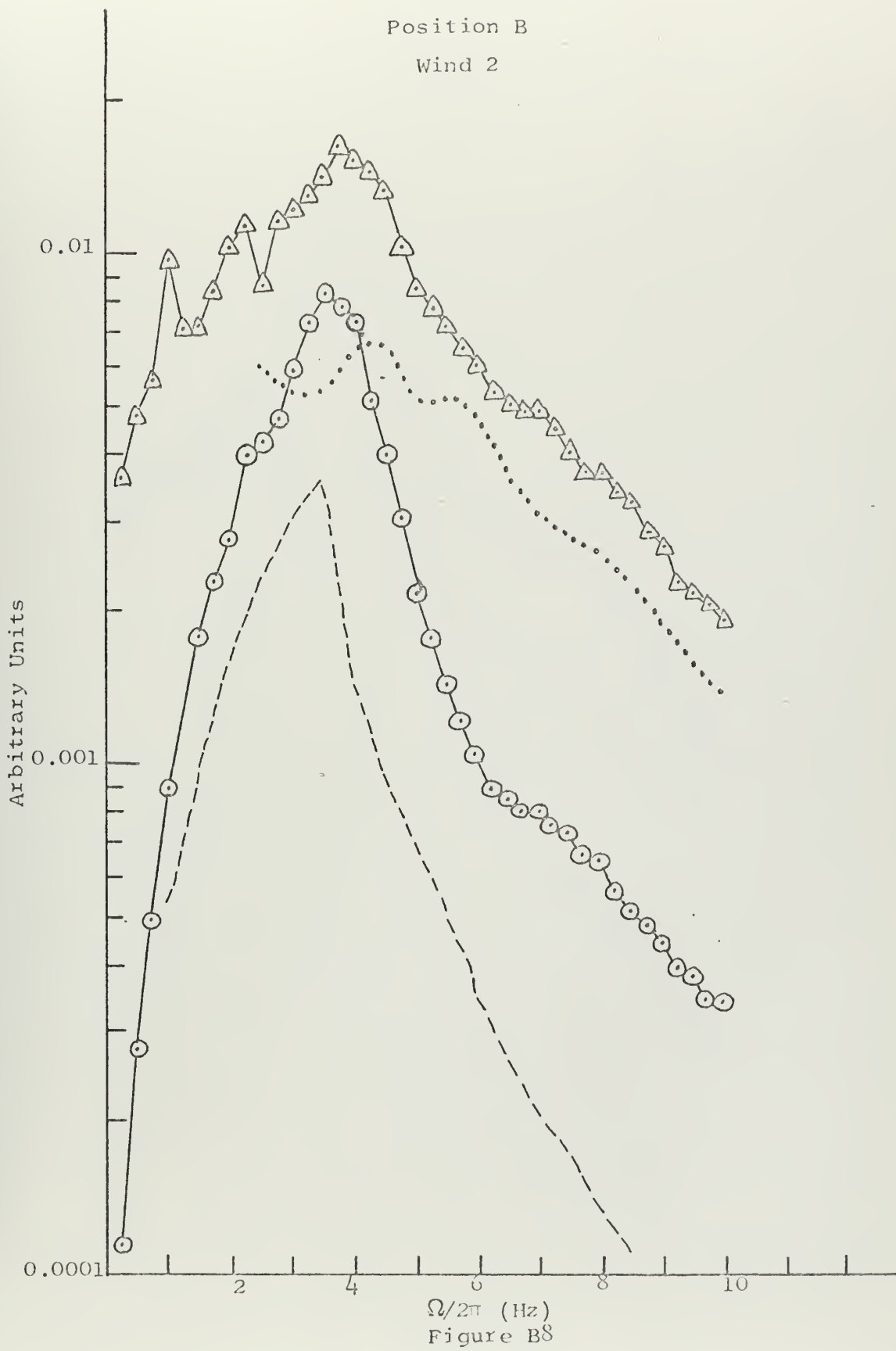


Figure B6



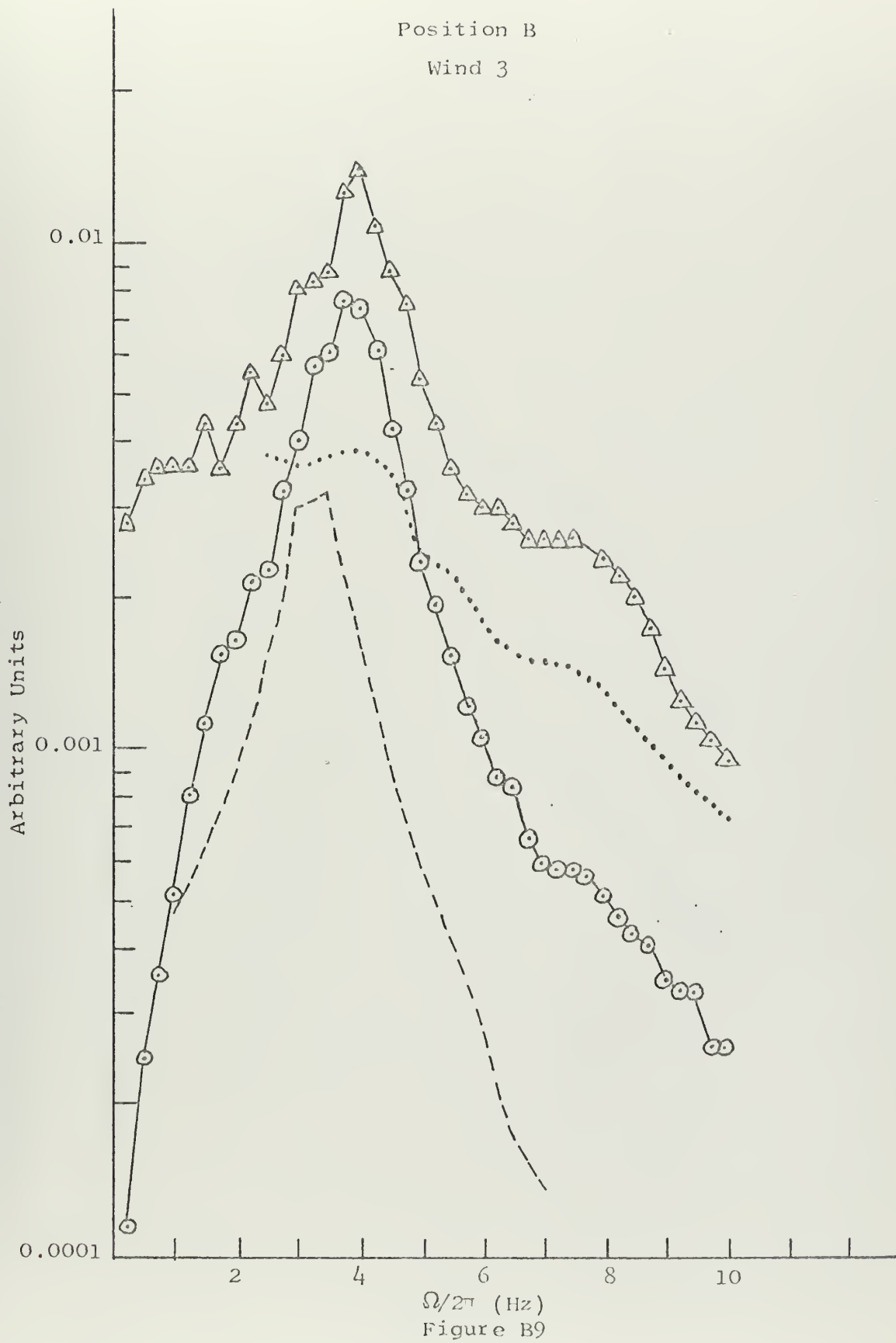




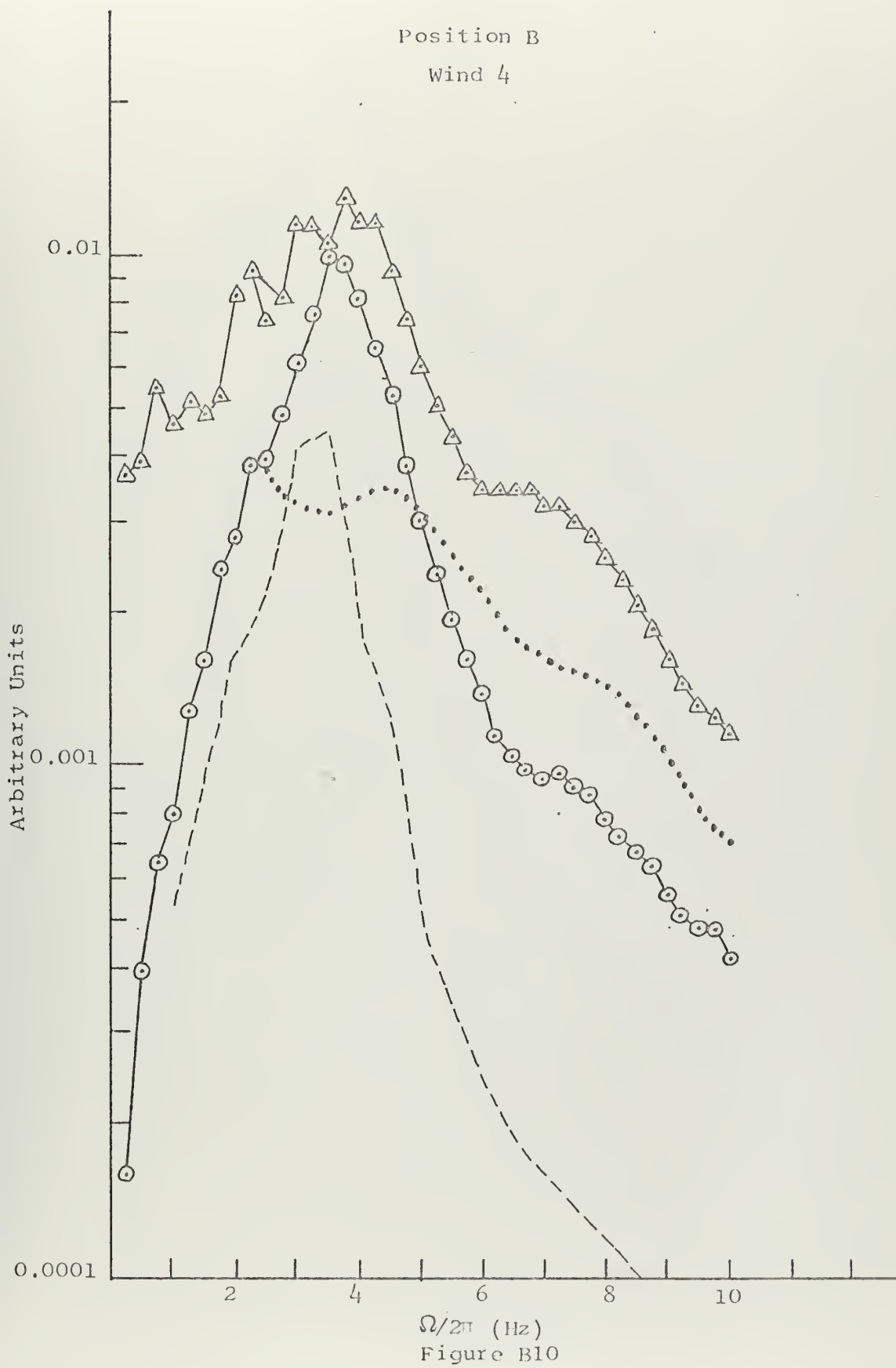




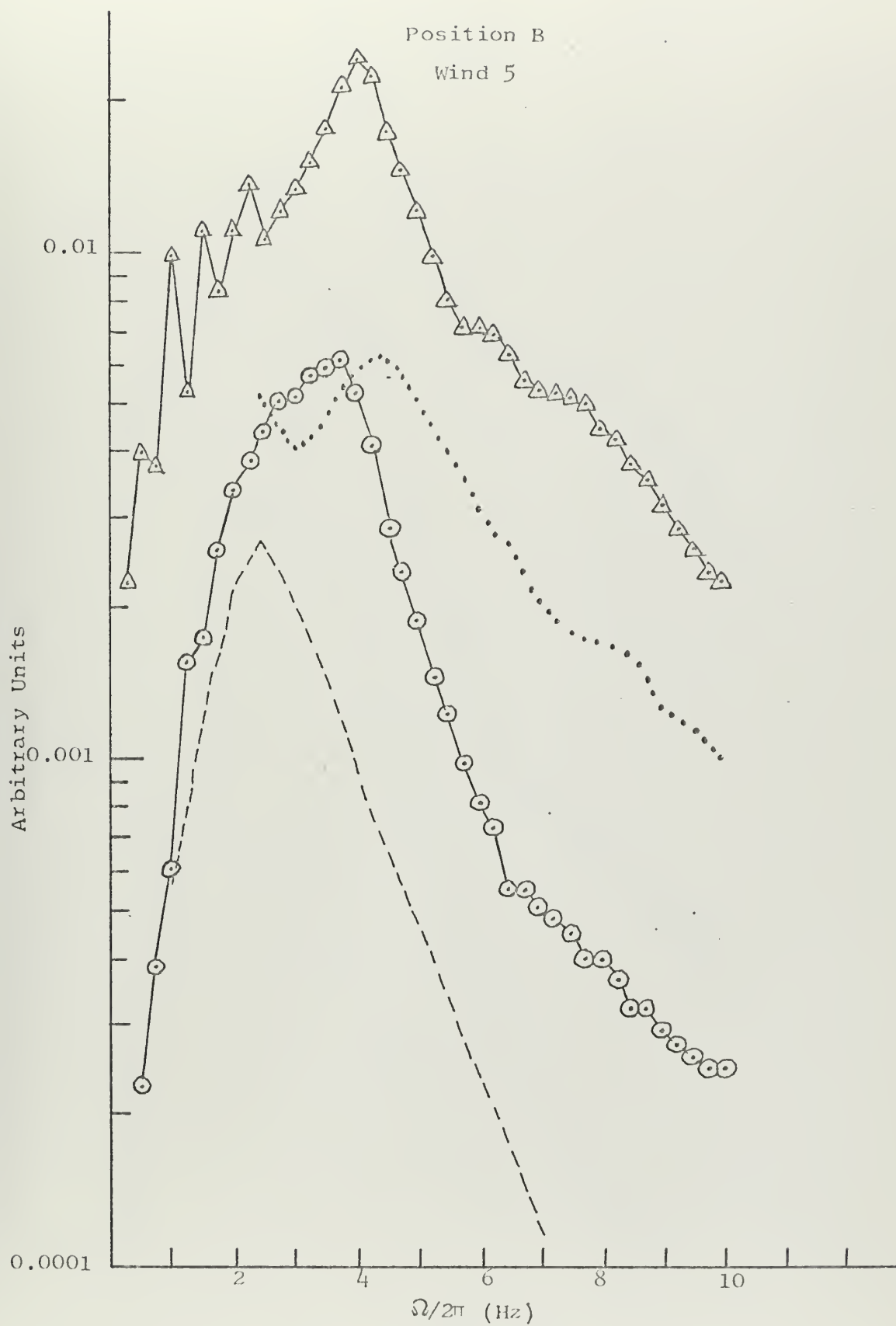
Position B  
Wind 3



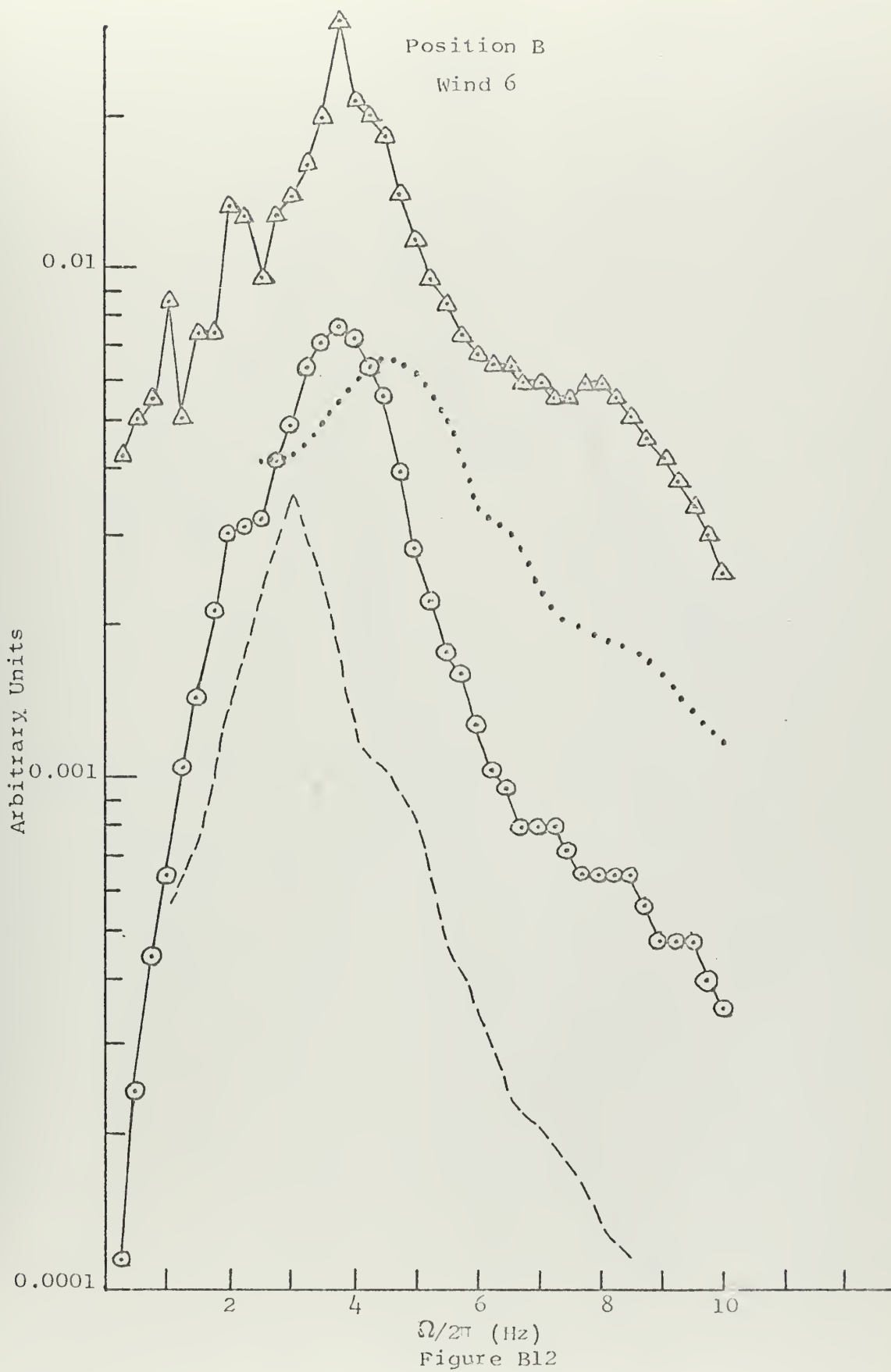




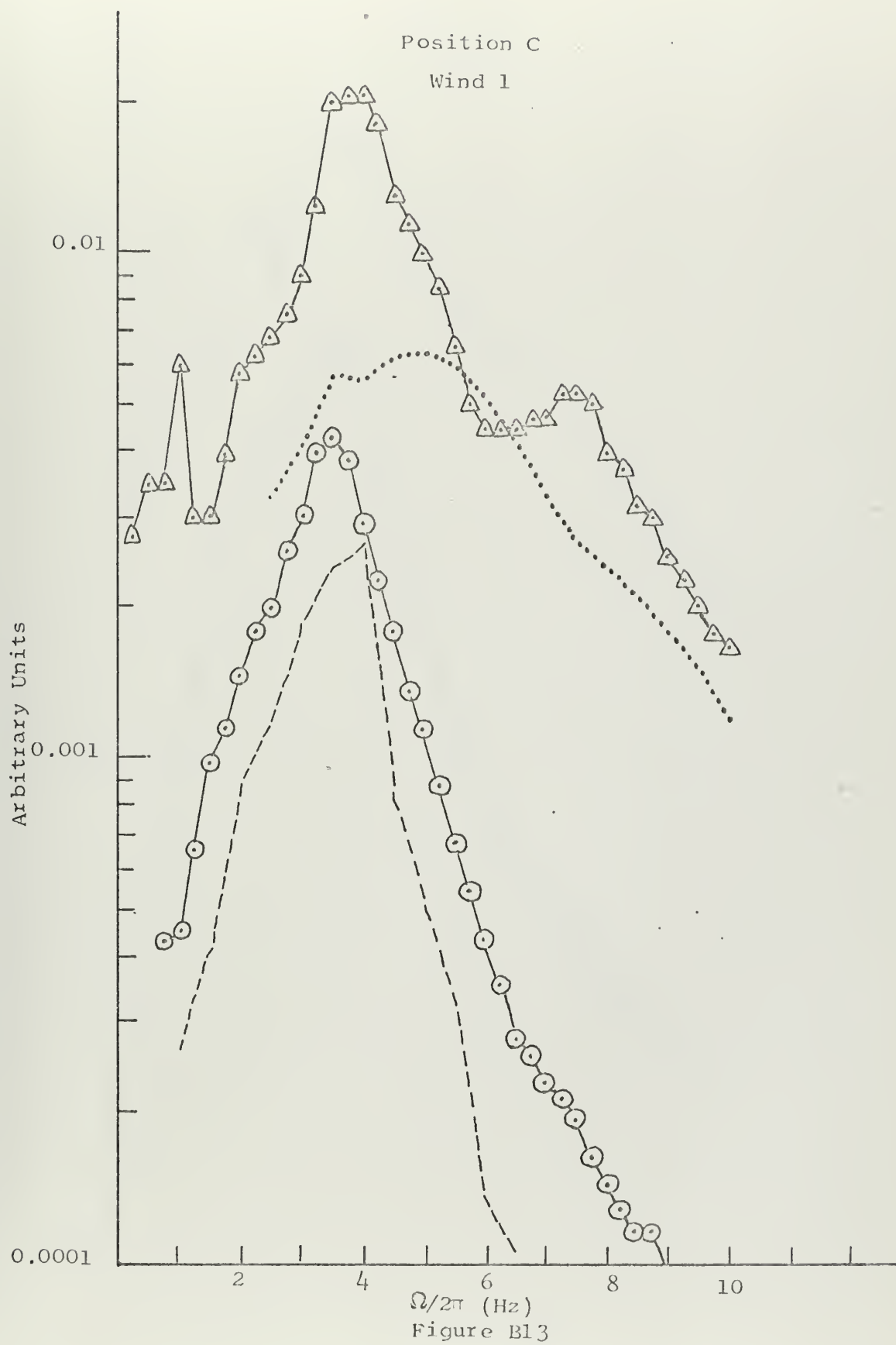




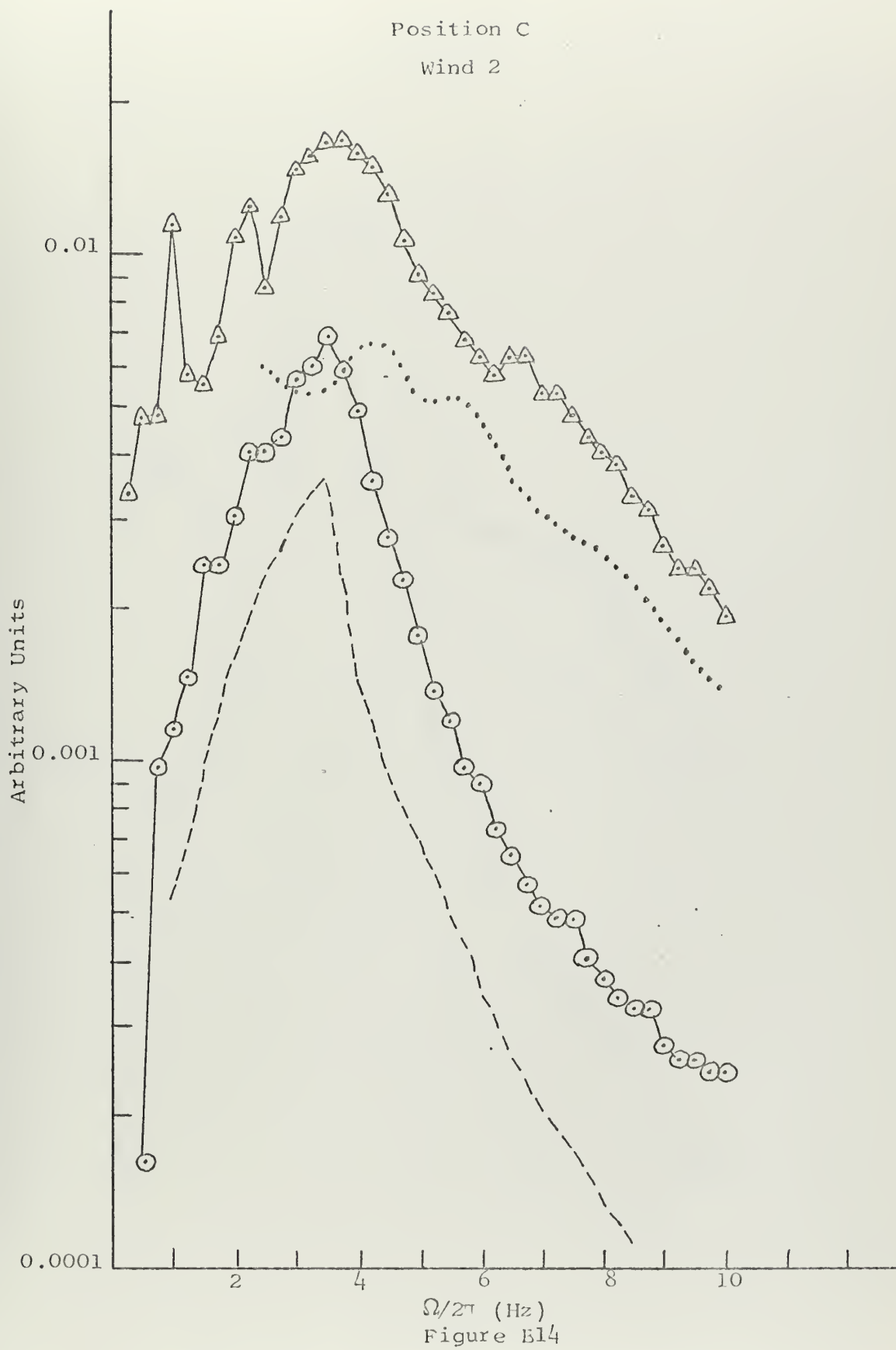














Position C

Wind 3

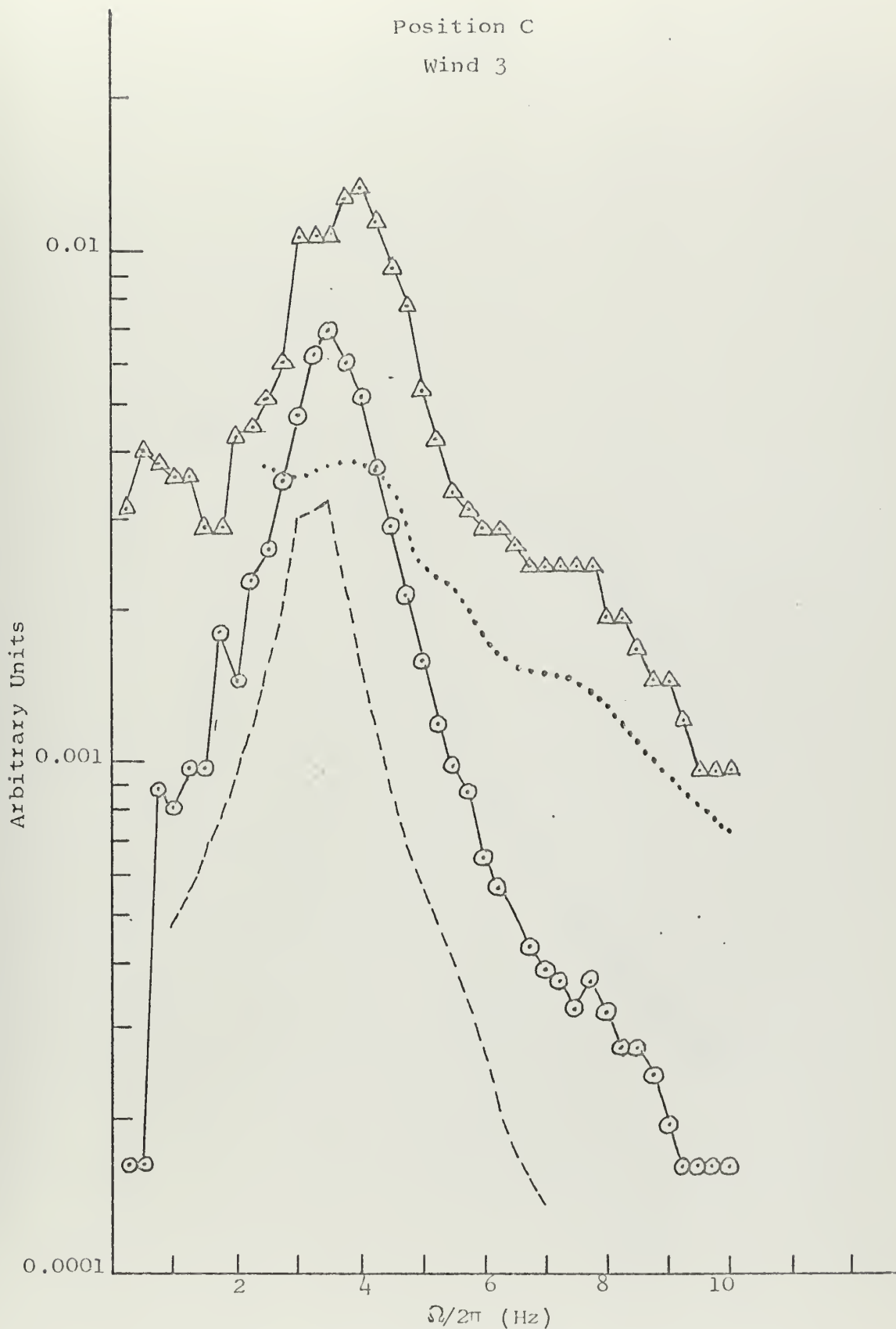
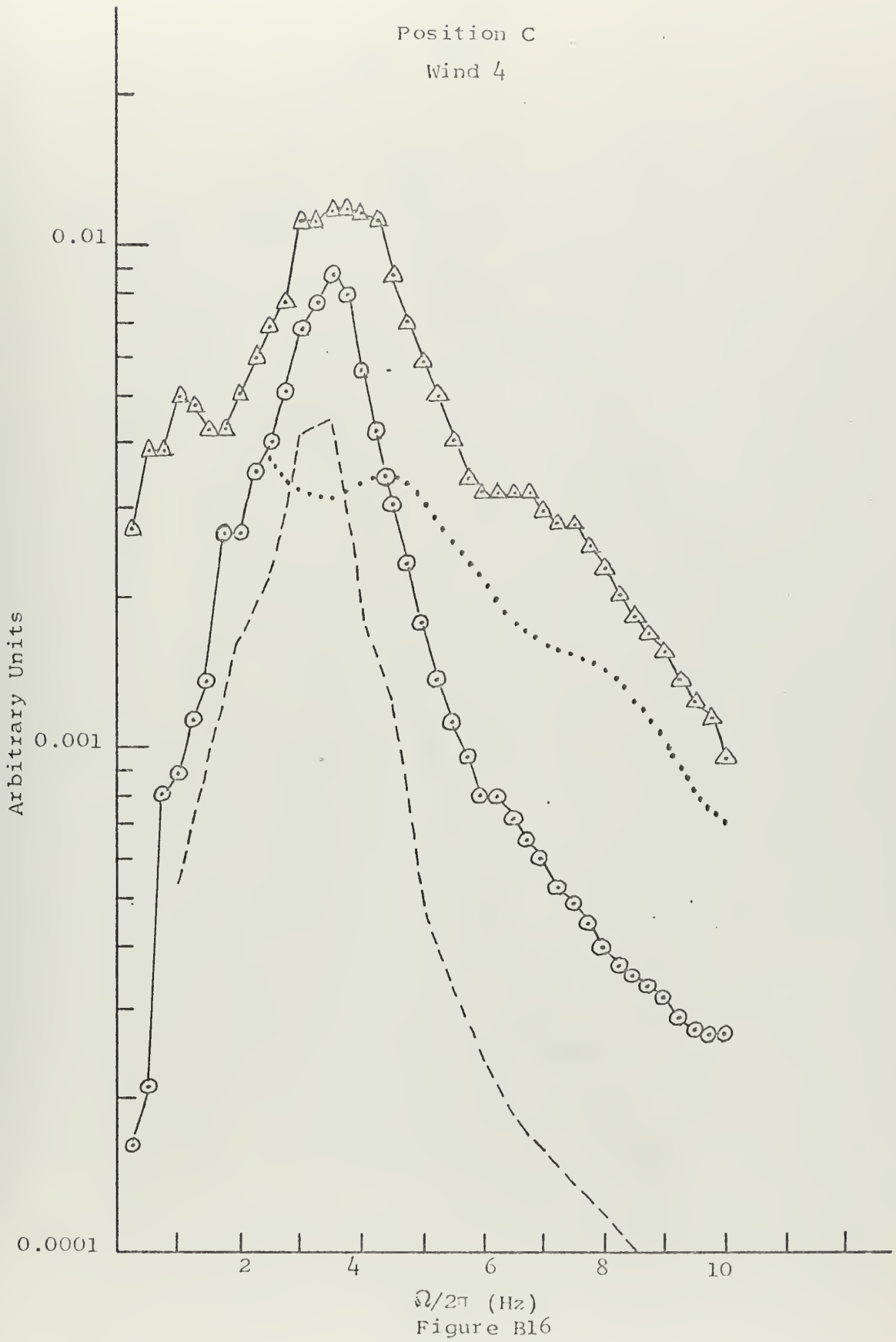


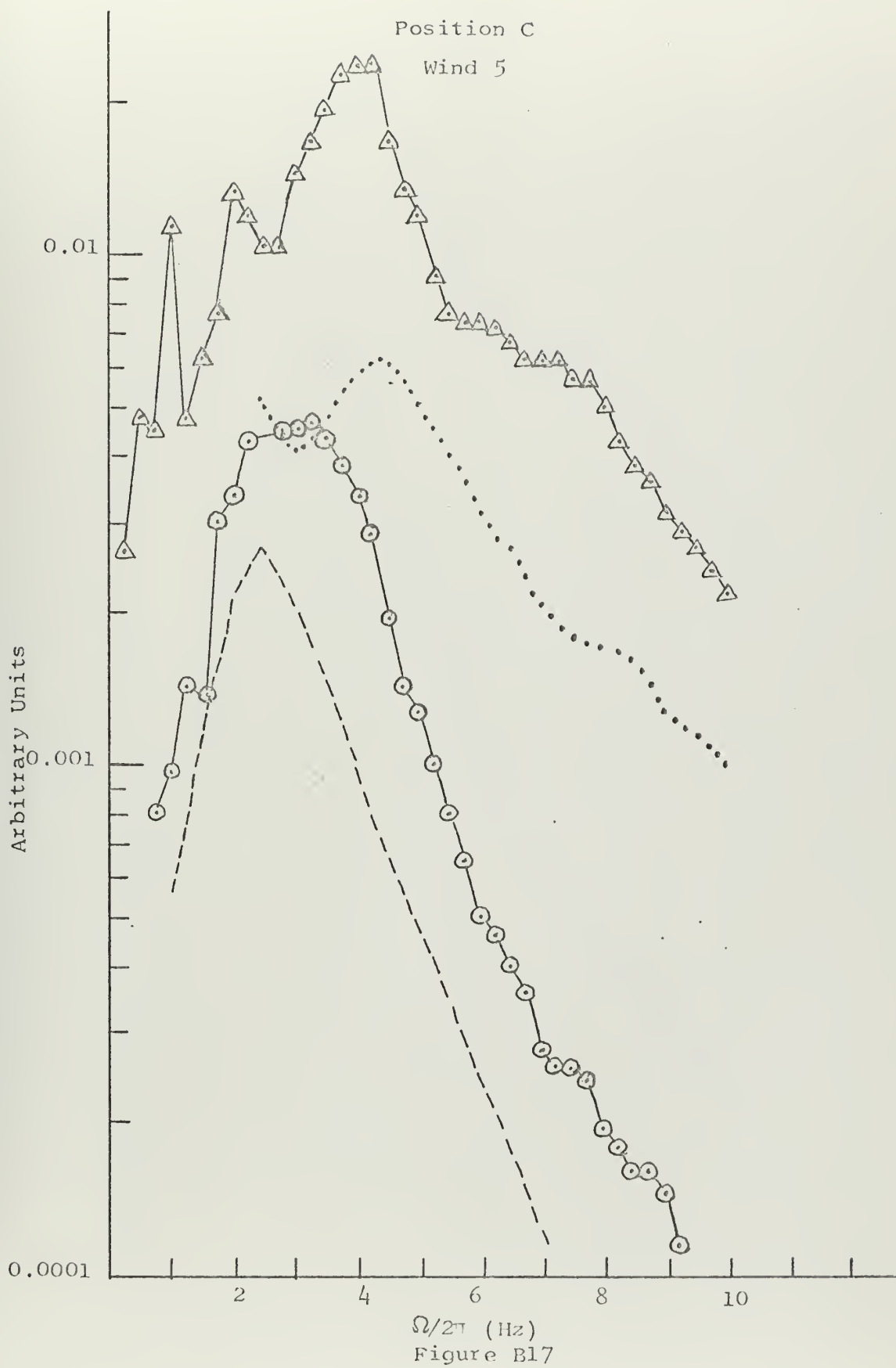
Figure B15



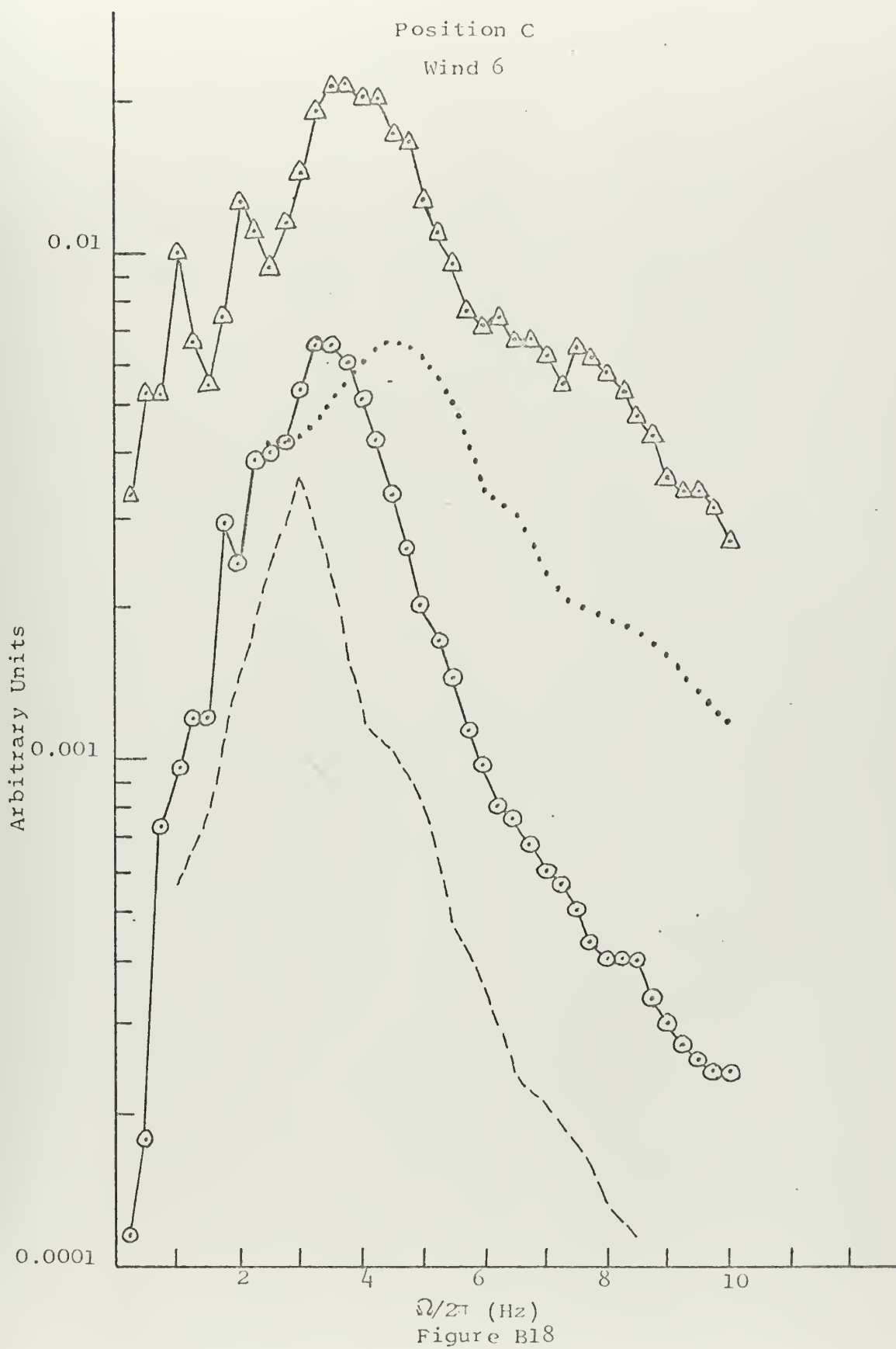
Position C  
Wind 4













## APPENDIX C

### Measured Values of $a/\epsilon$

The measured values of  $a/\epsilon$  at each receiver position for each wind condition are plotted as functions of surface wave frequency ( $\Omega/2\pi$ ). Standard RMS error flags are presented.



Position A

Wind 1

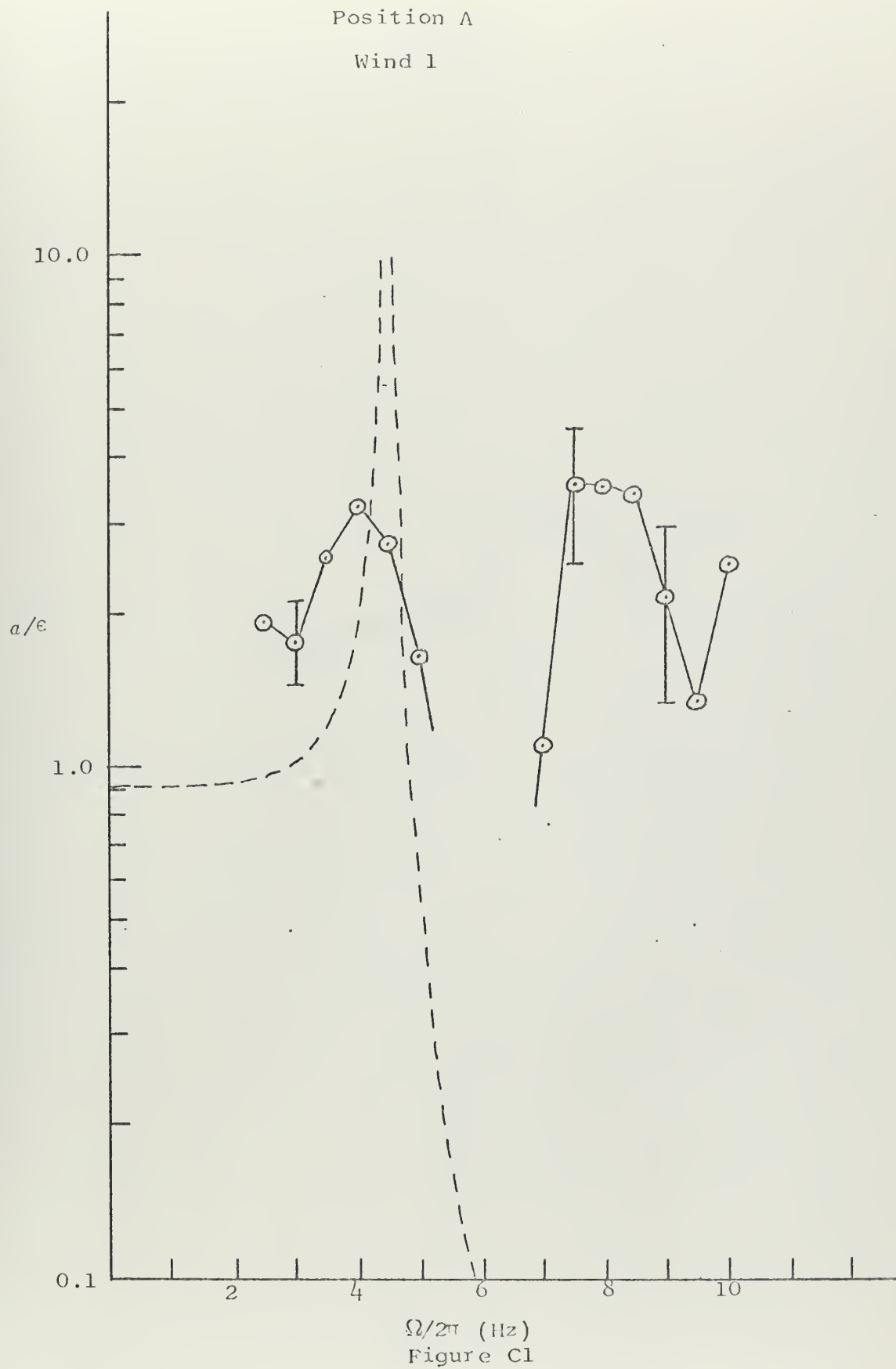
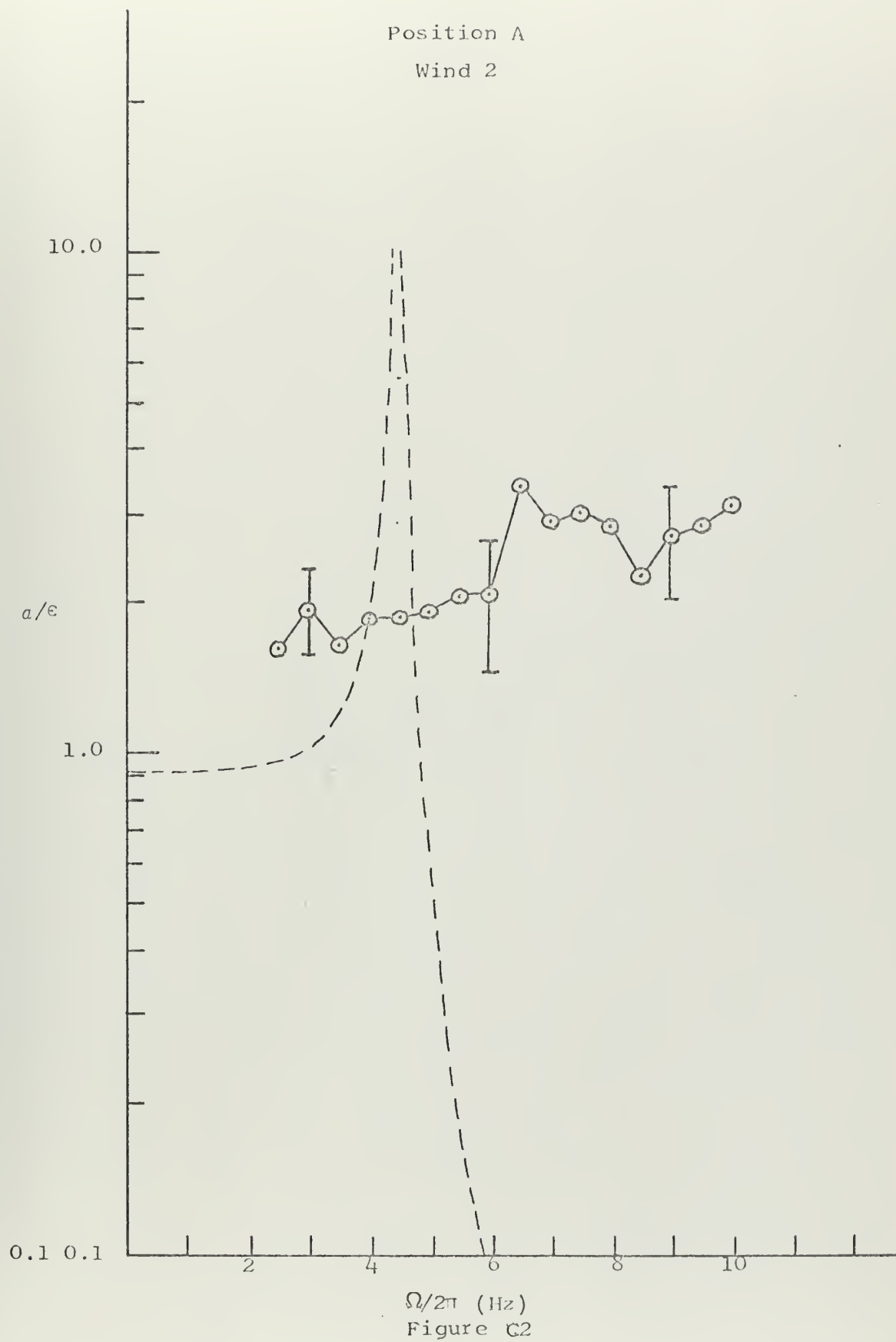


Figure C1

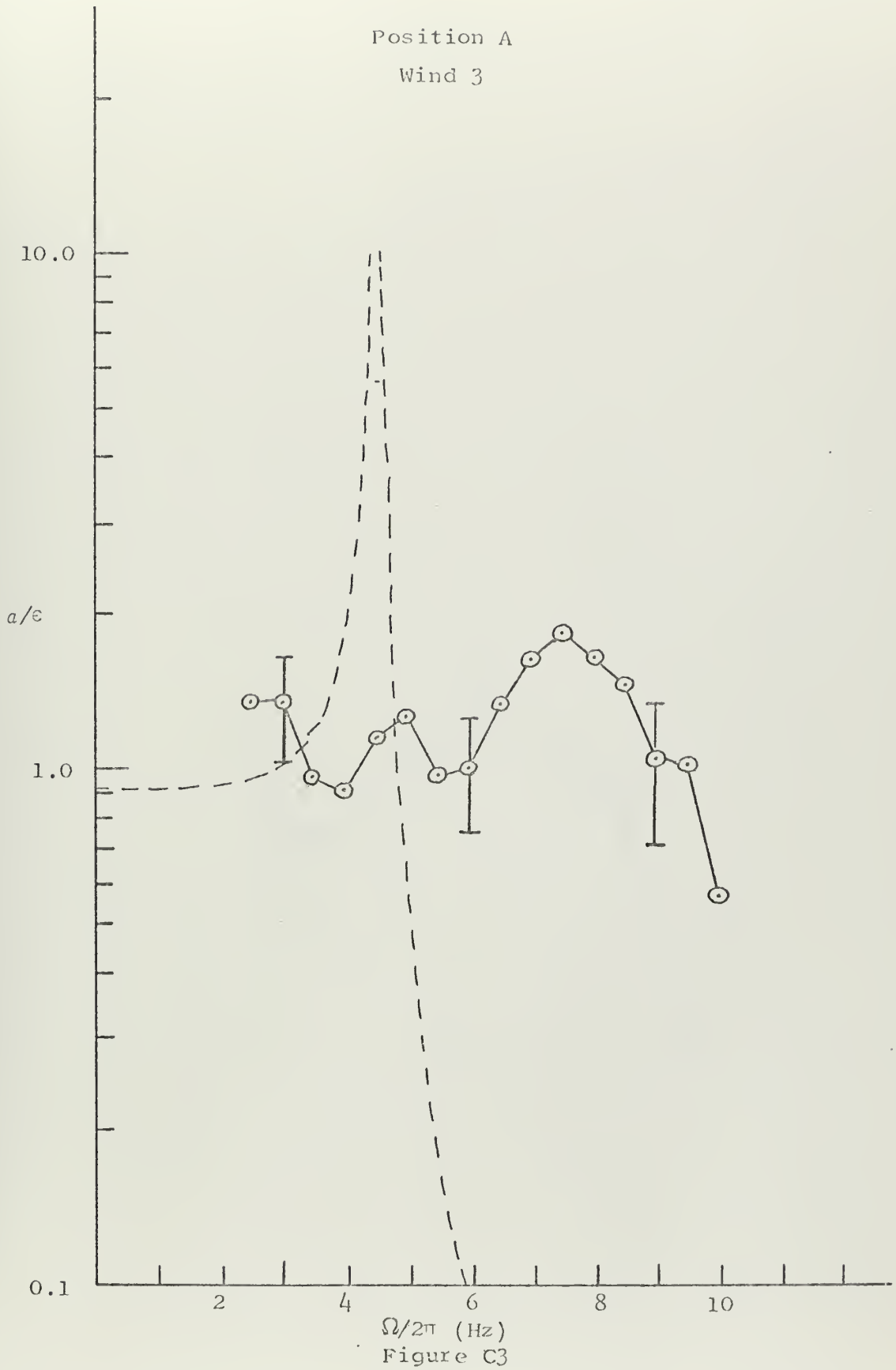


Position A  
Wind 2



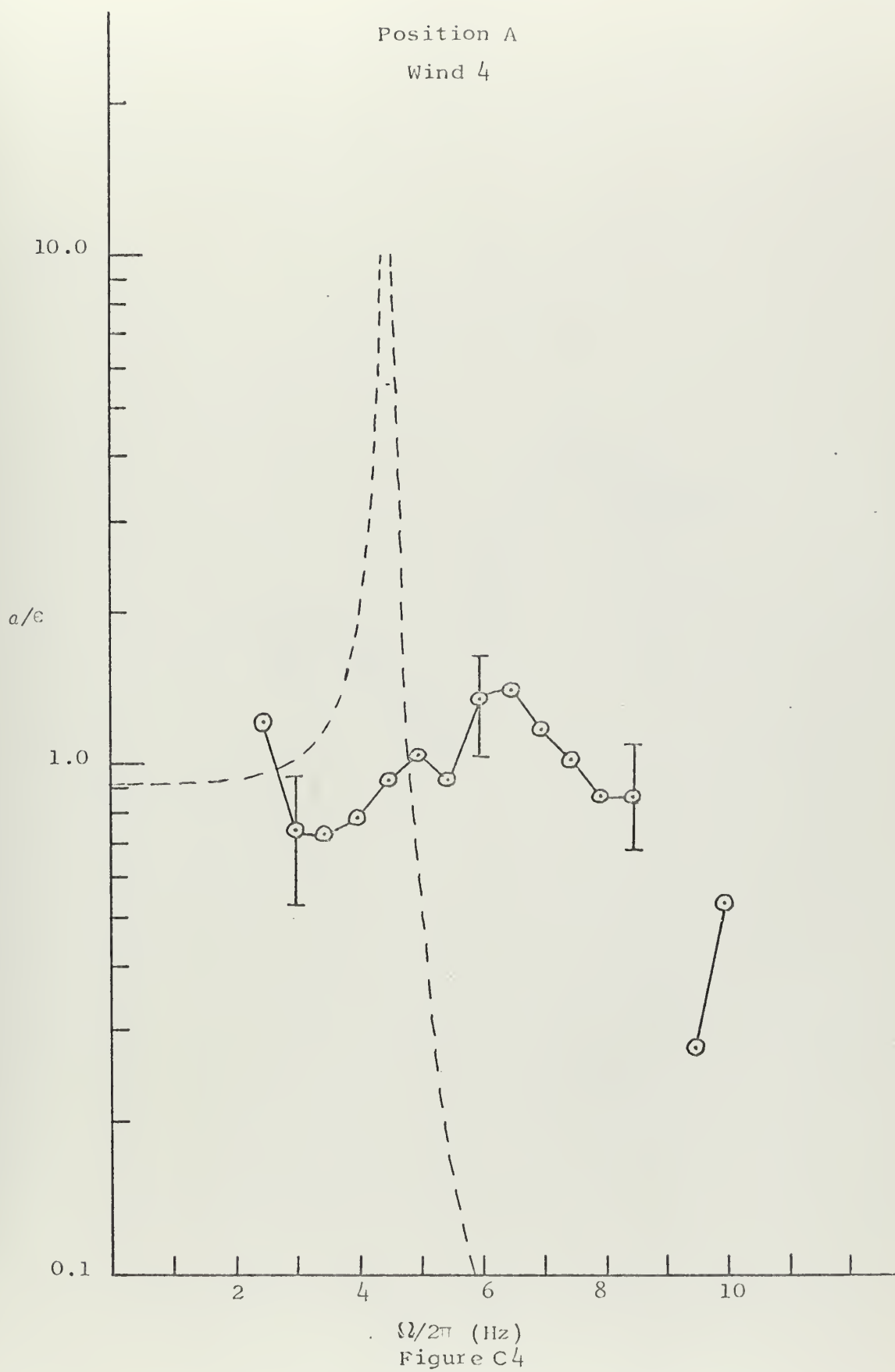


Position A  
Wind 3





Position A  
Wind 4





Position A  
Wind 5

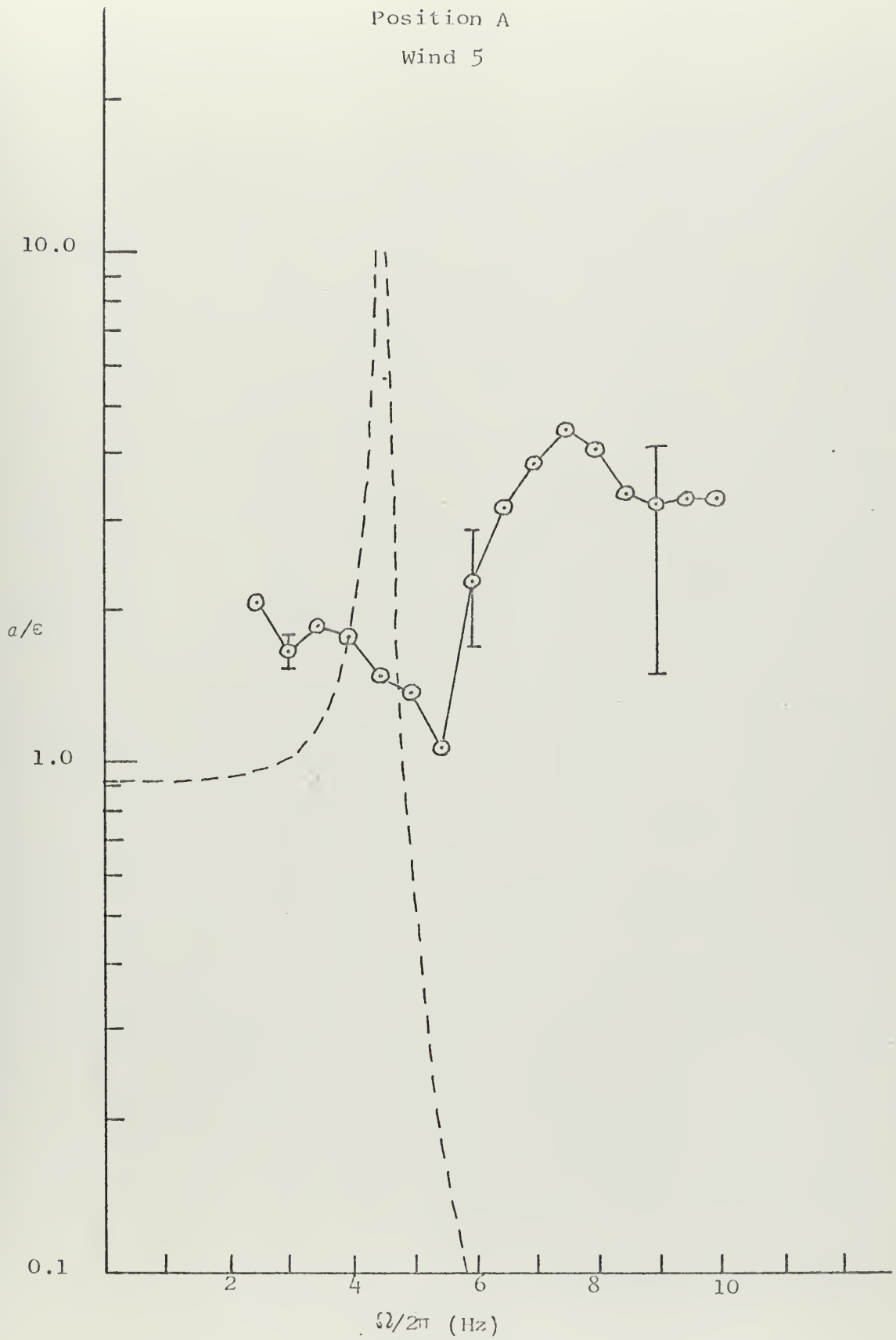


Figure C 5



Position A  
Wind 6

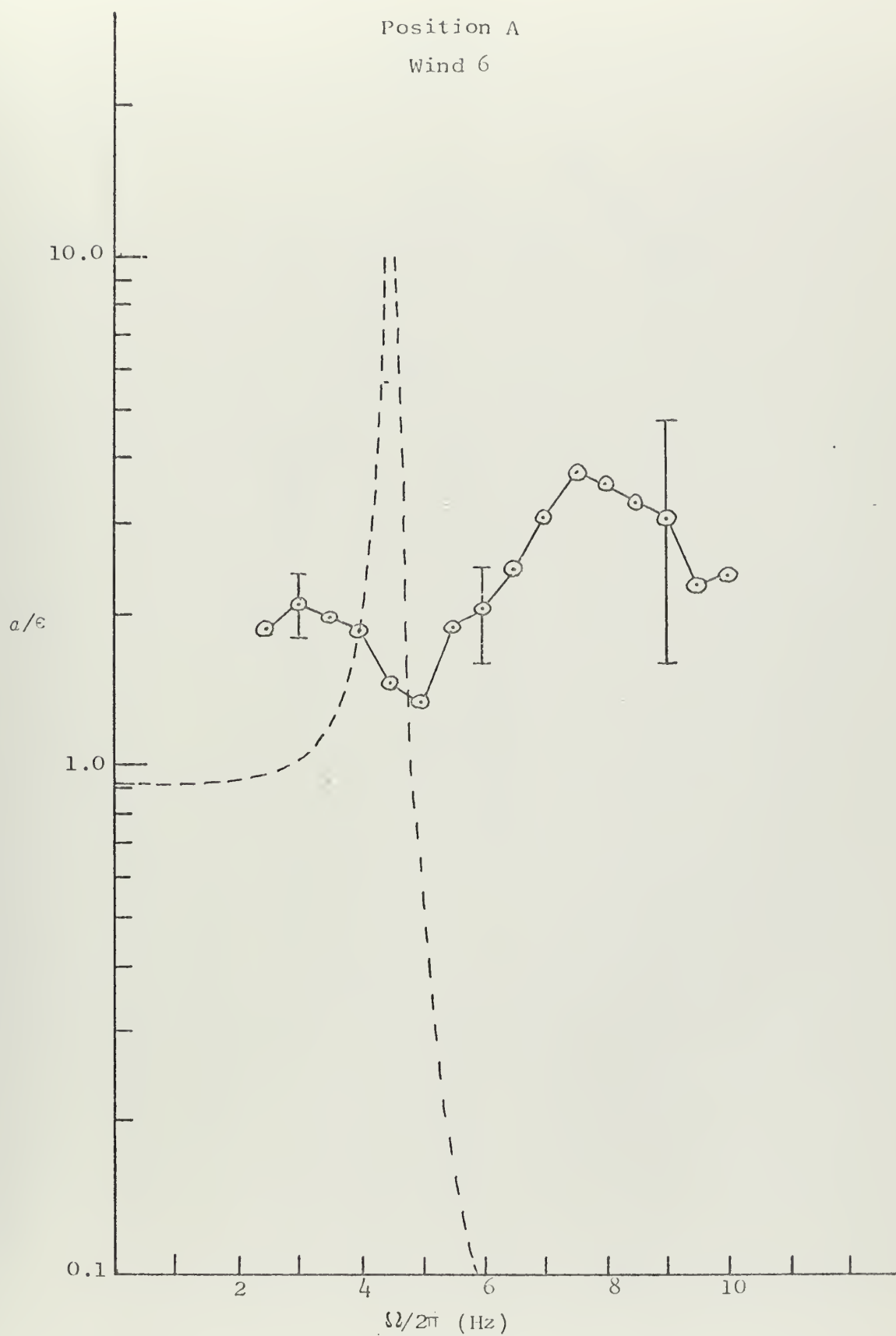


Figure C6



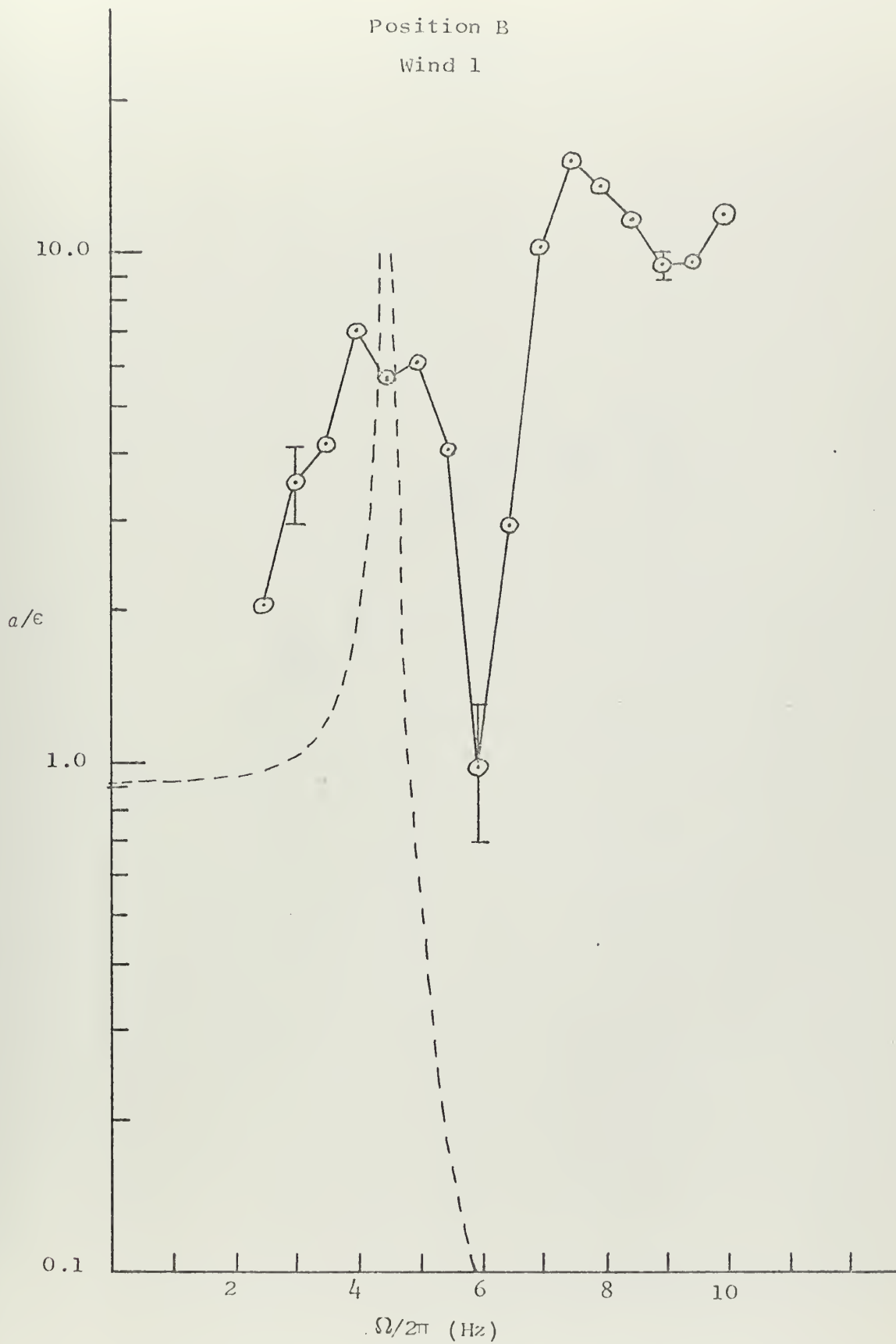
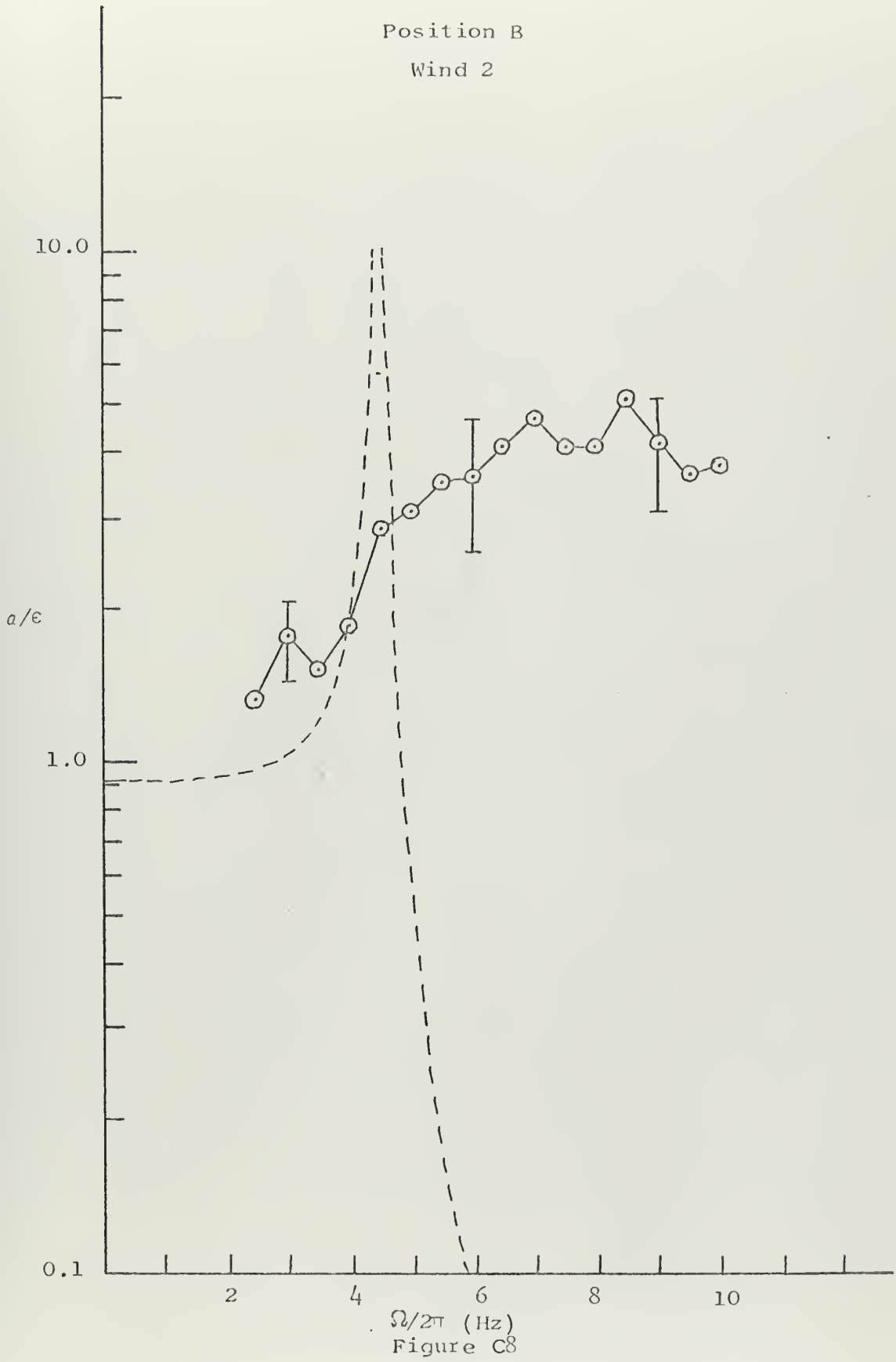


Figure C7

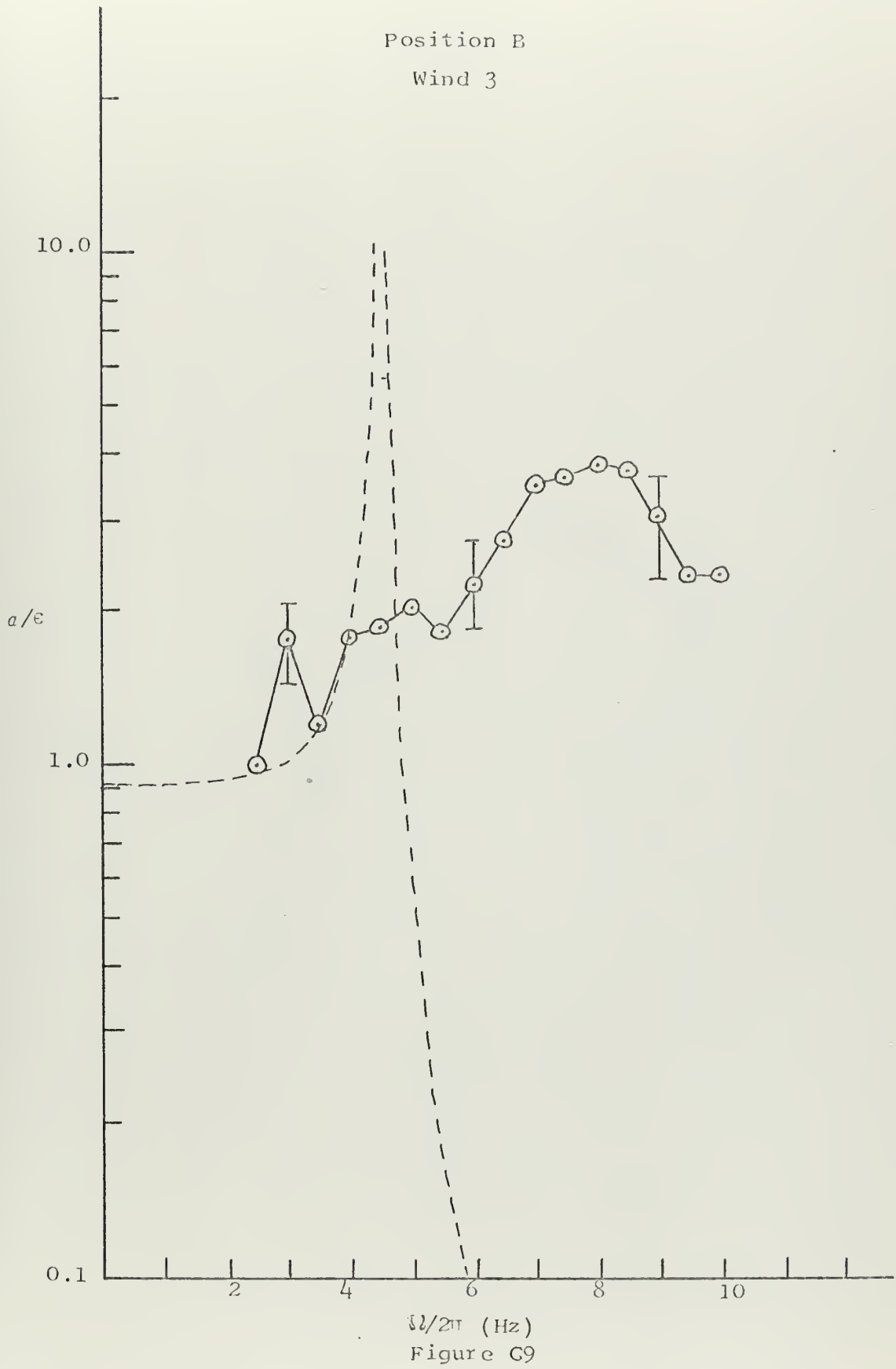


Position B  
Wind 2





Position B  
Wind 3





Position B

Wind 4

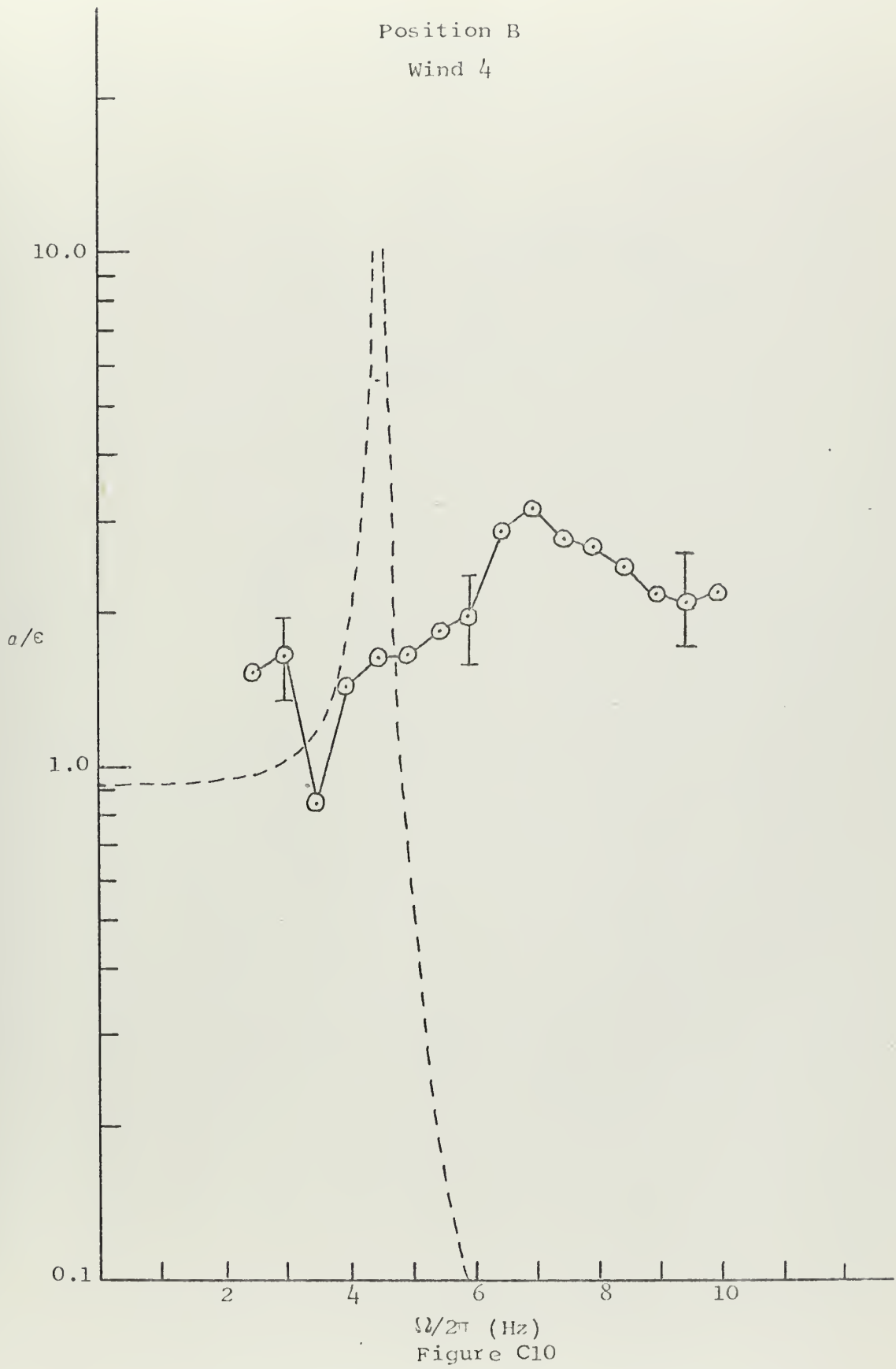


Figure C10



Position B  
Wind 5

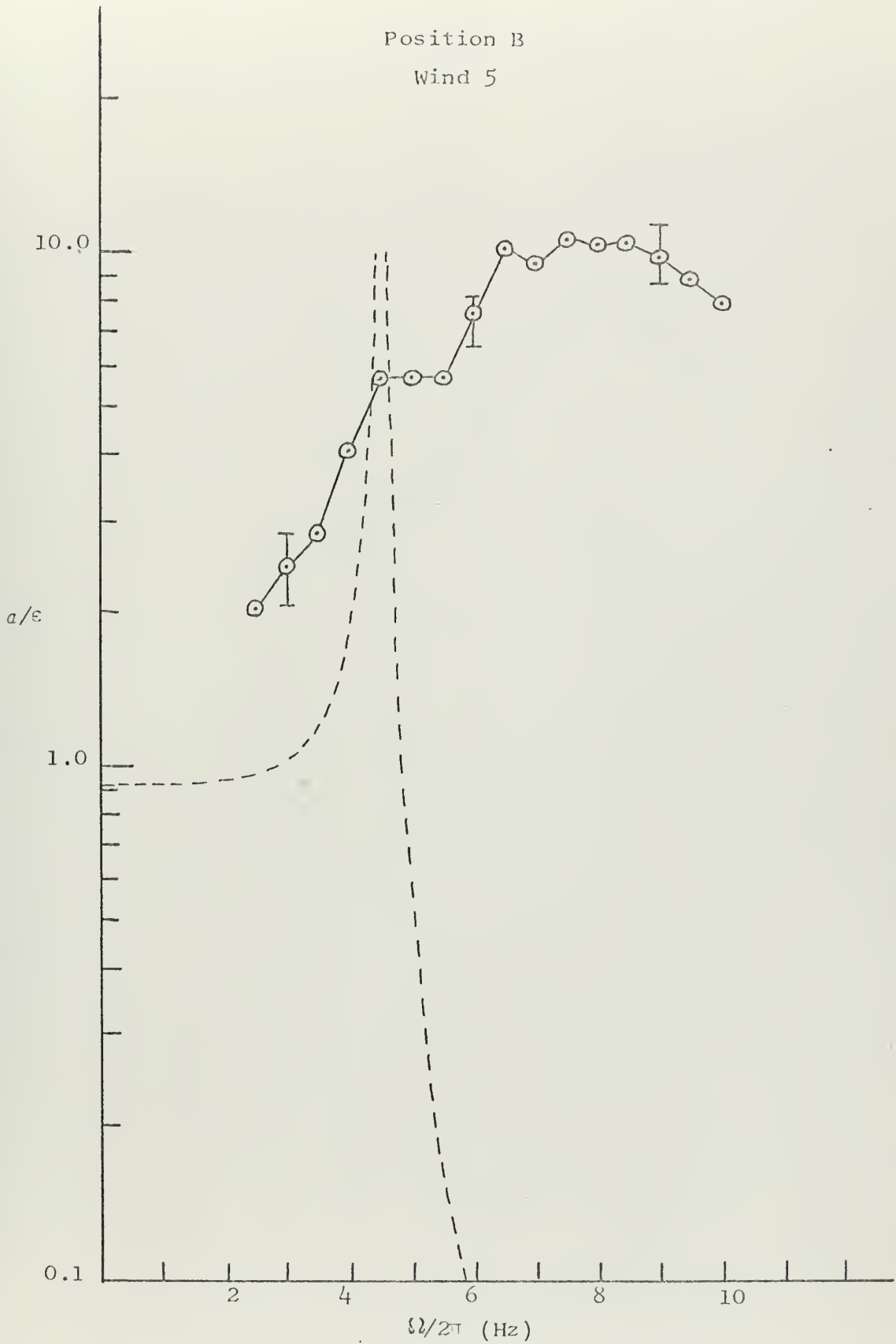
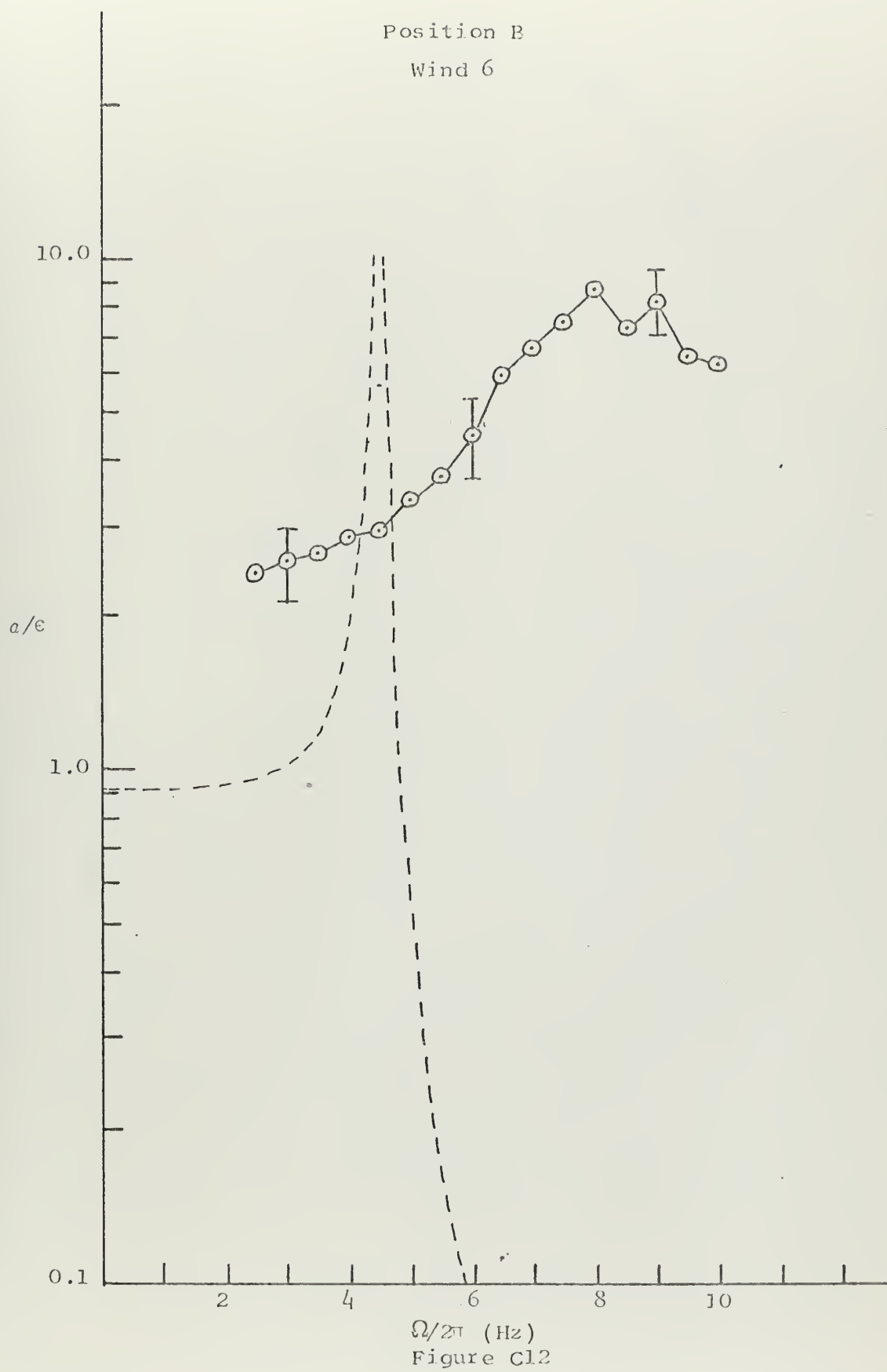


Figure C11



Position B  
Wind 6





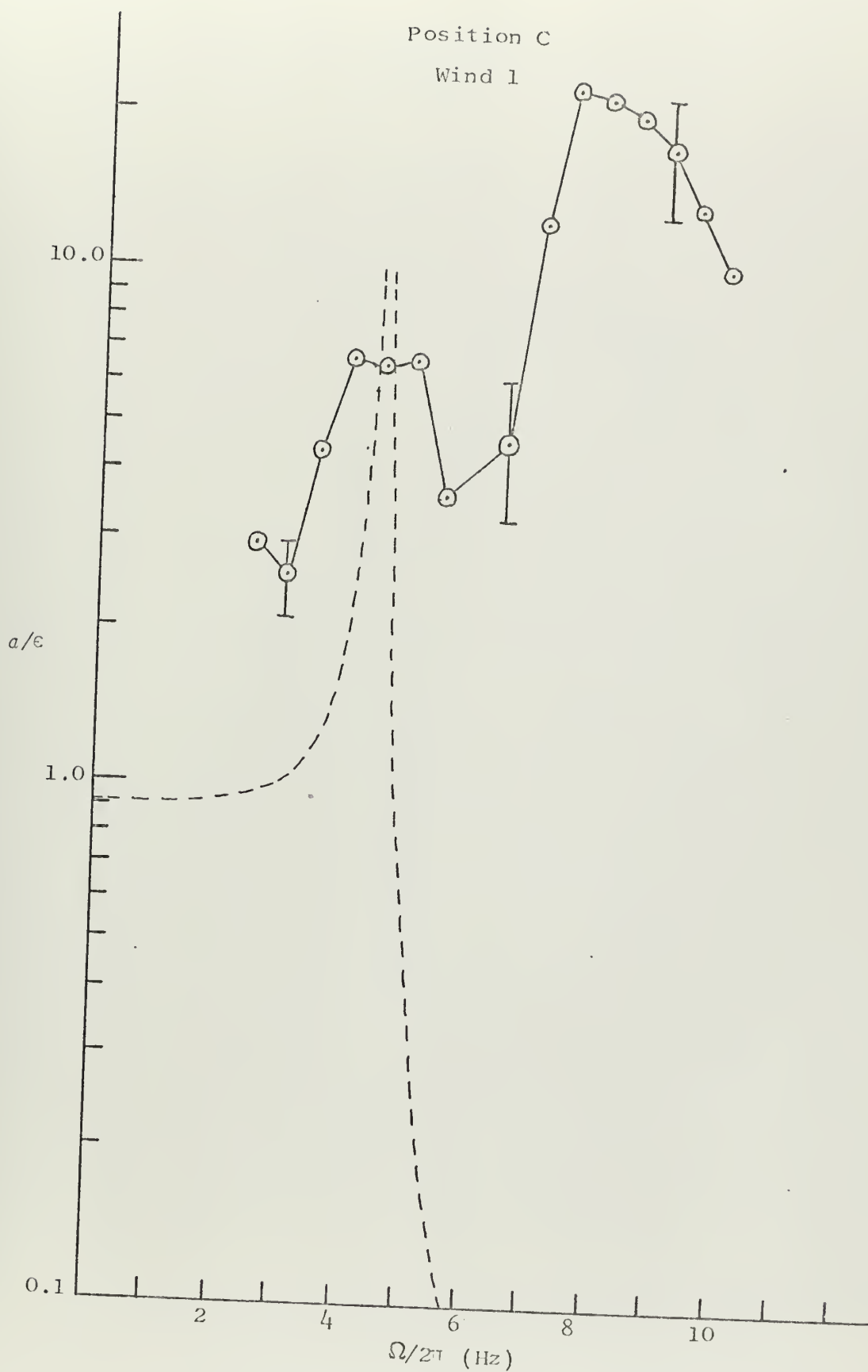


Figure C 13



Position C  
Wind 2

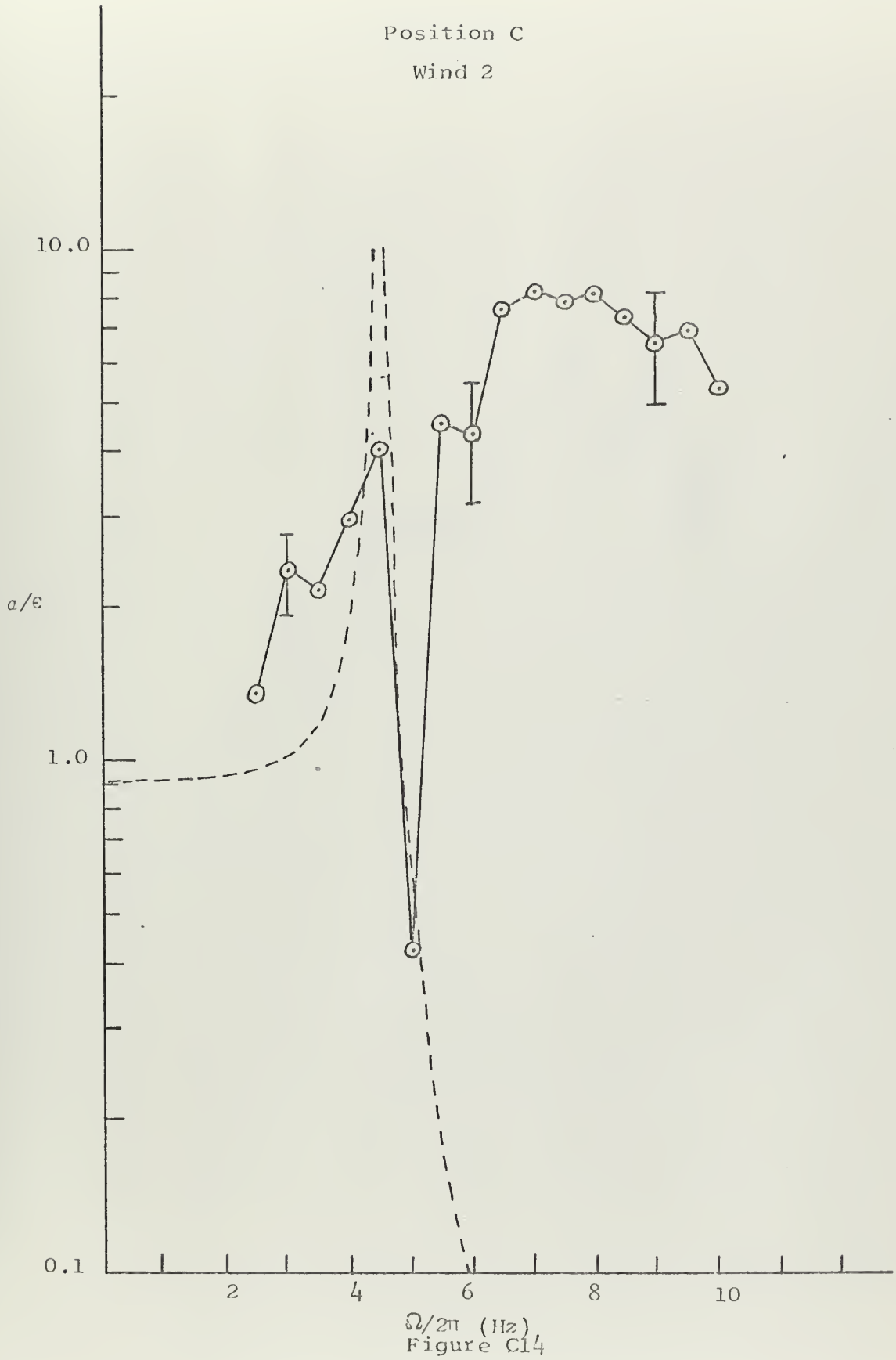


Figure C14



Position C  
Wind 3

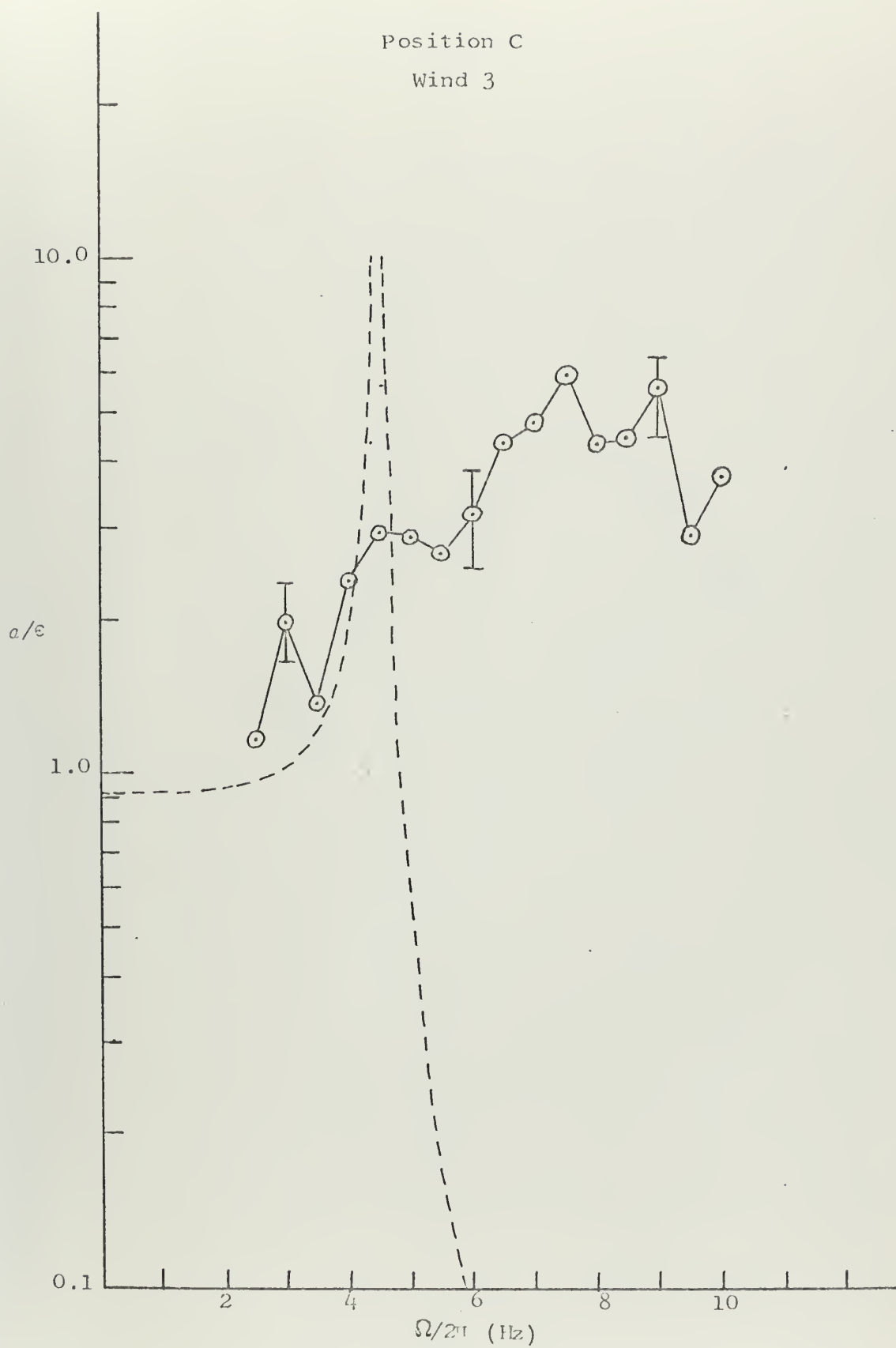


Figure C 15



Position C  
Wind 4

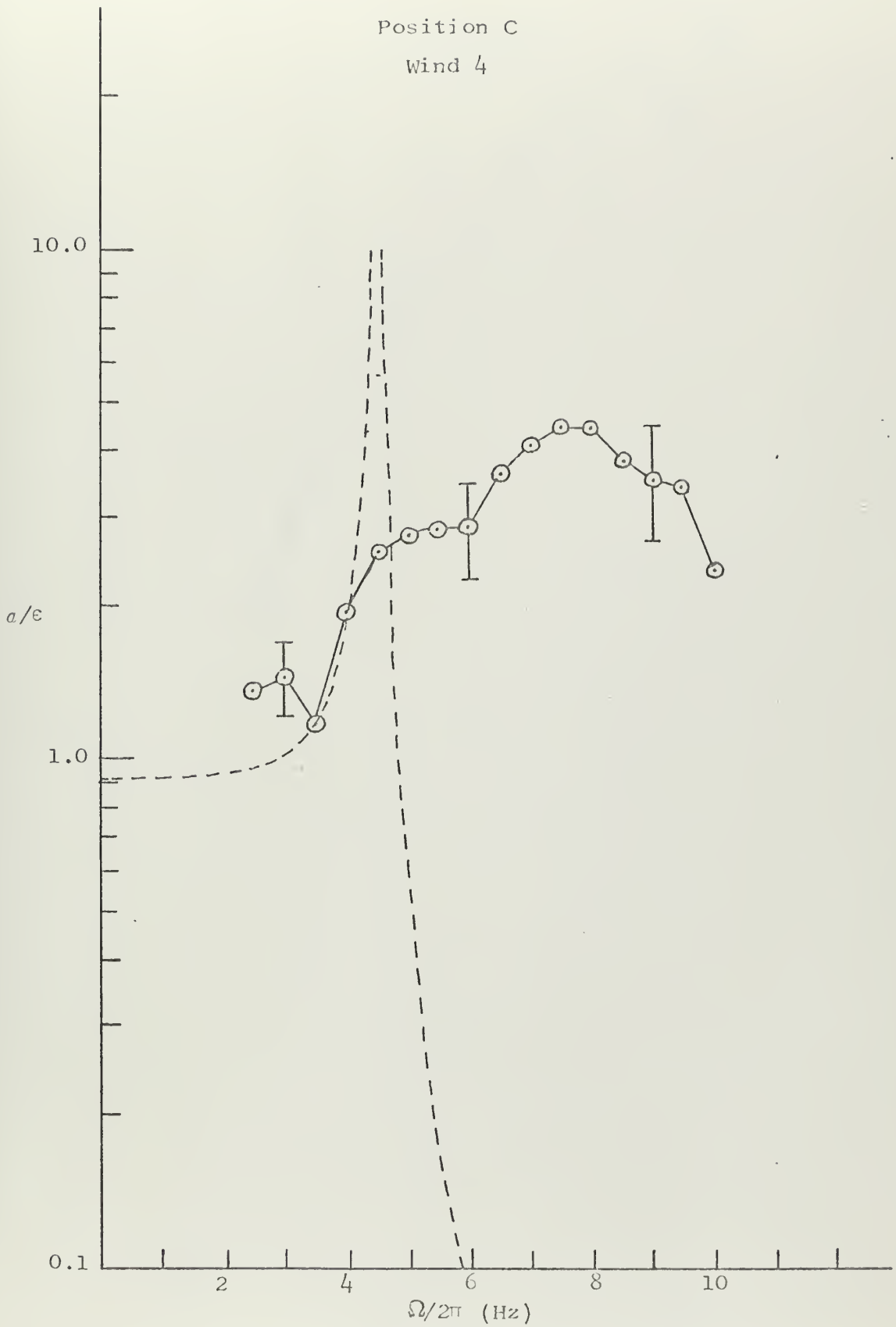


Figure C 16



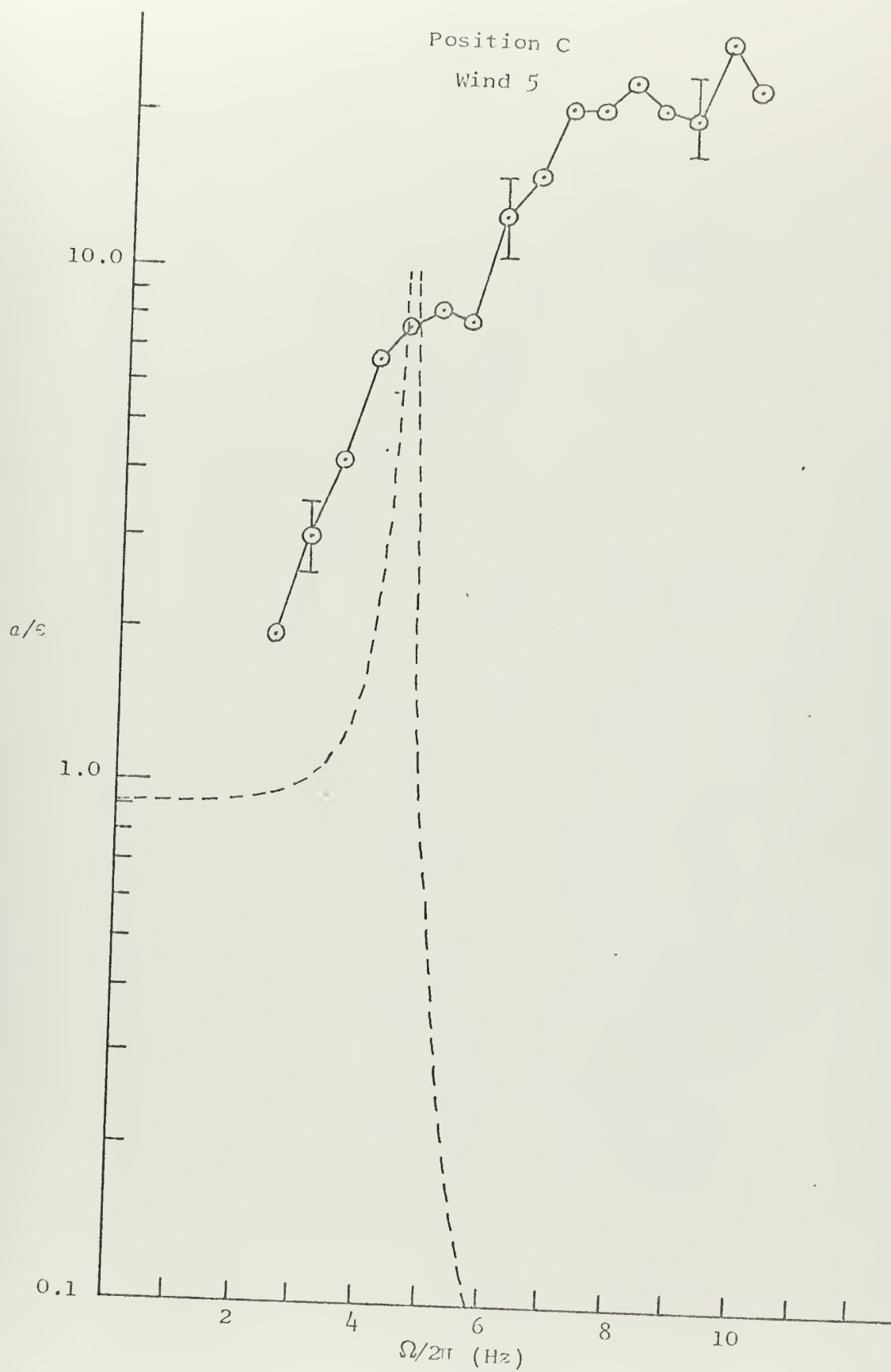


Figure C17



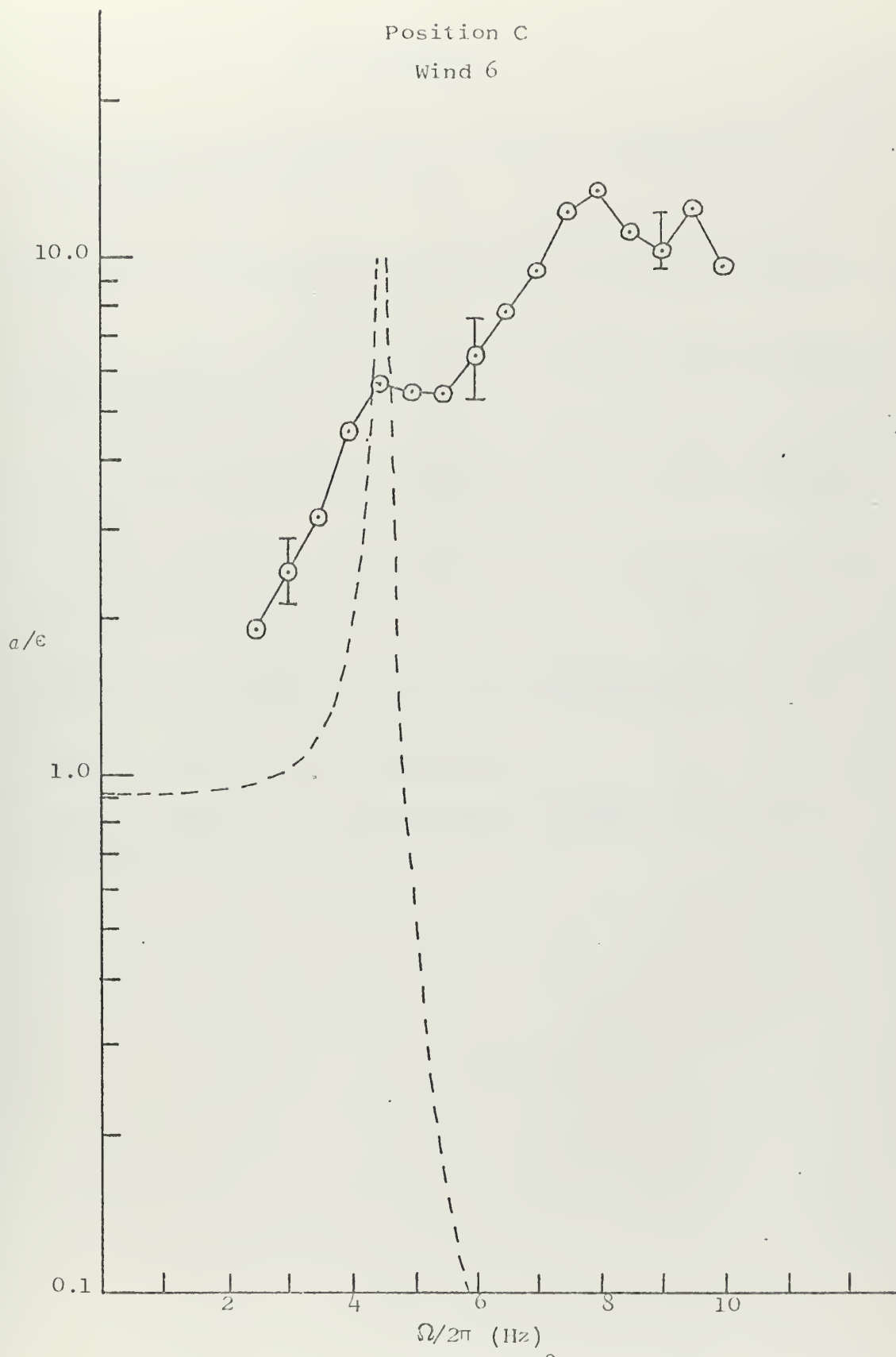


Figure C18



## BIBLIOGRAPHY

1. Wood, A.B., Model Experiments and Sound Propagation in Shallow Seas, J. Acoust. Soc. Am., Vol. 31, September, 1959: 1213-1234.
2. Fortuin, Leonard, Survey of Literature on Reflection and Scattering of Sound at the Sea Surface, J. Acoust. Soc. Am., Vol. 47, May, 1970: 1209-1228.
3. Pearson, J.D., The Transient Motion of Sound Waves in Tubes, Quart. Journal Mech. and Applied Math., Vol. VI, Part Three, 1953: 313-335.
4. Pierce, Allan D., Extension of the Method of Normal Modes to Sound Propagation in an Almost-Stratified Medium. J. Acoust. Soc. Am., Vol. 37, January, 1965: 19-27.
5. Scrimger, Joseph A., Signal Amplitude and Phase Fluctuations Induced by Surface Waves in Ducted Sound Propagation, J. Acoust. Soc. Am., Vol. 33, February, 1961: 239-247.
6. Tonakanov, O.S., Sound Fluctuations during Propagation in a Shallow Layer of Water, Soviet Physics-Acoustics, Vol. 7, October-December, 1961: 185-189.
7. Coppens, A.B., Private communication.
8. Lindsay, Robert Bruce, Mechanical Radiation, McGraw-Hill Book Company, Inc., 1950: 198.



# INITIAL DISTRIBUTION LIST

	No. Copies
1. Defense Documentation Center Cameron Station Alexandria, Virginia 22314	2
2. Library, Code 0212 Naval Postgraduate School Monterey, California 93940	2
3. Assoc. Prof. Alan B. Coppens, Code 61Cz Department of Physics Naval Postgraduate School Monterey, California 93940	5
4. LCDR Wesley E. Jordan, Jr. Armed Forces Staff College Norfolk, Virginia 23511	1



DOCUMENT CONTROL DATA - R & D

(Security classification of title, body of abstract and indexing annotation must be entered when the overall report is classified)

1. ORIGINATING ACTIVITY (Corporate author)		2a. REPORT SECURITY CLASSIFICATION	
Naval Postgraduate School Monterey, California 93940		Unclassified	
		2b. GROUP	
3. REPORT TITLE			
Preliminary Investigation of the Effect of Surface Fluctuations on Sound Amplitude in Guided Mode Propagation			
4. DESCRIPTIVE NOTES (Type of report and, inclusive dates)			
Master's Thesis; December 1970			
5. AUTHOR(S) (First name, middle initial, last name)			
Wesley Earl Jordan, Jr.			
6. REPORT DATE		7a. TOTAL NO. OF PAGES	7b. NO. OF REFS
December 1970		108	8
6a. CONTRACT OR GRANT NO.		8a. ORIGINATOR'S REPORT NUMBER(S)	
b. PROJECT NO.			
c.		9a. OTHER REPORT NO(S) (Any other numbers that may be assigned this report)	
d.			
10. DISTRIBUTION STATEMENT			
This document has been approved for public release and sale; its distribution is unlimited.			
11. SUPPLEMENTARY NOTES		12. SPONSORING MILITARY ACTIVITY	
		Naval Postgraduate School Monterey, California 93940	
13. ABSTRACT			
<p>A simple theoretical relation between a one-dimensional surface wave and the amplitude fluctuations of an acoustic standing wave in a cavity with idealized boundaries is presented. An experiment was designed to investigate the applicability of the theory to a more complicated configuration. A 237 cm x 117 cm x 9 cm water-filled cavity with pressure-release walls was excited in a normal mode by a source placed in one corner. The resulting acoustic signal was monitored at various locations throughout the cavity with a small probe receiver. Wind-driven surface waves were generated by a multi-fan blower placed at one end of the cavity. The relationship between the resulting fluctuation of the acoustic signal and the surface fluctuation above the receiver was investigated. The results are consistent with the simple theory at low surface-wave frequencies. Anomalous behavior was observed for the higher frequencies of the surface wave spectrum. Possible mechanisms for this inconsistency are postulated and discussed.</p>			



14

## KEY WORDS

## LINK A

## LINK B

## LINK C

ROLE

WT

ROLE

WT

ROLE

WT

Propagation

Normal Mode

Irregular Boundary

Amplitude Fluctuation

Surface Waves



Thesis  
J824  
c.1

Jordan

124440

Preliminary investi-  
gation of the effect  
of surface fluctua-  
tions on sound ampli-  
tude in guided mode  
propagation.

Thesis  
J824  
c.1

Jordan

124440

Preliminary investi-  
gation of the effect  
of surface fluctua-  
tions on sound ampli-  
tude in guided mode  
propagation.

thesJ824

Preliminary investigation of the effect



3 2768 002 11617 0

DUDLEY KNOX LIBRARY